UNIVERSITA' DEGLI STUDI DI ROMA

"TOR VERGATA"

FACOLTÀ DI SCIENZE M.F.N.

Dipartimento di Scienze e Tecnologie Chimiche

DOTTORATO DI RICERCA IN SCIENZE CHIMICHE XIX CICLO

"Novel receptor systems based on porphyrins and related macrocycles"

Relatori:

Prof. Roberto Paolesse

Dott. Donato Monti

Candidato:

Dott. Manuela Stefanelli

Coordinatore:

Prof. Bruno Crociani

Index

Chapter 1

Synthesis and Host-Guest Chemistry of a Porphyrin-Cavitand Supramolecular System

Introduction

Results and discussion

Experimental section

Chapter 2

Aggregation Chemistry of Porphyrin and Related Macrocycles

Introduction

Results and Discussion

Experimental section

Chapter 3

The Corroles Chemistry: novel aspects of their reactivity

Introduction

Results and Discussion

Experimental Section

Chapter 1

Synthesis and Host-Guest Chemistry of a Porphyrin-Cavitand Supramolecular System

Introduction

1.1 Origins and Concepts of Host-Guest Chemistry[1]

Supramolecular chemistry is a highly interdisciplinary field of science covering the chemical, physical, and biological features of the chemical species of greater complexity than molecules themselves, that are held together and organized by means of intermolecular (non-covalent) binding interactions. This relatively young area has been defined, conceptualized, and structured into a coherent system. Its roots extend into organic chemistry and the synthetic procedures for molecular construction, into coordination chemistry and metal ion-ligand complexes, into physical chemistry and the experimental and theoretical studies of interactions, into biochemistry and the biological processes that all start with substrate binding and recognition, into materials science and the mechanical properties of solids.

In any field of science, novelty is linked to the past. Where would the roots of supramolecular chemistry reach? It was Paul Ehrlich who recognized that molecules do not act if they do not bind thus introducing the concept of *receptor*. But binding must be selective, a notion that was enunciated by Emil Fischer in 1894 and very expressively presented in his celebrated "lock and key" image of steric fit, implying geometrical complementary, that lays the basis of *molecular recognition*.

Finally, selective fixation requires interaction, affinity between the partners, that may be related to the idea of *coordination* introduced by Alfred Werner, supramolecular chemistry being in this respect a generalization of coordination chemistry.

With these three concepts, fixation, recognition and coordination, the foundations of supramolecular chemistry are laid.

1.1.1 Principles of Molecular Recognition

Molecular recognition is defined by the energy and the information involved in the binding and selection of substate(s) by a given receptor molecule; it may also involve a specific function. Mere binding is not recognition, although it is often taken as such. One may say that recognition is binding with a purpose, like receptors are ligands with a purpose. It implies a pattern recognition process through a structurally well-defined set of intermolecular interactions. Binding of a substrate to a receptor forms a complex or supramolecule characterized by its thermodynamic and kinetic stability and selectivity, thus by the amount of energy and of information brought into operation.

Molecular recognition thus implies the molecular storage and supramolecular read out of molecular information. The latter may be stored in the architecture of the receptor, in its binding sites and in the ligand layer surrounding bound substrate. In addition to size and shape, a receptor is characterized by the dimensionality, the connectivity and the cyclic order of its structural graph; conformation, chirality and dynamics also come into play.

Recognition implies geometrical and interactional complementary between the associating partners, that is optimal information content of a receptor with respect to a given substrate. This amounts to a generalized *"double complementary principle"* extending over energetic features as well as over the geometrical ones represented by the "lock and key", steric fit concept of Fischer.

High recognition by a receptor molecule A consists in a large difference between the binding free energies of a given substrate B and of the other substrates. It results in a marked deviation from the statistical distribution. In

order to achieve large differences in affinity several factors must be taken into account:

- *steric* (shape and size) *complementary* between A e B, i.e. presence of convex and concave domains in the correct location on A and B;
- *interactional complementary*, i.e. presence of complementary binding sites (electrostatic such as positive/negative, charged/dipole, dipole/dipole, hydrogen bond donor/acceptor, etc.) in the correct disposition on A and B so as to achieve complementary electronic and nuclear distribution (electrostatic, H-bonding and van der Waals) maps;
- *large contact areas* between A and B;
- *multiple interaction sites*, since non-covalent interactions are rather weak compared to covalent bonds;
- *strong overall binding*; although high stability does in principle not necessary imply high selectivity, this is usually the case; indeed, the differences in free energy of binding are likely to be larger when the binding is strong; high binding efficiency (i.e. high fraction of bound with respect to free B) requires strong interactions; thus, in order to achieve efficient recognition, i.e. both high stability and high selectivity, strong binding of A and B is required.

In addition, medium effects play an important role through the interaction of solvent molecules which A and B as well as with each other; thus the two partners should present geometrically matched hydrophobic/hydrophobic or hydrophilic/hydrophilic domains.

Biological molecular recognition represents the most complex expression of molecular recognition leading to highly selective binding, reaction, transport, regulation etc. It is not surprising thus that nature's enzymes were used as a

blueprint by the first studies on the construction of artificial molecular receptors, whose structures have to share some features with the enzymatic ones.

1.1.2 Molecular Receptors: design principles.

Molecular receptors are defined as organic structures held by covalent bonds, that are able to bind selectively ionic or molecular substrates (or both) by means of various intermolecular interactions, leading to an assembly of two or more species, a supramolecule.

The factors mentioned in the previous paragraph must be taken into account in the design of a molecular receptor. In particular, complementarity depends on a well-defined three dimensional architecture with the correct arrangement of binding sites. Furthermore, host and guest will be in contact over a large area, if receptor is able to wrap around its substrate so as to establish numerous non-covalent binding interactions and to sense its molecular size, shape and architecture.

This is the case for receptor molecules that contain intramolecular cavities, clefts or pockets into which the substrate may fit. In such *concave* receptors the cavity is lined with binding sites directed towards the bound species; they are endopolarophilic and convergent and may be termed *endoreceptors*.

Macropolycyclic structures are of special interest for designing artificial receptors: they are large and may therefore contain cavities of appropriate size and shape; they possess numerous branches, bridges and connections that allow the construction of a given architecture endowed with a specific dynamic feature; they provide means for the arrangement of structural groups, binding sites, and reactive functions.

The balance between rigidity and flexibility is of particular importance for the binding and the dynamic properties of host and guest. Rigid “lock and key”-

type receptors are expected to present very efficient recognition, but on the other hand, flexible receptors that bind their substrate by an "induced fit" process may display high selectivity but have lower stability. Process of exchanges, regulation, cooperativity, and allostery require a built-in flexibility so that the host may adapt and respond to changes. Flexibility is of great importance in biological receptor-substrate interactions, where adaption is often required for regulation to occur. Such designed dynamics are more difficult to control than mere rigidity, and the developments in computer-assisted molecular design methods may greatly help. Receptor design thus covers both static and dynamic features of macropolycyclic structures.

Molecular receptors of extremely varied structural types have been conceived and investigated. Many of them are of macropolycyclic type.

Receptor molecules belonging to numerous types of geometries can be imagined. A selection of such structures resulting from the combination of non-cyclic and cyclic elements is presented in Fig.1.1 .

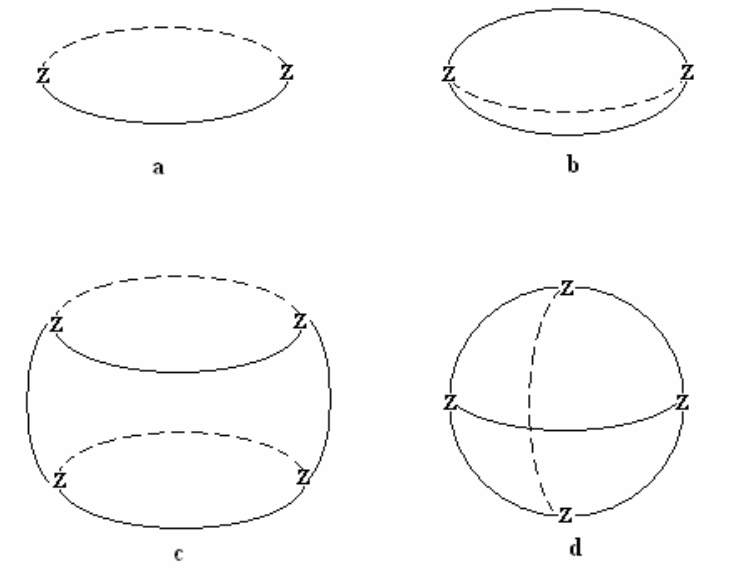

Fig. 1.1 *– Some macropolycyclic structures: a) macrocyclic, b) macrobicyclic, c) cylindrical macrotricyclic, and d) spherical macrotricyclic..*

The size and shape of the binding cavity that they define and their rigidity or flexibility are determined by the nature of structural subunits from which they are formed. The great accessibility of chemical structures characterized by all kinds of electronic and structural features brought a large number of molecular receptor till today. Without being exhaustive, one may mention the acyclic *podands*, the macrocyclic *crown ethers*, *coronands* or *torands*, the *clathrochelates* and *coordinatoclathrates*, the macropolycyclic *cryptands* and *speleands*, the *spherands*, *cavitands* and *carcerands*, the *calixarenes*, the *cyclophane* receptors, the *cryptophanes* etc.

Taking its inspiration form enzymatic models in nature, the investigation of the potentiality of these molecular containers was initially devoted to catalysys[2]. The first, simple examples of enzyme mimics were crown ethers and cryptands with catalytically active functionalities attached in the correct position near the reacting group of a complexed substrate. From the early 1970s on, cyclodextrins (CDs), naturally abundant cavity molecules, have been extensively used as binding sites in supramolecular catalysts., showing to be a particularly selective catalysts for ester hydrolysis[3].

Covalently built capsules have proven their value as catalysts of a wide range of chemical reactions, and in several cases impressive efficiencies and selectivities have been achieved. However, as the scale and complexity of the target products of their reactions increase, designing and preparing capsule-shaped catalysts in a covalent fashion rapidly became very difficult, involving costly multistep syntheses that often produce only milligram yields of material. Moreover, the resulting catalysts were not so versatile because they were often highly specific to only a limited number of reactions.

For this reason in the past decade a shift has been observed in the approach to construct these catalysts, from traditional covalent chemistry to multicomponent self-assembly of relatively small complementary building blocks.

1.1.3 Molecular receptors with enclosed cavities: supramolecular assembled capsules and boxes[2].

Self-assembled capsules are receptors with enclosed cavities that are formed through reversible, noncovalent interactions between two or more complementary subunits. Typically, such capsules self-assemble through hydrogen-bonding and metal-ligand interactions. Hydrogen-bonding are highly directional and specific, whereas metal-ligand bonds are generally much stronger, yielding more robust self-assembled structures.

The group of Rebek has become one of the leading groups in the exploration of self-assembly of complementary concave receptors into a myriad of hydrogenbonded capsular species[4].

The first capsule they reported[5], the so-called "tennis-ball" **1-1** (Fig 1.2), consists of two bis-glycoluril units which self-assemble into a closed cavity. The self-assembly is governed by the specific curvature encoded within the building block, and the concomitant formation of eight hydrogen bonds between the self-complementary C=O and N-H functions of the two subunits.

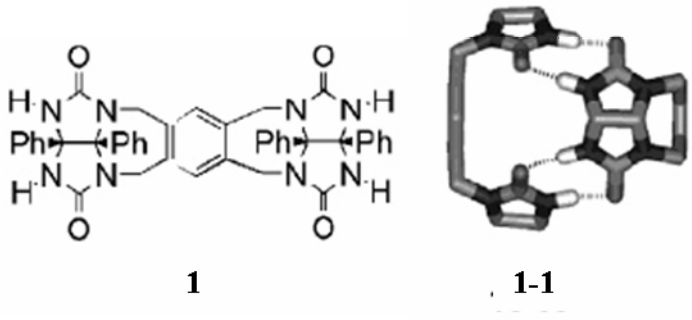

1 **1-1**

Fig. 1.2 *– Glycoluril-based capsule which are self-assembled by hydrogen-bonding interactions: a "tennis-ball".*

The inner volume of the capsule (~50 $Å^3$) is rather small and only allows the encapsulation of small molecules such as methane and noble gases. To complex larger guests, the spacers between the glycoluril moieties were varied,

generating a number of dimeric and higher order capsules with inner compartments of varying sizes. By comparing the binding properties of these capsules, it turned out that the encapsulation process was largely determined by the size and shape of the guest. An extensive study toward the understanding of the factors that govern the binding of guests within Rebek's capsules revealed the "55% occupance" rule, which implies that in the absence of specific intermolecular interactions between the guest and the capsule the binding is most efficient if only 55% of the available inner space is filled.

A typical example of a larger capsule generated by the assembly of extended subunits is the "molecular softball" **2-2**, in which the glycoluril moieties are connected across seven fused rings[6] (Fig.1.3). The central ring contains an ethylene bridge function that encodes the extra curvature that is required for the specific formation of a hydrogen-bonded dimer, resulting in a capsule which is now held together by a seam of 12 hydrogen bonds.

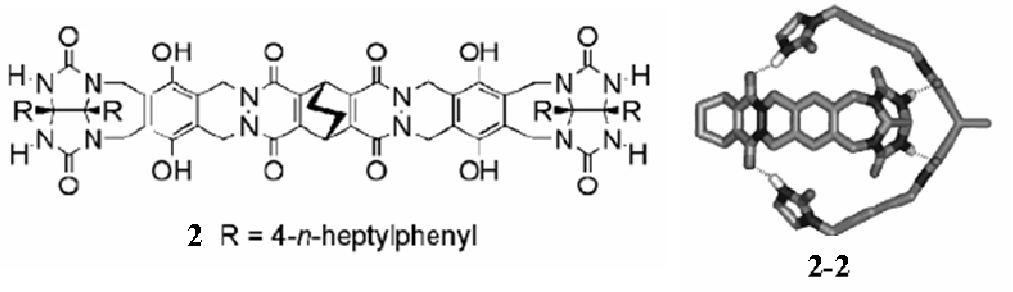

Fig. 1.3 *– Glycoluril-based capsule which are self-assembled by hydrogen-bonding interactions: a "soft-ball".*

The complexation of guest molecules within the softball is, interestingly, an entropy-driven process, which was concluded from the fact that the association constants increase with temperature. Moreover some experiments showed that the "softball" was capable of encapsulating two aromatic solvent molecules. This propensity stimulated the researchers to utilize the "softball" as a microreactor for bimolecular reactions.

An example is depicted in Fig. 1.4 and reported the Diels-Alder reaction between 2,5-dimethylthiophene dioxide and *p*-benzoquinone catalyzed by the microreactor[7] **2-2**.

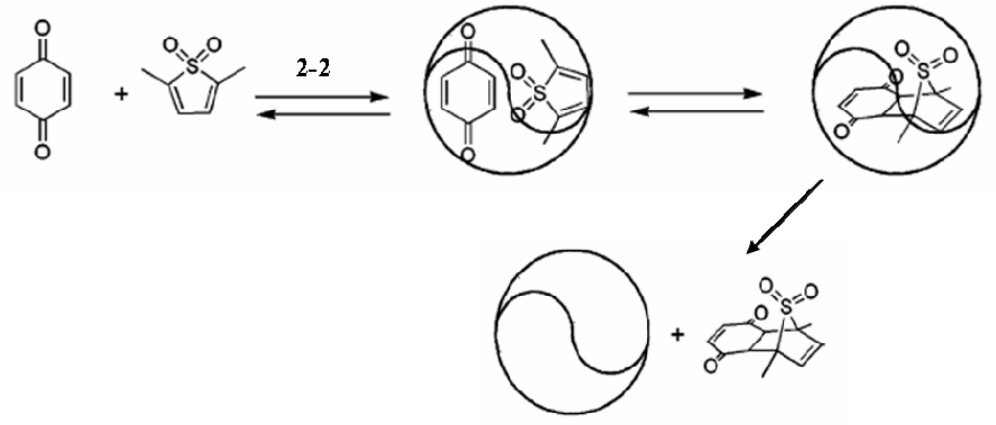

Fig. 1.4 *– The Diels-Alder reaction between two dienes accelerated by microreactor* ***2-2.***

Self-assembled capsules can be formed by metal-ligand interactions too[8].

In contrast to hydrogen-bonding motifs, which are linear in nature and thus require the presence of curvature elsewhere in the building block for a capsule to be formed, the specific coordination angles between ligands and metal centers can be used themselves as codons for curvature.

Fujita and co-workers have elaborated on the conceptual design and synthesis of well-defined cages by multicomponent transition metal-mediated self-assembly processes[9] for the use as reaction chambers for several types of bi- and multimolecular reactions.

The building blocks of these highly symmetrical metallocapsules are simple triangular heterocyclic ligands and cis-enforced square-planar Pd-and Pt-complexes. Coordination cage **3**[10], which is the single product of a spontaneous self-assembly process of four tris(4-pyridyl)triazine ligands and six palladium complexes, has an inner compartment with a volume of about 500 $Å^3$ and is capable of encapsulating a variety of neutral organic molecules in aqueous environments (Fig. 1.5).

For this reason, the capsule was expected to be an effective mediator for phase-transfer catalysis reactions in water. For example, in the absence of cage 30, the Wacker oxidation of styrene to acetophenone, catalyzed by $[Pd(en)](NO_3)_2]$ (en = ethylenediamine) in water, proceeded only to a small extent (4%).

In the presence of a catalytic amount of the capsule, however, a dramatic increase in the yield of acetophenone to 82% was observed[10d]. When the reaction was carried out in the presence of 1,3,5-trimethoxybenzene, a molecule that effectively competes with styrene for encapsulation by cage, the acetophenone production dropped to 3%.

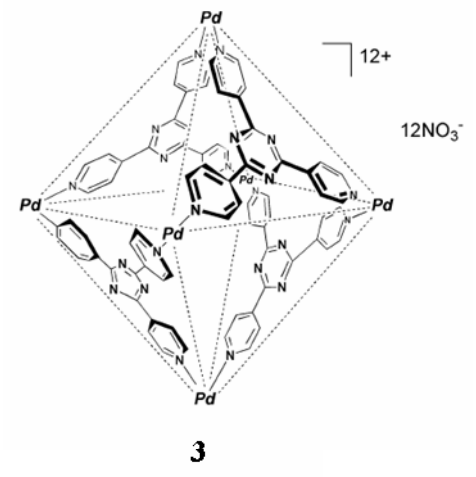

Fig. 1.5 *– Structure of metallo-cage* ***3*** *elaborated by Fujita's group.*

An elegant example about generation of a cage promoted by metal-ligand interactions was recently reported by Dalcanale and co-workers.[11]

They synthesized a cavitand, functionalized with four alkylthioether groups at the lower rim, and four tolylpyridine groups at the upper rim. This structure was able to bind to a gold surface by its thioether groups, and formed the coordination cage **4** with $[Pd(dppp)(NEt_3)_2(OTf)_2]$ by its pyridine groups (Fig. 1.6).

Monitoring the self-assembly process by atomic force microscopy (AFM) they observed that cages of nanosized dimensions can be effectively formed in a controlled fashion on gold, using different approaches. More insight they pointed out that metal-directed self-assembly of cages is a reversible process, also on surfaces.

When a gold substrate with inserted cages was exposed to a solution of triethylamine in ethanol, this ligand was able to shift the equilibrium towards the formation of $[Pd(dppp)(NEt_3)_2(OTf)_2]$ plus free cavitand by competing with Pd coordination centres.

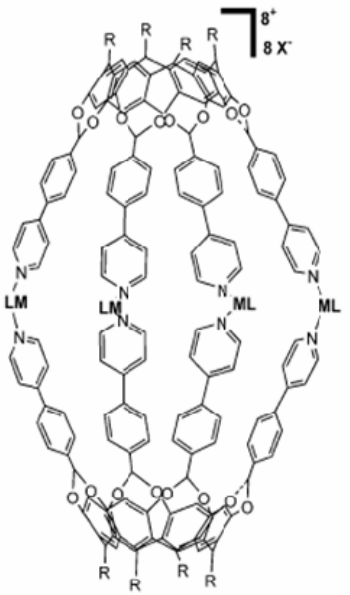

Fig. 1.6 *– Structure of metallo-cage* ***4*** *elaborated by Dalcanale's group.*

.

This aspect conveys interesting properties, such as self-repairing ability and responsiveness to external stimuli that are very important for a supramolecular receptor.

1.1.4 Chirality in Encapsulation Complexes[12]

Chiral supramolecular complexes are always popular topics, especially when noncovalent interactions direct the assembly of achiral components into chiral suprastructures. In the absence of a chiral bias the structures appear as racemates, but with chiral information present in the system, the spontaneous formation of an excess of the appropriate supramolecular structure can be the outcome.

Several studies have taken advantage of the intimate relationship between encapsulated molecules and the supramolecular capsules that bridle them, thus granting a unique perspective on the transfer of information within complexes that is governed by noncovalent interactions. At the outset, the larger distances (compared to covalent bonds) and the flexibility of the weak, often non directional forces, did not guarantee success.

The tendency for calixarene-tetraurea monomer functionalized with aryl sulfonamides to exclusively (>98%) form heteromeric capsules with monomer functionalized with a simple aryl group, has been reported by Castellano and co-workers (Fig.1.7a)[13]. When heteromeric dimmers such as 5a-5b form, the cyclic directionality of the urea hydrogen bonding seam results in the generation of racemic chiral species[14] (Fig.1.7b). The head-to-tail arrangement of the urea units at the equator can be clockwise or counterclockwise, given a reference point of the poles. Interconversion of these enantiomers occurs trough the rotation of functional groups that make up the hydrogen-bonding seam, or through complete dissociation and recombination of monomers.

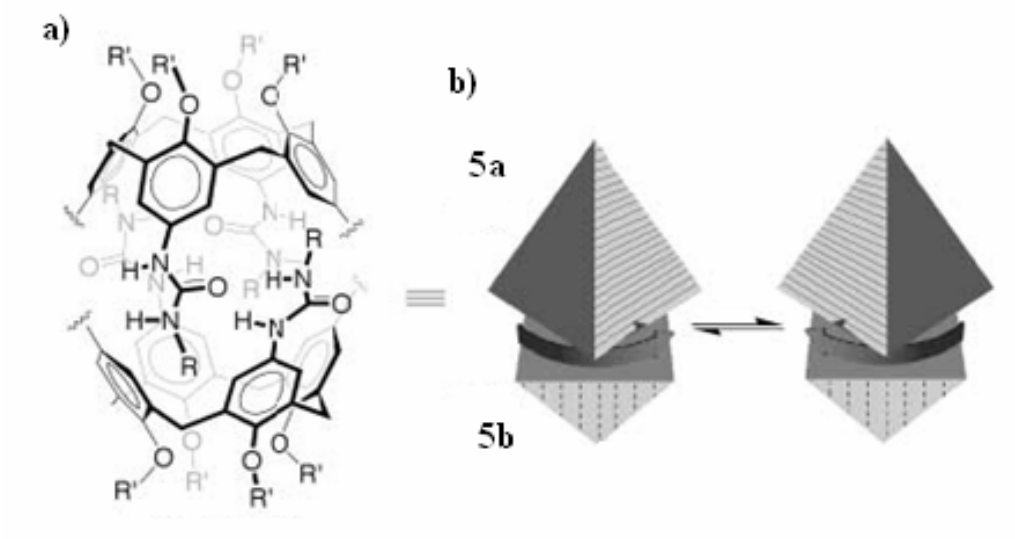

Fig. 1.7 *– Chirality in calix[4]arene-tetraurea capsules.*

Either mechanism would require the eventual breaking of all 16 hydrogen bonds, and as such the reversal of hydrogen bonding directionality (and thus interconversion of enantiomers) is slow on the NMR time scale.

Chiral guests however, were not capable of significant differentiation of the two resulting enantiomeric capsules 5a-5b.

Glycoluril-based monomers (Fig.1.3) have also been employed in the construction of chiral self-assembled capsules. The simple monomers contain two mirror planes, which are both preserved in the dimeric assembled state. Analogous monomers **6** lacking one of the two mirror elements have been synthetized[15]. These monomers are achiral, but self-assemble into dimeric supramolecular capsules that retain no mirror planes in the assembled state (Fig.1.8). Again the chiral capsule formed from these achiral components are formed as an equilibrating racemic mixture. The use of monomer **6**, which incorporate symmetry-breaking elements adjacent to the encapsulate guest, results in a host-guest pair capable of significant transfer of chiral information[16]. The binding of an enantiomerically pure guest can bias the self-assembly process (a form of imprinting) such that one enantiomeric capsule is favored over the

other by as much as a factor of four. In a reversal of the flow of chiral information, this diastereomeric host-guest complex can then be used for noncovalent chiral templating.

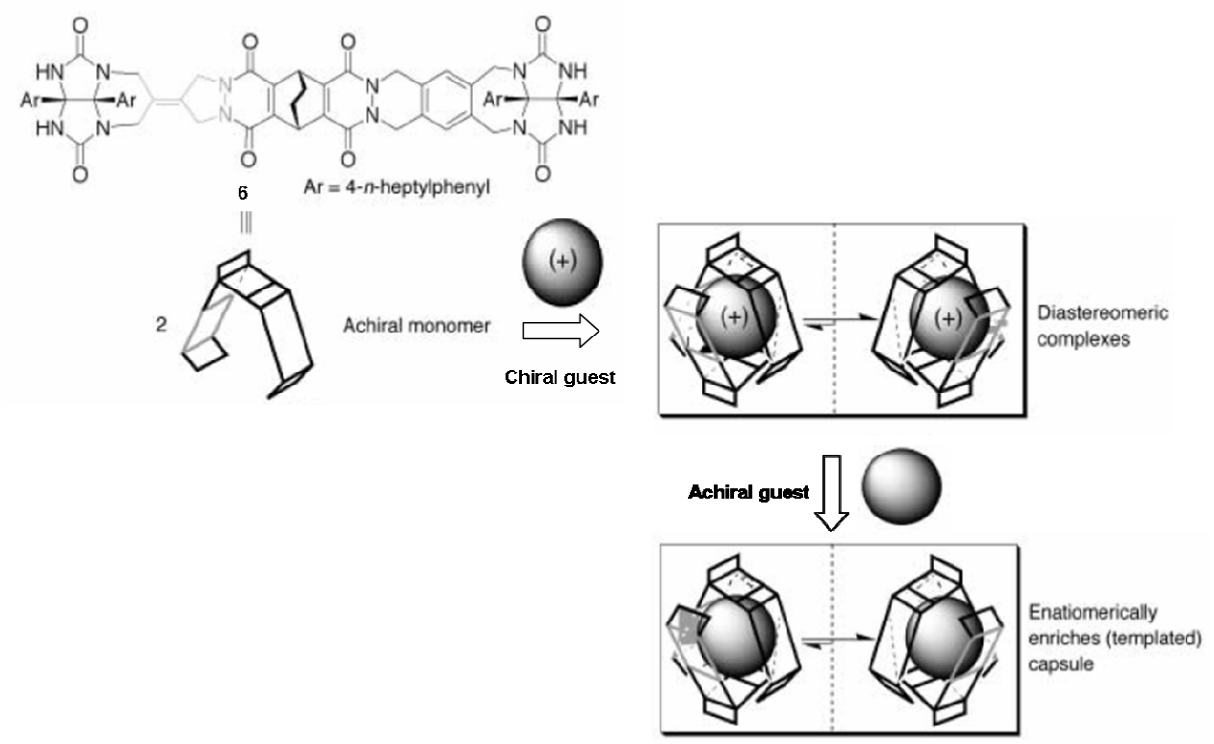

Fig. 1.8 *–"Softball" monomers possessing only one mirror element spawn dimeric structures lacking any mirror symmetry.*

In this procedure, an optically pure guest is used to imprint the formation of a single chiral softball enantiomer and is then rinsed out rapidly by an excess of an achiral guest or solvent molecule. Since the exchange of guests in glycouril-based capsule is much faster than the dissociation of the capsule, the exchange occurs without racemization of the capsule itself. The ghost of the chiral guest allows the chiral capsule to discriminate between guest enantiomers for several hours before it returns to its thermodynamically determined state.

1.2 Cavitands

Cavitand is a synthetic compound defined as a molecular container with an enforced concave surface large enough to complex complementary organic compounds or ions[17]. The molecular cavity is generally open at one end. Inclusion of guest species within a cavitand results in a *cavitate*.

Molecules or fragments that possesses intrinsic curvature (i.e. are structurally bent or curved) may be used to bind guest molecules in both solution as well as the solid state since dissolution of the host does not result in disappearance of the cavity.

Intrinsically curved molecular building blocks that are reasonably synthetically accessible are relatively uncommon, and as a result cavitand hosts and a wide range of related species tend to fall into loose families. These families may be grouped according to the kinds of building blocks used to impart curvature and hence achieve a concave binding pocket.

In general, the binding of strictly neutral, nonpolar organic molecules in nonpolar solvents by the majority of cavitands is relatively weak because there is no significant enthalpic gain from strong host-guest interactions. Solid-state complexes are widespread, however, because of the need to pack efficiently in the crystals lattice.

On the other hand, significant binding of polar or charged organic guests is observed in many species, with binding of alkyl ammonium cations being particularly common. Such binding often takes the form of dipole-dipole or hydrogen bond interactions, often with charge (ion-dipole) assistance. Hydrophobic portions of the guest are sequestered within hydrophobic portion of the host. In water, organic guest binding is enhanced dramatically because of hydrophobic effects.

Calixarenes and resorcinarenes represent the main protagonists of the intracavity inclusion chemistry.

1.2.1 Syntheses of Resorcinarenes

Resorcinarenes can be prepared in high yields via simple, one-step procedures without using templates or high dilution techniques[18]. Most cases involve the acid-catalysed condensation reaction between resorcinol and an aliphatic or aromatic aldehyde. Recently, two novel procedures were described, involving the Lewis acid-catalysed tetramerisation of 2,4-dimethoxycinnamates* and the treatment of 2,4-dimethoxybenzyl alcohol with trifluoroacetic acid*. The main synthetic procedures are reported below.

- **Resorcinol-aldehyde condensation**

The rational investigation of the acid-catalysed condensation reaction between resorcinol and an aldehyde was carried out by Cram and co-workers[19]. They addressed the question of which group substituted on the resorcinol and aldehyde moieties tolerate the fourfold oligomeric cyclization reactions leading to the C_{4v} isomers of the structure reported in Fig.1.9.

The standard procedure they employed entailed the condensation of equimolar amounts of an aliphatic aldehyde and resorcinol, at 25°C in solutions of 2:2:1 respective volumes of EtOH, H_2O and concentrated aqueous HCl with reaction times of 1 day or longer (Scheme 1.1).

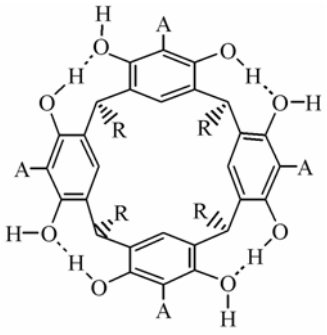

Fig. 1.9 – *Structure of Resorcinarene.*

Generally, the product crystallized from solution and was recrystallized and characterized. With aliphatic aldehydes only the C_{4v} isomers were isolated, although small amounts of other isomers were undoubtedly present in the filtrates. Table 1.1 reports the structures and yields (not optimised) of resorcinarene produced from the aliphatic aldehydes. As expected, as the R groups became longer, the octols became more soluble in hexane, benzene, and chloroform.

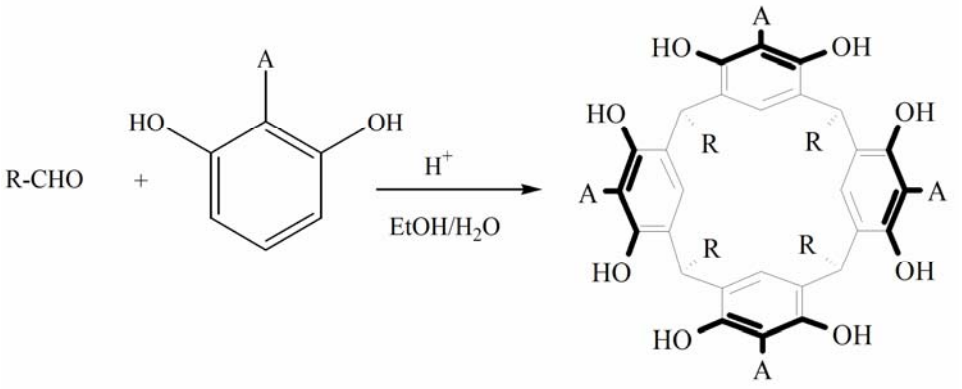

Scheme 1.1 *– Acid catalysed condensation of resorcinol and aldehyde affording resorcinarene.*

The yields of the C_{4v} isomeric products varied from 56 to 95% when the A group was H and the R groups were CH_3, CH_3CH_2, $CH_3(CH_2)_2$, $CH_3(CH_2)_3$, $CH_3(CH_2)_4$, $CH_3(CH_2)_{10}$, $(CH_3)_2CHCH_2$, $HO(CH_2)_4$, $Cl(CH_2)_5$, $C_6H_5CH_2$, $C_6H_5CH_2CH_2$, 4-$O_2NC_6H_4CH_2CH_2$, and 4-$BrC_6H_4CH_2CH_2$.

The reaction was also successful with A=CH_3, and R=CH_3 or $CH_3(CH_2)_4$. However, it failed to give readily isolable amounts of the desired C_{4v} isomeric product, when R=CH_3, and A=CO_2H, Br or NO_2. No cyclic oligomer was detected when resorcinol and $ClCH_2CHO$ or glucose were condensed under this experimental conditions. With R=CH_3, and A=CO_2H, an unresolved mixture of cyclic oligomers was produced.

Table 1.1. Yields and Melting Points of Resorcarene produced from Aliphatic Aldehydes and Resorcinol or 2-substituted Resorcinols

R	A	% yld	mp, °C
CH_3	H	60	>360
CH_3CH_2	H	88	>360
$CH_3(CH_2)_2$	H	92	>360
$CH_3(CH_2)_3$	H	89	344-345
$CH_3(CH_2)_4$	H	77	329-330
$CH_3(CH_2)_{10}$	H	68	285
$(CH_3)_2CHCH_2$	H	95	340-342
[a]$OH(CH_2)_4$	H	80	280-284
$Cl(CH_2)_5$	H	67	170-175dec
$C_6H_5CH_2$	H	70	>300
$C_6H_5CH_2CH_2$	H	69	>280
$4\text{-}O_2NC_6H_4CH_2CH_2$	H	64	285-290
$4\text{-}BrNC_6H_4CH_2CH_2$	H	56	>280
CH_3	CH_3	79	>360
$CH_3(CH_2)_4$	CH_3	80	260 dec
CH_3	CO_2H	UM[b]	-
CH_3	Br	Olig[c]	-
CH_3	NO_2	OP[d]	-

[a]Failed to obtain satisfactory elemental analysis. [b]Unseparated mixture of cyclic oligomers. [c]Unseparated mixture of oligomers. [d]Other product.

The condensation of equimolar amounts of benzaldehyde or 4-substituted benzaldehydes with resorcinol or 2-substituted resorcinols has also been studied in 95% ethanol-concentrated hydrochloric acid at 80°C. Table 1.2 reports the results.

When A = H and Ar = C_6H_5, 4-$CH_3C_6H_4$, or 4-$C_2H_5C_6H_4$, of the products characterized, the C_{4v} configuration was detected in the solid that separated from the reaction mixture. When A = H and Ar = C_6H_5, the C_{2v} isomer was isolated (10%) and fully characterized.

Table 1.2. Yields and Configurations of the dominant products of Resorcarene produced from Aromatic Aldehydes and Resorcinol or 2-substituted Resorcinols

R	A	% yld of isom mixt	Composite C_{4v}/C_{2v}	mp, °C
C_6H_5	H	83	>97/3	285-300 dec
4-$CH_3C_6H_4$	H	96	>97/3	>305
4-$CH_3CH_2C_6H_4$	H	73	>97/3	>360
4-BrC_6H_4	H	43	>97/3	>390
4-$CH_3OC_6H_4$	H	93	3/2[a]	-
4-$AcNHC_6H_4$	H	52	1/2	-
4-$C_6H_5C_6H_4$	H	99	3/2	-
4-$HO_2CC_6H_4$	H	79	2/5	-
4-NCC_6H_4	H	52	>3/97	-
4-$(CH_3)_3CC_6H_4$	H	28	>3/97	-
C_6H_5	CH_3	78	>3/97	-
4-$O_2NC_6H_4$	H	0	no ppt	-
4-$OCHC_6H_4$	H	0	no ppt	-
C_6H_5	Br	0	no ppt	-
$CH_3(CH_2)_3C\equiv C$	H	0	no ppt	-
4-$(CH_3)_3CC_6H_4$	NO_2	0	no ppt	-

[a]Reaction run at 25°C. When run at 80°C, only the C_{2v} isomer could be detected in the product.

When A = H and Ar = 4-$O_2NC_6H_4$ or when A = Br and Ar = C_6H_5, no crystalline solids precipitated from the reaction medium.

Hogberg[20] previously reported that in the reactions of resorcinol with benzaldehyde or 4-bromobenzaldehyde, the ratio of C_{4v} to C_{2v} isomeric products varies with reaction time, longer reaction times favouring the C_{4v} product. Cram's research group observed that increasing the scale of the 4-bromobenzaldehyde reaction from 1 g to 64 g of starting aldehyde increased the time necessary for complete conversion to the C_{4v} isomer from less than 1 day to greater than 28 days. Differences in mixing efficiency may be responsible. In contrast, the reaction of resorcinol with 4-methoxybenzaldehyde gave increasing amounts of the C_{2v} isomer as the reaction progressed. The values listed in the tables refer to reaction times of 48 h and are believed to closely approximate terminal (equilibrium) values.

The non-planarity of resorcinarenes implies that they can, in principle, exist in many different isomeric forms. The stereochemistry is generally defined as a combination of the following three stereochemical elements:

- The conformation of the macrocycle ring, which can adopt five extreme, symmetrical arrangements: the crown *(C_{4v}),* boat (C_{2v}), chair (C_{2h}), diamond (C_s) and saddle (D_{2h}) conformation;
- Their relative configuration of the substituents at the methylene bridges, giving the all-cis (ccc), cis-cis-trans (cct), cis-trans-cis (ctc) and trans-cis-trans (tct) arrangement, as shown in Fig. 1.10;

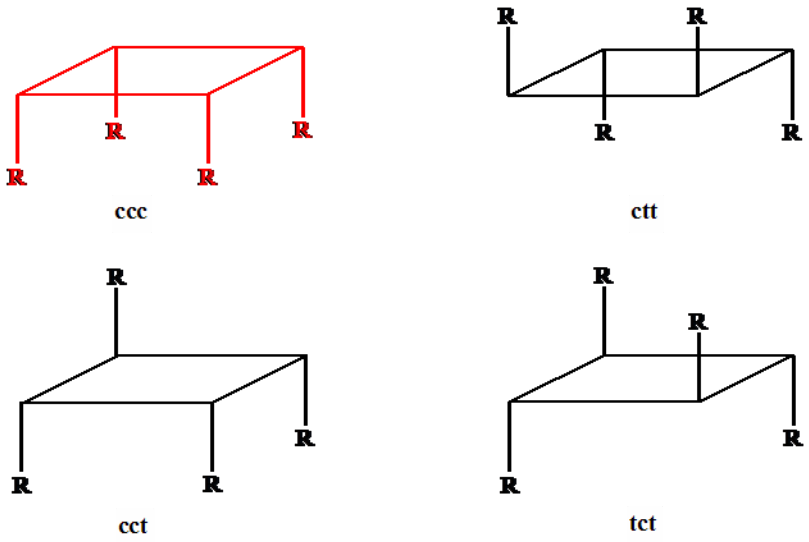

Fig. 1.10 *– Different configurations of the R groups at the –CH- bridges.*

- The individual configuration of the substituents at the methylene bridges which, in conformations of the macrocycle with *C* symmetry, may be either axial or equatorial.

As a matter of fact, resorcinarenes possess effectively the ccc configuration in solution.

Hogberg[21] gave a convincing argument for the virtual absence of the cct and tct isomers when benzaldehyde is condensed with resorcinol**.** He also demonstrated that under the conditions of cyclooligomerization, the ctt isomer was formed faster than the ccc isomer but that the ctt isomer converted to the more stable ccc isomer through reversible protoalkylation-protodealkylation reactions under the conditions of their formations.

Cram and his group observed that a large number of octols precipitated from the reactions, and they believe that in many cases the insolubility of the ccc isomers relative to their diastereomeric counterparts provided the driving force for the observed stereoselectivity.

In reactions involving alkyl and substituted alkyl groups attached to the aldehyde function and with resorcinol or 2-methylresorcinol as starting materials, the ccc isomer dominated. Substitution of electron- withdrawing groups such as $C0_2H$, Br, or NO_2 in the 2-position of the resorcinol starting material did not lead to a single dominant product but to either no detectable cyclic oligomers or to mixtures of many isomeric products. These three substituents deactivate the resorcinol moiety toward electrophilic substitution, both with respect to forming cyclic oligomers and equilibrating them once formed.

In conclusion they interpreted the stereoselectivity shown in most cases as being due to a combination of higher intrinsic stability associated with the ccc isomers, coupled with the reversibility of the condensation reactions and the relatively high insolubility of the ccc isomers in the reaction medium.

The intrinsic stability of the ccc isomers must be mainly associated with the tendency of the R groups of the aldehyde to be more stable in the axial than in the equatorial positions of the bowl conformations. As these R substituents become longer, they can intramolecularly associate with one another only when in axial conformations. The ccc isomers are unique in the sense that they alone provide the conformation that maximizes the proximity of like groups on the hydrophilicity-lipophilicity scale.

- **Other types of condensation reactions**

Another high-yield synthesis of resorcinarenes involves the Lewis acid-catalysed tetramerisation of 2,4-dimethoxycinnamates.

Treatment of (*E*)- 2,4-dimethoxycynnamic acid methyl ester with $BF_3 \cdot Et_2O$ in $CHCl_3$ at room temperature for 15 hours gave the corresponding octamethylated resorcarene in 75% yield, as a 3:2 mixture of ccc and cct isomers[22].

A similar treatment of isopropyl ester yielded, in addition to the same isomers, a third isomer in which the ring adopts a saddle (D_{2d}) conformation with the substituents in all-cis arrangement.

When 2,4-dimethoxybenzyl alcohol is treated with trifluoroacetic acid (5% in $CHCl_3$) resorcinarene is obtained in 95% yield[23]. The octamethylated resorcinarene cannot be synthesised by the acid-catalysed condensation of resorcinol and formaldehyde, since this reaction only gives polymeric products. Because of the absence of alkyl chains at the methylene bridges, resorcinarene is conformationally flexible and different isomers can therefore not be isolated.

These synthetic strategies are reassumed in Scheme 1.2.

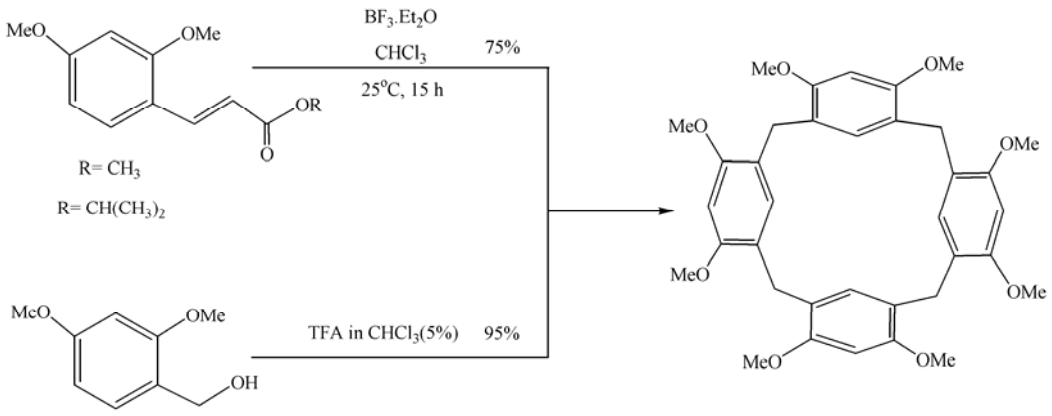

Scheme 1.2 *– Other types of condensation reactions for Resorcinarenes.*

1.2.2 Syntheses of Cavitands from Resorcinarenes

Resorcinarenes do not generally possess significant solution affinity for organic molecules, but their binding ability may be enhanced markedly by elaboration of the cavity. Synthesis of deeper cavities has the dual effect to increase the degree of guest shielding from solvent and often results in rigidification of the host, increasing its degree of preorganisation and preventing the cavity from collapsing on itself[17].

Many research groups contributed in the last 20 years to the preparation of a range of multiply bridged resorcinarenes, which exhibit significantly reduced conformation mobility in solution. They are particularly attractive because the rims of this compounds can be varied by different R^1 substituents and bridging groups A for shaping the bowl cavity and for manipulating the solubilities of the cavitands, or for introducing potentially cooperating functional groups to act as catalysts (Fig. 1.11)

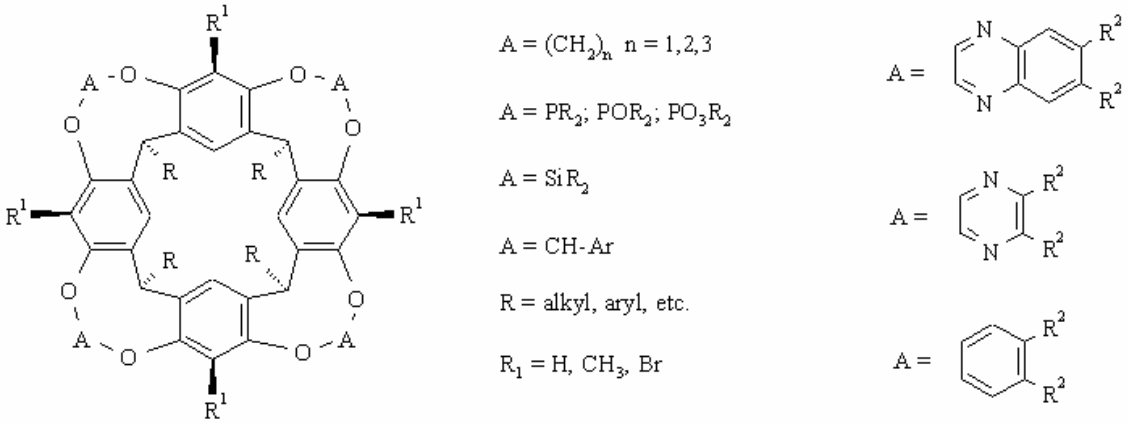

Fig. 1.11 *– Different types of cavitands preparated from resorcinarenes.*

The multiply methylene-bridged resorcinarenes (Fig. 1.12) were obtained by four-fold ring closures to build methylene or polymethylene bridges anchored by the four sets of the proximate oxygens. The reagents involved were $BrCH_2Cl$,

$TsOCH_2CH_2OTs$ or $TsO(CH_2)_3OTs$ with Cs_2CO_3-DMSO, and the yields ranged from 23 to 90%[24].

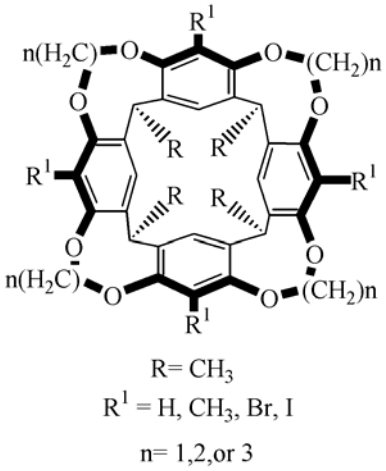

Fig. 1.12 *– Multiply methylene-bridged resorcinarenes.*

Higher yields were always observed when R= CH_3 or Br than R= H, probably because with the two substituents present steric inhibition of intermolecular reactions leading to non-cyclic oligomers was greater than that of their intramolecular reactions leading to ring closure.

Practical amounts of mono-, bis- and tris-bridged compounds were also prepared by appropriate manipulation of the reaction conditions*.

A deeper type of cavitand was preparated by Cram and co-workers functionalizing the upper rim of resorcinarene with pyrazine and quinoxaline groups (Fig.1.13).

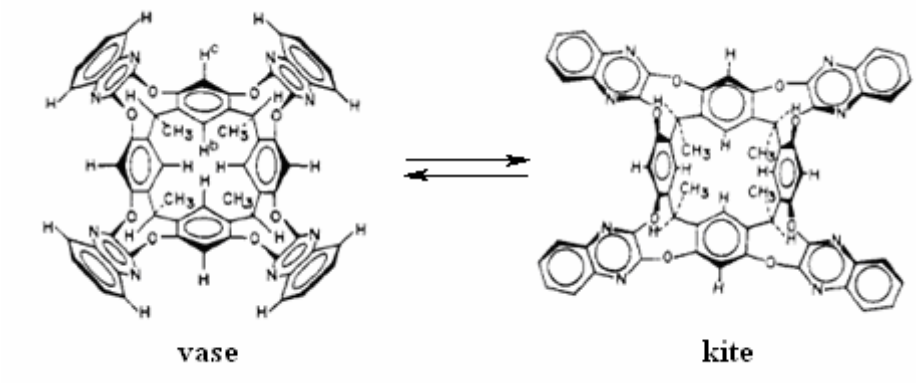

Fig. 1.13 *– Equilibrium between the two conformers of quinoxaline-bridged cavitands.*

The reaction carried out in KOH-$(CH_3)_2NCHO$ (yield ~30%) has shown successful, but the use of Cs_2CO_3-DMSO as the reaction medium raised the yield to more than 80%, depending on the R group. In this latter case cavitands exists in principle as an equilibrium of two conformations, namely *vase* and *kite* (Fig.1.13), in which the pyrazines or quinoxalines are all in the axial and the equatorial orientation respectively[25]. It is possible to shift the equilibrium toward a specific conformer by varying temperature. In particular at sufficiently low temperatures, the *kite* is the more stable conformer in solution because its more favourable enthalpy of solvation overrides the sum of the unfavorable TS of solvation and the greater strain energy of this conformer. As the temperature increases, the unfavourable TS cancels more of the favorable enthalpy until the free energy of solvation no longer overrides the greater strain energy of the *kite***.** Above this temperature, the *vase* conformer dominated in the equilibrating mixture, since its stability in solution does not depend as much as that of *kite* on its free energy of solvation.

The presence of a rigid molecular cavity means that the reported compounds invariably crystallize with an intracavity guest, and a large number of X-ray structures have been obtained by Cram's group with guests such as SO_2, CS_2, MeCN and CH_2Cl_2 or aromatic solvents. In Fig. 1.14 the X-ray structure of a quinoxaline-bridged cavitand is reported.

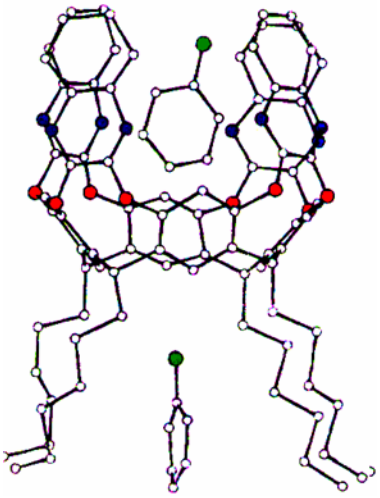

Fig. 1.14 *– X-ray structure of a quinoxaline-bridged cavitand.*

It's interesting to note that toluene possesses two different orientations into the structure: the aromating ring occupies the large cavity of the cavitand, giving the rise to π-π interactions, while methyl group is exposed in the lower rim of the cavitand, interacting with the long alkyl chains by means of dispersion forces.

1.3 Porphyrins

Porphyrins (Fig.1.15) and related tetrapyrrolic pigments occur widely in nature, to provide natural systems with brilliant colors and play very important roles in various biological processes. In particular heme, the iron(II) protoporphyrin-IX complex, is the prosthetic group in hemoglobins and myoglobins responsible for oxygen transport in red blood cells, and oxygen storage in living tissues.

All porphyrins are derived from the cyclic porphyrin formula, $C_{20}H_{14}N_4$, consisting of four pyrrole units connected by four methane (*meso*) carbons. Their peculiar chemical and physical properties made them very attractive candidates for a large number of applications.

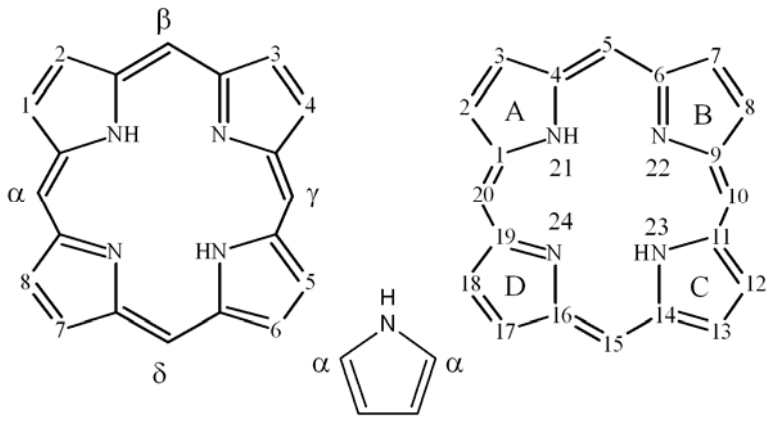

Fig. 1.15 *– Structure and numeration of Porphyrin (IUPAC and Fischer).*

1.3.1 General properties of Porphyrins

The porphyrin macrocycle is an aromatic system containing 22π electrons of which 18 are involved in any one delocalization pathway. Porphyrins obey Hückel's rule of aromaticity (4n+2π electrons, where n=4). The aromatic character of porphyrins is also evident in their NMR spectra. ^{1}HNMR spectroscopy of porphyrins shows that the N-H protons appear at δ = ~ -5 ppm (upfield from TMS), indicative of NHs located in an anisotropic aromatic shielding cone. Whereas the methine protons appear at ~ 10 ppm, a δ-value indicating a highly deshielding environment resulting from the aromatic ring current. All visible absorption spectra of porphyrins display the following characteristic spectra (Fig.1.16):

***B* band**: An exceedingly intense band (referred to as the "Soret" band) appears between 380 and 420 nm. It is the origin *B* (0,0) of the second excited singlet state and has molar extinction generally from 2 to 4 x 10^{5} M^{-1} cm^{-1}. This is characteristic of a highly conjugated porphyrin macrocycle. Better resolved spectra sometimes show another band ~ 1250 cm^{-1} to the blue; it is attributed to addition of one mode of vibrational excitation and is denoted *B*(1,0).

***Q* bands**: There are several weaker absorptions at longer wavelengths between 500 and 700 nm: four visible bands are seen (sometimes called "satellite" bands). The lower-energy band (sometimes called α) is the electronic origin $Q_{x,y}(0,0)$ of the lowest–energy excited singlet state. The higher-energy band (sometimes called β) includes one mode of vibrational excitation and is denoted $Q_{x,y}(1,0)$; it is actually a merging of several different vibrations. It was originally identified as a vibration on the basis of the relative constant energy gap between $Q_{x,y}$ (1,0) and $Q_{x,y}$ (0,0). The $Q_{x,y}$ (1,0) band has molar extinction coefficient in a narrow range between 1.2 and 2 x 10^{4} M^{-1} cm^{-1}, in fact they are not allow by selection rules.

All these bands are interpreted as (π,π*) in origin.

The basic porphyrin ring, as shown in Fig.1.15, provides the electronic "heart" of a porphyrin. The ring is structured with a basic fourfold symmetry, including four nitrogen atoms directed toward the center. This electronic "heart" is responsible for porphyrin-type optical spectra, which are then perturbed to a greater or lesser extent by various chemical modifications to the basic structure. Variations of the peripheral substituents on the porphyrin ring often cause minor changes in the intensity and wavelength of these absorptions. Protonation of two inner imine nitrogen atoms or insertion a metal into the porphyrin cavity also changes the visible absorption spectra. These absorptions can often be very helpful in elucidating certain structural features on a porphyrin. X-ray structural determinations of both metalloporphyrins and free-base porphyrins have basically shown the core porphyrin to be planar, a fundamental requirement for perfect aromaticity.

The porphyrin ring is very stable on both concentrated acid and base, and the macrocycle can act both as an acid and a base. Strong bases such as alkoxides remove the two central protons (pK_a ~16) on the inner nitrogen atoms of a porphyrin to form a dianion. However, trifluoroacetic acid easily protonates the two free pyrrolenine nitrogen atoms (pK_b ~9) to form a dication.

Porphyrins also undergo a number of chemical reactions typical of aromatic compounds. For example, electrophillic substitution reaction such as nitration, halogenation, acetylation, and formylation are often performed on porphyrins. Only the *meso* carbons and the β-pyrrolic carbons participate in these reactions. The α-pyrrolic carbons rarely take part in any kind of reaction.

Porphyrins are also capable of being metallated and demetallated. Almost every metal in the periodic chart has been inserted into the porphyrin macrocycle but most typically are: Fe, Zn, Cu, and Ni, which can be inserted into the porphyrin cavity by using simple metal salts. Demetallation can usually be achieved by treatment with acids of various strengths.

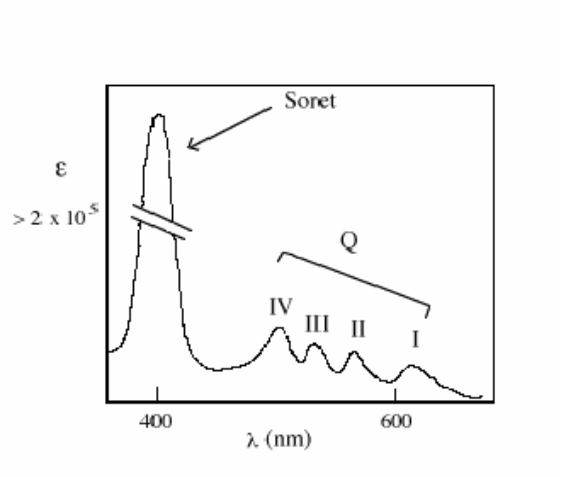

Fig. 1.16 *- Typical UV-Visible absorption spectrum of a Porphyrin.*

1.3.2 Main synthetic procedures for Tetraarylporphyrins[27]

The synthetic chemistry of porphyrins is extremely rich, as its history began in the mid-1930s. An enormous number of synthetic procedures has been reported until now, and the reason can be easily understood analysing the porphyrin skeleton.

In principle, there are many chemical strategies to construct it, involving different building blocks, like pyrroles, aldehydes, dipyrromethane, dipyrromethene, tripyrranes and linear tetrapyrroles (Fig. 1.17)

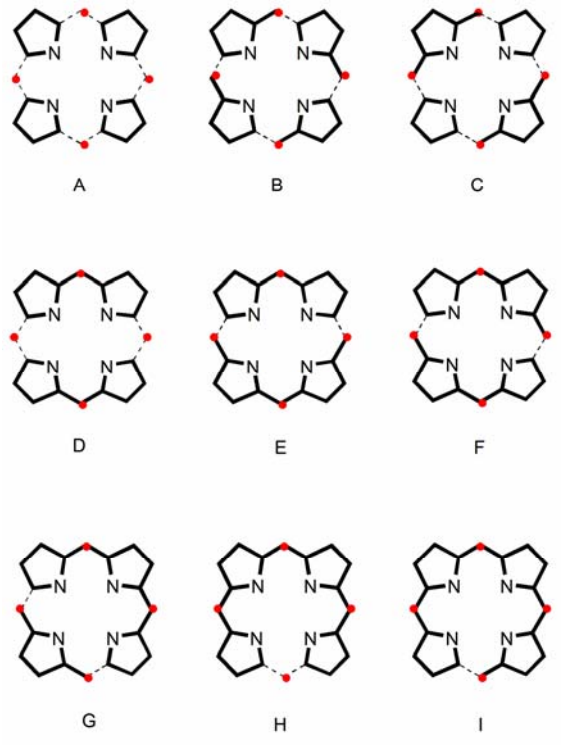

Fig. 1.17 *– Different synthetic paths for the construction of the porphyrin skeleton.*

While pattern B is widely employed for the synthesis of the *β*-substituted porphyrins, A is the common approach for the synthesis of *meso*-substituted porphyrins and consists in condensation of pyrrole and aldehyde. In the course of the years, many studies have been carried out to make the synthesis of *meso*-substituted porphyrins easily accessible. These macrocycles in fact have found wide applications as biomimetic models and useful components in material chemistry and their availability became a pressing demand.

The main synthetic approaches to tetra-arylporphyrins developed in the last century can be summarized as follows.

- **Rothemund method**

The chemistry of *meso*-substituted porphyrins had its genesis with the work of Rothemund in 1935. He first investigated the synthesis of *meso*-tetramethylporphyrin by reaction of acetaldehyde and pyrrole in methanol at various temperatures, obtaining a crystalline porphyrin.

Similar studies were performed with other aldehydes, both alkylic and aromatic. In most cases, a careful examination of each reaction product showed the present of a second porphyrinic compound at the 10-20% level compared with porphyrin. This contaminant was later isolated and shown to be a chlorine, that can be converted by oxidation to the corresponding porphyrin.

In 1941 Rothemund described in detail the preparative synthesis of *meso*-tetraphenylporphyrin (H_2TPP).

Heating 10 mL of pyrrole (3.6 M) and 20 mL of benzaldehyde (4.9 mL) in 20 mL of pyridine in a sealed vessel at 220°C for 48 hr, followed by slow cooling over 10-18 hr, gave the title porphyrin in 7.5-9% yields (Scheme 1.3).

In summary the distinguishing features of the Rothemund method are reaction at high concentration and high temperature in a sealed vessel in the absence of an added oxidant.

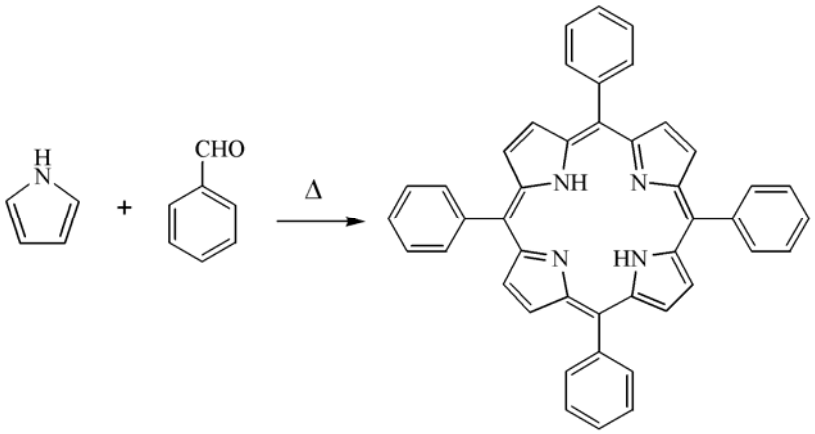

Scheme 1.3 *– Rothemund method.*

This method achieves reaction at high concentration but the low yields limit the scope of application. Several high-temperature synthesis have been developed that go further and avoid the solvent altogether. These include the use of a metal salt, as zinc acetate, of an acidic support like silica gel, but the yields were almost the same, with the exception for the tetramesitylporphyrin, obtained by the reaction of pyrrole, mesitaldehyde, pyridine and zinc acetate at 180°C for 48 hr followed by oxidation on air and treatment with concentrated HCl (yield 48%).

- **Adler-Longo method**

In the mid-1960s, Adler, Longo and co-workers re-examined the synthesis of *meso*-substituted porphyrins. They performed condensations of benzaldehyde and pyrrole (0.02 M each) in a variety of acidic solvents at reflux in glassware open to the atmosphere. The main solvents employed were acetic acid, acetic acid in the presence of a metal salt or benzene containing chloroacetic acid or trifluoroacetic acid. Yields of 30-40% were obtained with acetic acid or acidified benzene, but lower yields were observed in the presence of metal salts.

Further study of these reaction conditions led to the use of propionic acid (bp 141°C) in place of acetic acid (bp 118°C), higher concentrations of aldehyde an pyrrole (0.27M each), refluxing for 30 min in an open beaker, and isolation of porphyrin crystals upon cooling, filtration, and washing. This approach is known as the Adler-Longo method (Scheme 1.4)

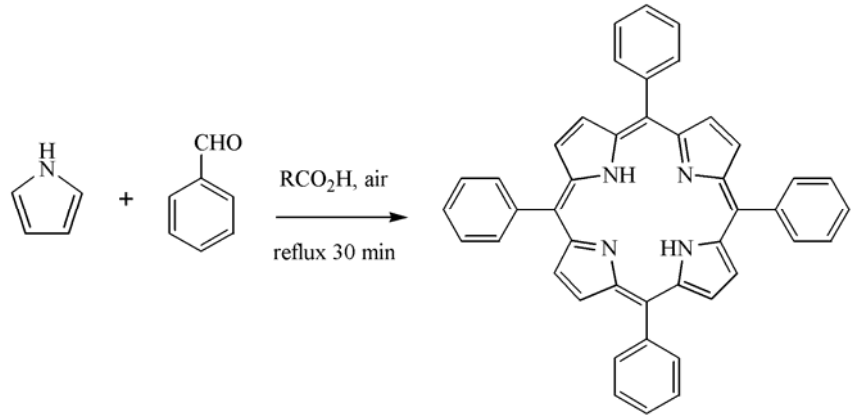

Scheme 1.4 *– Adler-Longo method.*

The reaction was faster in propionic acid than in acetic acid but the yield was 20% rather than 40% respectively. However, H_2TPP crystallized more readily from propionic acid than from acetic acid , affording a cleaner product.

The advent of this method made readily available a variety of *meso*-substituted porphyrins, particularly tetra-arylporphyrins with different aryl substituents. Of the three different reaction media, propionic acid is the most popular, because it can solubilize different aldehydes, producing crystalline porphyrins directly from the crude reaction mixture.

The Adler method affords ~20% yields with many *p*-substituted aryl aldehydes, but the yields obtained with most *o*-substituted benzaldehydes are usually lower.

A mixed-aldehyde condensation is also possible following this method. Although this procedure is inelegant, it's an expedient replacing elaborate synthesis with elaborate separation. The variation of the molar ratio of the different aldehydes employed, considering their diverse reactivity, results in

different distributions of the porphyrin components. Purification of isomers results very laborious and results efficient only when these compounds are remarkably different in polarity or steric dimensions.

- **Lindsey method**

The development of this method was motivated by the need of discover more gentle conditions for the condensation of aldehydes and pyrrole, in order to enlarge the number of the aldehydes utilizable and then the porphyrin available.

This method was mainly inspired by the following observations:

- Pyrrole an benzaldehyde are reactive molecules and they should not require high temperatures for condensation;
- The biosynthesis of porphyrins proceeds via a porphyrinogen intermediate that is oxidized at the last step of the process;

These considerations and others not reported her, prompted the development of a "biomimetic" strategy for the synthesis of *meso*-substituted porphyrins, using a sequential process of condensation and oxidation steps, as shown in Scheme 1.5.

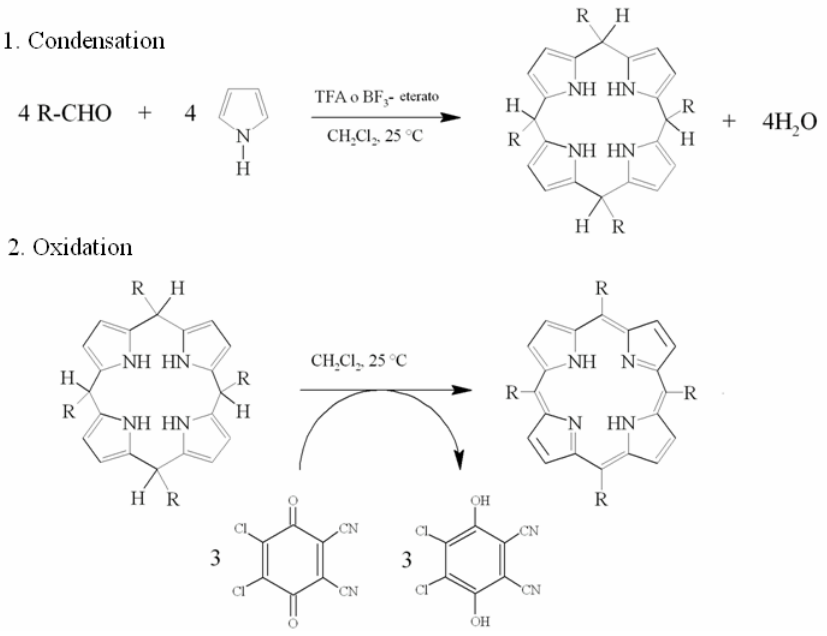

Scheme 1.5 *– Lindsey method.*

The first step consists in the acid-catalysed condensation between pyrrole and aldehyde under inert atmosphere, leading to the porphyrinogen; the subsequent oxidation by using a stoichiometric quantity of an oxidant affords the desired porphyrin.

This reaction was found to be quite sensitive to concentrations, both of the reagents and the catalyst. The better conditions were found to be equimolar quantities of pyrrole and benzaldehyde (10 mM) in dichloromethane, trifluoroacetic acid or BF_3- etherate as catalysts, DDQ or p-Chloranil as oxidant. (Yields 35-40%). Room temperature is also required.

1.4 Cavitand-Porphyrin conjugates

The moderate dimensions of the synthetic cavities represent the most serious limitations to the practical uses of this molecules. The more guest-accessible, self-assembling capsules as "softballs", generally encapsulated a single guest molecule, while catalysis most often requires two molecules placed in close proximity. A second, related limitation is functionality: how to provide space for a guest or two *and* a functional group positioned to influence their behaviour? Here the central theme is the functionalization of concave surfaces. While there has been progress on the problem of size, especially carried out by Cram and Reinhoudt in the mid 1990s, there is much less progress on interior functionality.

Molecular clefts, concave reagents, and endohedral functions all testify the existence of the problem but fail to provide independent binding and functional group sites.

Rebeck and co-wokers recently afforded a successful solution to this problem, reporting on some new cavitand-porphyrin hybrids, possessing intriguing binding features[28].

They positioned metalloporphyrin on the host structures to assess the independent contributions of the cavitand and porphyrin to the recognition of guests. The newest cavitand-porphyrin conjugates they reported possess one or even two deepened self-folding cavities and a metalloporphyrin wall (Fig. 1.18).

In general, the electron-rich cavities possess typical affinities toward adamantanes while the Zn-porphyrin wall strongly complexes pyridines.

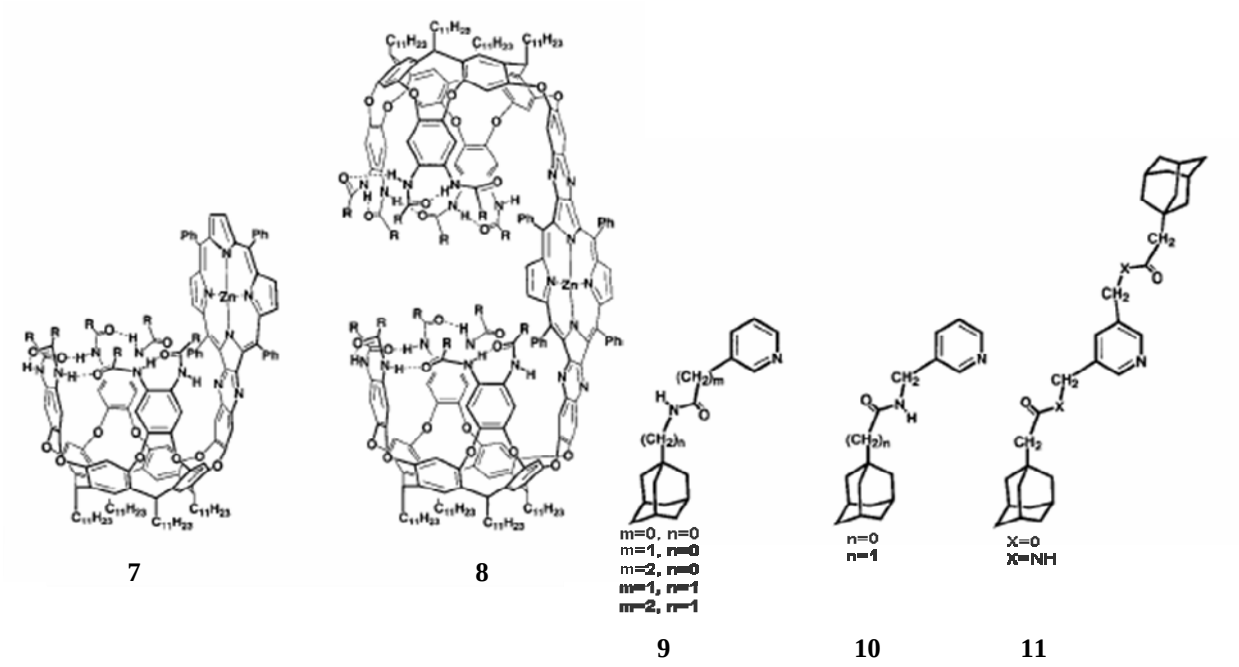

Fig. 1.18 *– Structures of cavitand-porphyrin hosts and ditopic guests employed in the studies reported by Rebeck and co-workers.*

Therefore a series of amide/ester-linked guests of various lenghts, containing either adamantly, pyridyl, or both fragments (Fig.1.18) were used to determine the hosts binding abilities in solution by using UV-vis and ^{1}H NMR specroscopies.

Strong binding ($-\Delta G$~7.5-9.5 kcal mol^{-1} in toluene) was detected for adamanthyl-pyridines guests of opportune length (guest **9** with m= 2, n=0 and m=1, n=1) by host **7**, reflecting simultaneous participation of the cavity and the

Zn-porphyrin in the complexation event. With the shorter or longer guests, such as **10** with n=0 and **9** with m=2, n=1 respectively, lower binding energies were measured (-ΔG between 5.6 and 7.0 kcal mol^{-1}).

The bis-cavitand host **8** features cavities that are well preorganized for cooperative binding, and it readily forms kinetically stable complexes with the longer guests tested containing two adamantyl ends with a pyridyl in the center.

Binding studies between this host and monoadamantyl and bis-adamantyl **11** guests in toluene showed very strong association (-ΔG between 7.5 and 9.2 kcal mol^{-1}). Obviously, the cavities and the Zn-porphyrin wall were involved in the complexation. The fact that diester is less strongly complexed than diamide reflects the involvement of the guest's C(O)-NH proton in the hydrogen bonding with the cavity's amide walls.

The internal space of the reported hosts is nanoscale, and in particular the dimensions of the bis-cavitand molecular container (~10×25 Å) place it among the largest synthetic hosts prepared to date. The constant flow of substrates into and products out of the cavity may be envisioned in their use in catalysis; furthermore, the porphyrin functions contribute to high binding affinities of appropriate guests and raise the possibility of metal-catalyzed reactions as alkane hydroxylations or alkene epoxidations in these containers.

Although large cavities are in general required for practical applications, very recently Nakazawa and co-workers reported the synthesis of a new flexible cavitand-porphyrin conjugate (CH_2P) endowed with the smallest cavity among known cavitand-based compounds[29]. This host is formed by cavitand and porphyrin connected by two ether linkages that ensure a certain flexibility to the structure (Fig. 1.19).

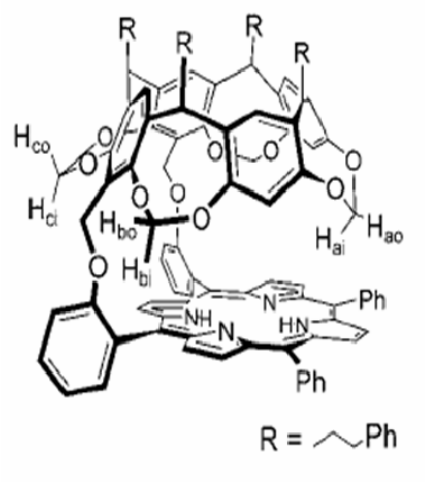

Fig. 1.19 *– Structure of cavitand-porphyrin coniugate CH_2P.*

The authors have successfully demonstrated size-selective and reversible encapsulation of small hydrocarbons within the conjugate cavity. To evaluate the affinity and selectivity of guest binding they determined the 1:1 binding constant K_{11} of the hydrocarbon encapsulation.

Acetylene exhibits the greatest affinity of encapsulation in the cavity, and the binding constants decrease in the following order:

acetylene>methane>ethylene>cyclopropane >ethane

Among the saturated hydrocarbons examined in this work, large differences in K_{11} values were observed (methane/ethane/propane=8.6:1.0:≈0). The selectivity of encapsulation appears to be related to the volume and shape of the guest molecules. However, the remarkable large binding constant of acetylene cannot be explained only in terms of molecular volume. Since the acetylene protons favor stronger CH-π interactions with electron-rich aromatic π systems that act as electron donors, the high affinity of acetylene may be due to this attractive effect induced by the aromatic walls of the host molecule.

The authors also described very recently a stable self-assembled cavitand-porphyrin ($C \bullet H_2P$) formed with four hydrogen bonds without template guest molecules and reported reversible binding of small organic molecules[30] (Fig.1.20).

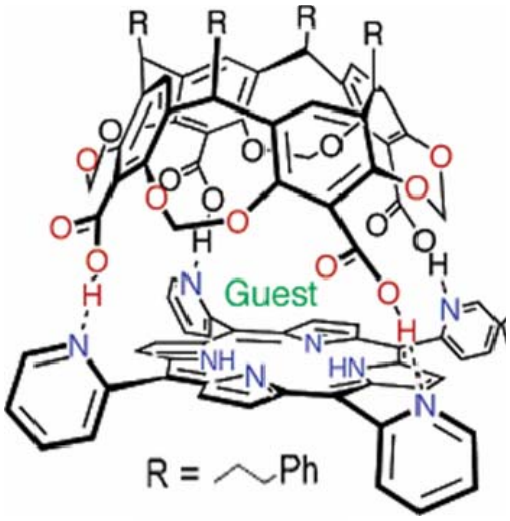

Fig. 1.20 *— Structure of cavitand-porphyrin coniugate C•H_2P.*

Tetracarboxylcavitand and *meso*-tetra(2-pyridyl)porphyrin are appropriate components for formation of a self-assembled capsule through quadruple hydrogen bonding as a result of considerations of convergence and relative separation of functional groups and symmetry. Self-assembly of the two molecules has been carried out in 1,1,2,2-tetrachloroethane-d_2 at room temperature and followed by ^{1}H NMR spectroscopy. Signals assignment and symmetry considerations suggested that the cavitand is located above the porphyrin plane and provides a capped structure with respect to the porphyrin. The associated C•H_2P capsule resulted thermodynamically stable despite being assembled solely by quadruple hydrogen bonds between the pyridyl and the carboxyl groups.

Methane, acetylene, ethylene, ethane, propane, and other small organic molecules were encapsulated by C•H_2P while molecules such as benzene that are larger than cyclopentane, were not encapsulated.

The host CH_2P exhibited higher guest size selectivity than C•H_2P for smaller guests as a result of its cavity size. On the other hand, C•H_2P could encapsulate guests of various sizes ranging widely from methane to cyclopentane as a result of both its larger cavity size and its flexibility provided by the four hydrogen bonds of the host capsule.

Signal analyses provided crucial informations about the "encapsulation mode". It suggested that encapsulation occurs by an "induced-fit" type of complexation. Upon entry of a small guest molecule, the capsule size contracts in size as a result of flexibility of the host hydrogen bonds, to optimize the van der Waals contacts between the host and guest. However, molecules requiring a larger capsule size than the original cavity cannot be encapsulated. Thus, C•H_2P is able of encapsulating various guests ranging in size of methane to cyclopentane as a result of its larger cavity and the flexibility imparted as a result of self-assembly.

After all, it's to be mentioned that capsule C•H_2P has fewer hydrogen bonds than any of the previously reported self-assembled systems.

Results and Discussion

1.5 Chiral supramolecular capsule by self-assembly of Resorcinarene-ZnPorphyrin conjugates

The construction of nano sized supramolecular hosts via self-assembly of molecular components is a fascinating field of researches[1]. Such intriguing class of architectures, beside the intrinsic intellectual stimuli, is of importance in many fields of chemistry and technology such as material chemistry[31], catalysis[2, 12, 4c], and sensor applications[32]. Within this scenario, the achievement of self-assembled structures possessing a chiral cavity[16] opens the way to chiral molecular recognition and asymmetric catalysis.

According to such interesting target, we entailed the synthesis of two zinc Resorcinarene-Porphyrin conjugates (**ZnP1**, and the corresponding methylene-bridged, **ZnP2**) with the aim of building up a supramolecular capsule able to offer a cavity for the recognition of properly shaped organic molecules. We surmised that the presence of both the Zn-porphyrin platform and the resorcinarene cavity, would result in a combined ligand to metal coordination and "cage effect" (cavitand bowl) motif, upon interaction with bidentate ligands such as, for example, diamines and alike.

1.5.1 Synthesis of Resorcinarene-ZnPorphyrin conjugates ZnP1 and ZnP2

Synthetic approach consists of linking the two subunits, metalloporphyrin and resorcinarene respectively, by an esther linkage in order to have a covalent, flexible ditopic receptor. Indeed the hydroxyl groups on the upper rim of resorcinarene can be easily exploited as nucleophiles for the reaction with a carboxylic function on a peripheral position of porphyrin macrocycle. Resorcinarene used in this synthesis (Res-$C_{10}H_{21}$) was prepared by following published procedures[19].

Porphyrin derivative was suitably synthetised in two steps.

The parent porphyrin methyl ester ***1a*** was prepared by acid catalysed Adler condensation of pyrrole, bezaldehyde, and methyl 4-formylbenzoate in the required molar proportion (Scheme 1.6).

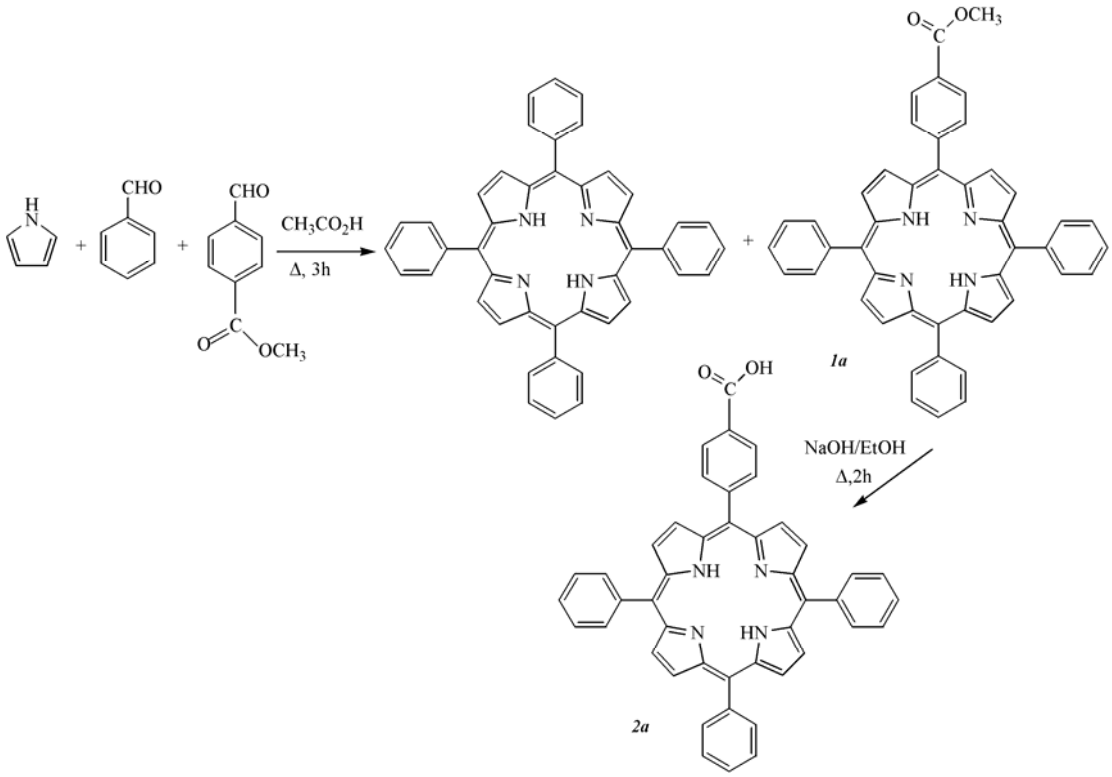

Scheme 1.6 *– Synthesis of porphyrin monoderivatives* ***1a*** *and* ***2a****..*

The choice to employ the corresponding ester instead of the acidic one was due to easier work-up of the crude of reaction and a higher overall yield than using 4-carboxybenzaldheyde as reagent (12% compared to 4% respectively).

The tetraphenylporphyrin was the prevalent product of reaction, but it was easily removed by column chromatography. The desired porphyrin derivative was then converted in good yield into the corresponding carboxylic acid derivative ***2a*** by alkaline hydrolysis in refluxing ethanol.

Synthesis of the conjugate ***3a*** was performed in three steps. The first reaction was performed between porphyrin ***2a*** and oxalyl chloride to give the corresponding acid chloride, which is considerably more reactive in nucleophilic reactions.

The subsequent coupling with the resorcinarene Res-$C_{10}H_{21}$ was straightforwardly accomplished in dry chloroform/THF mixture, in the presence of catalytic amount of pyridine. Standard workup gave the desired free-base receptor (**H_2P1**) along with some starting (hydrolised) material.

The reaction mixture has been found to be of difficult purification and separation by standard SiO_2 chromatography. We noted that an easier separation could be obtained on the corresponding Zn-derivatives. According to this observations, we performed zinc insertion directly on the crude product mixture, which could be then easily purified and separated by standard column chromatography, obtaining the desired receptor ***5a*** in a overall 3% yield.

The corresponding bridged-derivative ***4a*** **ZnP2** has been prepared by Williamson coupling of ***3a*** with bromochloromethane in dry DMF, in satisfactory 30% yield, after standard workup and column cromatograpy.

The synthetic paths for the preparation of **ZnP1** and **ZnP2** conjugates are depicted in Scheme 1.7.

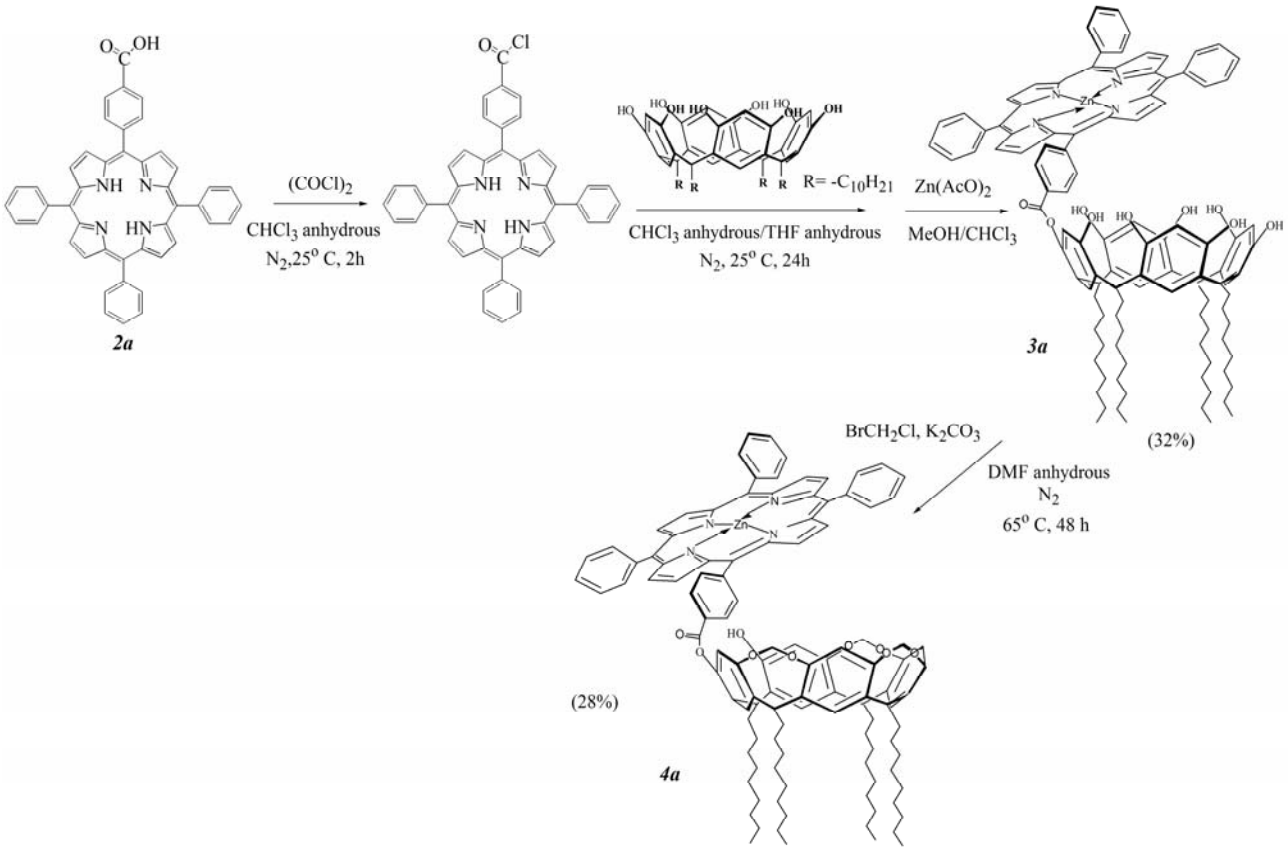

Scheme 1.7 *– Synthesis of conjugates ZnP1(**3a**) and ZnP2(**4a**)*

1.5.2 Complexation studies of amines on ZnP1 and ZnP2

The recognition properties of **ZnP1** and **ZnP2** conjugates towards a particular class of guests were investigated by UV-vis spectroscopy, evaluating the typical UV-visible spectral changes, in the porphyrin Soret region, upon Zn-coordination. According to HSAB theory we choose some amines as ligands, featuring different electronic and structural properties. In particular, we have surmised that the presence of two binding site on the receptor molecule, namely zinc metal and aromatic cavity of resorcinarene, may present a particular affinity for bidentate, aromatic ligands, such as bipyridyl and related structures.

In order to verify our hypothesis we performed complexation studies on receptors, using different amines, whose structures are reported in Fig. 1.22.

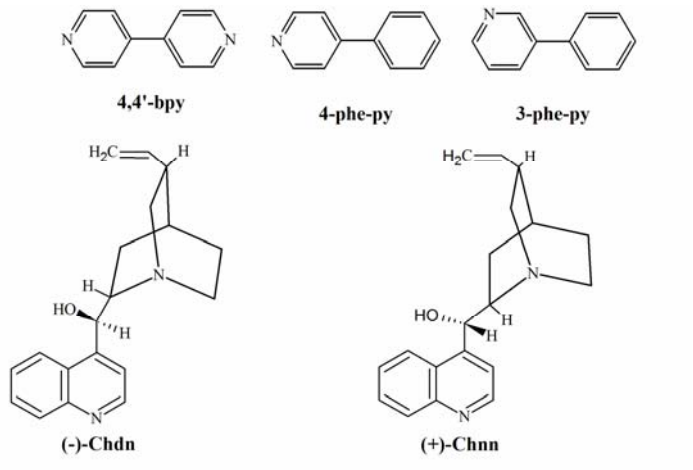

Fig. 1.22 *– Structures of guests used in these studies.*

Binding studies have been carried out in chloroform, at 298 K, by following the typical UV-visible spectral changes, in the porphyrin Soret region, due to the transition of zinc atom from tetra- to penta-coordination. The spectral variations showed an evident red-shift of the Soret band, with the contemporary diminishing of the band of free receptor and the increasing of the complex formed during titration. Moreover the presence of several clean isosbestic points (Fig. 1.23), indicated a 1:1 complexation process.

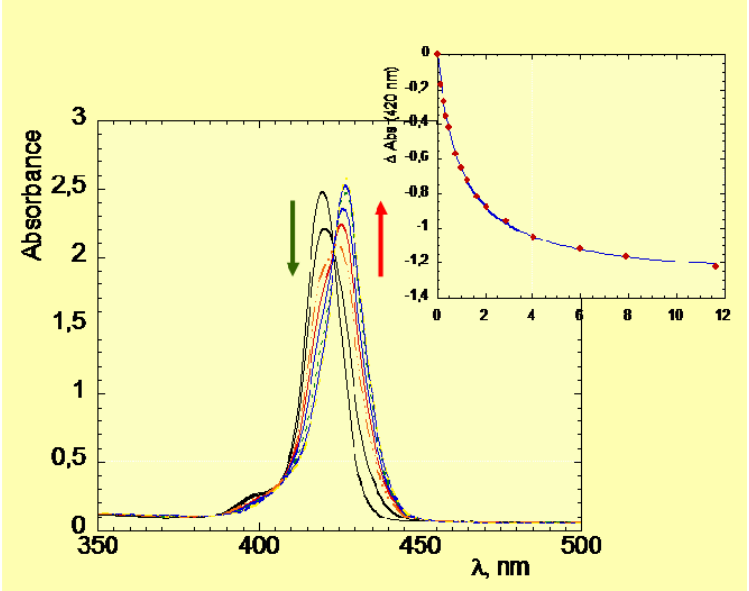

Fig. 1.23 *– UV-vis titration spectra (Soret region) of ZnP1 with 4,4'-bpy.*

The experimental data points has been nicely fitted by a typical Langmuir-type equation (Fig. 1.23, inset), to give the corresponding binding constant values (*K*) reported in Table 1.3. These findings, along with the increase up to two order of magnitude of the binding constant values with respect to the reference, monotopic ZnTPP, may be suggestive of either a 1:1 or a 2:2 complex formation. Some considerations would indicate the latter mode as the most probable one.

In the case of **4,4'-bpy**, for example, the formation of a 1:1 supramolecular complex, i.e. self-complexation, is hampered by a severe strain energy caused by the folding of py-py bond, owing to the open conformation of the host, which is reported in Fig. 1.24a.

A more energetically comfortable configuration is the one considering a nitrogen py-terminus bound to a ZnTPP platform, while the other end is bound within the aromatic cavity of the resorcinarene bowl of a second receptor by C-H.....π interactions (Fig. 1.24b).

Table 1.3. Binding constant values, *K*, M^{-1}, for the interactions of ligands to selected receptors[a].

	ZnTPP	ZnP1	ZnP2
4,4-Bpy	2.0×10^3 6.7×10^{3b}	1.0×10^5 4.4×10^{4b}	3.0×10^5
4-phe-py	4.5×10^3	4.8×10^3	4.6×10^3
3-phe-py	4.5×10^3	4.4×10^3	
(+)-Chnn	2.4×10^2	1.0×10^4	3.8×10^2
(-)-Chdn	2.0×10^2	2.0×10^4	6.8×10^2

[a] In $CHCl_3$, at 298K. Uncertainities are within ± 5%.
[b] In toluene, at 298K.

This would also explain the fact that neither **3-phe-py**, nor **4-phe-py**, ligands lacking a second pyridine moiety, do not form supramolecular structures upon complexations. This is also corroborated by MM calculations accomplished by MMFF94 Spartan 02 program, which indicate the 2+2 system as the more stable one.

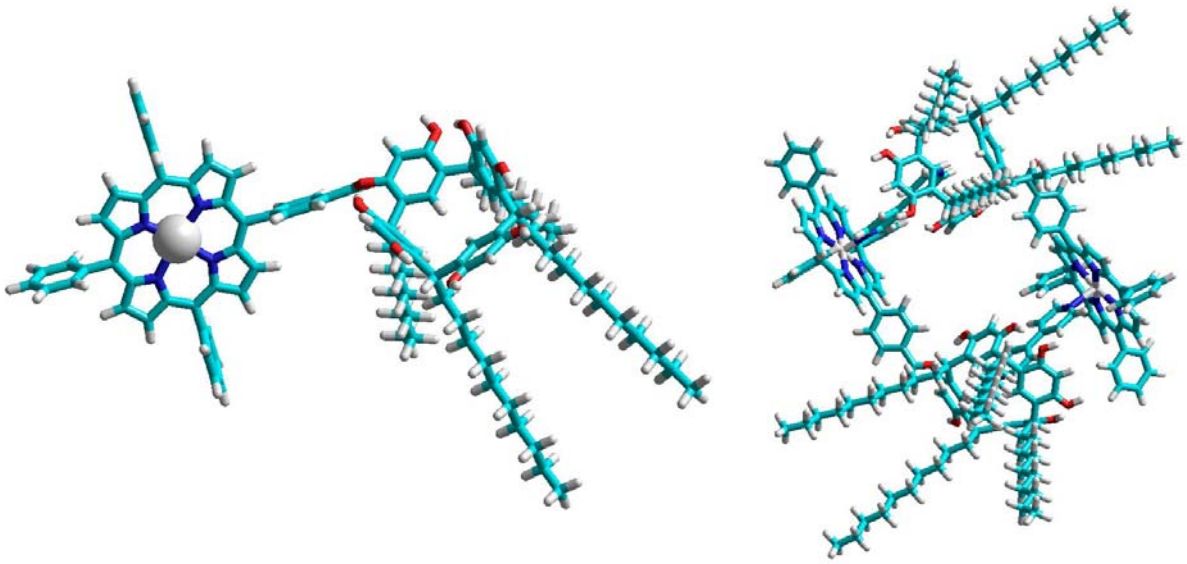

a b

Fig. 1.24 *– Energy-minimized structures of ZnP1 and [ZnP1-4,4'-bpy]$_2$ (MMFF94 Spartan 02).*

The extension of the studies to **ZnP2**, a receptor with a more rigid cavity, gave useful informations on the interaction involved in the formation of the porphyrin bowls. A small, but significative increase of binding strength (up to three-fold) can be evidenced, indicating a better interaction of the terminal pyridine moiety with the aromatic, π-basic bowl.

The importance of these interaction can be witnessed by the fact that in aromatic solvents such as toluene (see Table 1.3), the strength of the binding of **4,4'-bpy** to **ZnP1** is lowered by a factor of two, whereas its binding to the reference ZnTPP shows a three fold increase, as expected in the case of a less polar medium.

This also should rule out the involvement of hydrogen bond in the molecular recognition event, which, on the contrary, should be increased in a less polar, not competitive solvent.

1.5.3 ^{1}H PGSE NMR diffusion studies of supramolecular capsule [ZnP1-4,4'-bpy]$_2$.[33]

Pulsed gradient spin-echo (PGSE) technique was introduced about 40 years ago by Stejskal and Tanner and is a useful method for the characterization a variety of organic supramolecular systems in solutions, representing a possible supplement to mass spectroscopy.

The basic NMR experiment is based on a spin-echo sequence and two incorporated pulsed field gradients separated by a waiting time, Δ (Fig. 1.25).

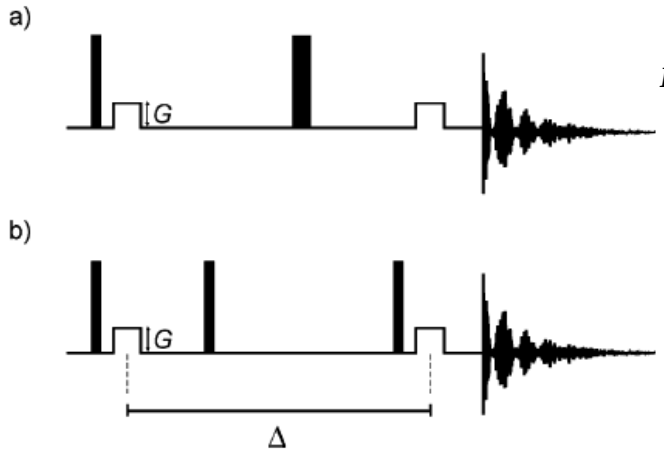

Fig. 1.25 *– Typical pulse sequences for the PGSE experiments: (a) the Stejskal-Tanner experiment; (b) the Stejskal-Tanner experiment modified via substitution of two 90° pulses for a single 180° pulse.*

The effect of the two gradients is to initially defocus and then refocus the magnetization; however, if during the time Δ the molecules diffuse from their positions after the first gradient pulse, the effective magnetic field experienced by the spins will be different during both gradient pulses. This results in incomplete refocusing of the spins and a consequent decrease in the intensity of the resulting NMR signals.

Repetition of the experiment with increasing gradient strengths, G, affords a set of signals from which the diffusion coefficient, D (often called a "self-diffusion constant", in literature), can be obtained (see Eqn 1).

$$\ln(I/I_0) = -\gamma_x^2\delta^2G^2(\Delta-\delta/3)D \qquad \textit{Eqn. 1}$$

where:

γ_x) gyromagnetic ratio of the X nucleus;

δ) length of the gradient pulse;

G) gradient strength;

Δ) delay between the midpoints of the gradients;

D) diffusion coefficient

A typical plot of the observed intensity changes, $\ln(I/I_0)$, as a function G^2 is shown in Fig. 1.26. Molecules (or ions) possessing larger volumes will diffuse more slowly than smaller molecules and thus afford smaller slopes.

More elaborate pulse sequences have been proposed and the stimulated spin-echo (see Figure 1.25b), in which three 90° pulses are used, has the advantage that the signals decay according to T_1 (spin-lattice relaxation time) rather than according to T_2 (spin-spin relaxation time).

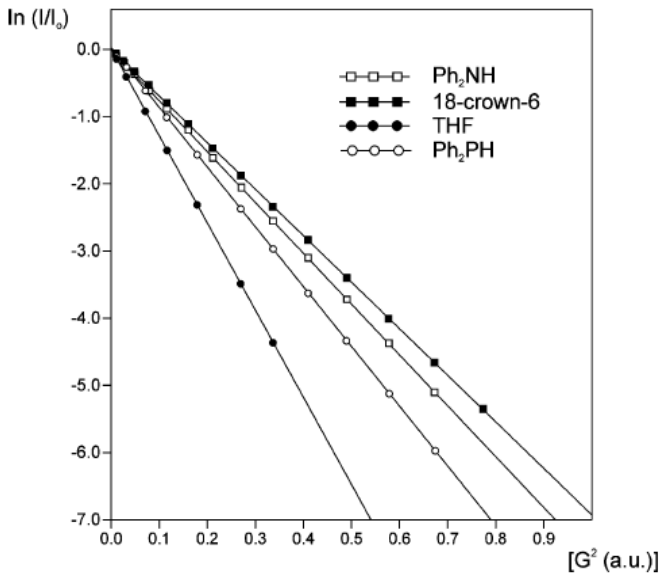

Fig. 1.26 *– Typical plot of the observed intensity changes ln(I/I$_0$), as a function of G^2 showing various translation rates depending on their molecular sizes for various species in solution.*

PGSE data may also be presented as one component of a 2D spectrum in which the chemical shift is displayed in the first dimension and the diffusion coefficient in the second one.

Such an experiment is called **DOSY** (Diffusion Ordered Spectroscopy) and has also been referred to as "NMR chromatography", for its ability to facilitate and visualize the resolution and assignment of complex mixtures.

DOSY methods have proven especially valuable where the molecules are relatively large and thus the NMR spectra are fairly complicated. Although the DOSY methodology is potentially quantitative, integrating cross-peaks is not always straightforward. The PGSE approach routinely gives diffusion constants that are accurate to ± 2%.

The resolution of this technique is sufficient to distinguish between molecules or assemblies with different molecular weight (M_r).

It is necessary to understand the relation between M_r and the diffusion coefficient of a particular assembly for a correct interpretation of the experimental results. Indeed it should be realized that the shape of a given molecular specie can significantly affect the relation between M_r and D which complicate a direct comparison of the data.

However a correlation of experimental D with calculated values of molecular weight is possible.

The ratio of diffusion coefficients for two different molecular species (D_i/D_j) is inversely proportional to the square-root or to the cubic-root of the ratio of their M_r (see Eqn.2) for rod-like and spherical molecules respectively.

$$\sqrt[3]{\frac{M_{rj}}{M_{ri}}} \leq \frac{D_i}{D_j} \leq \sqrt{\frac{M_{rj}}{M_{ri}}} \qquad \textit{Eqn 2}$$

Using this relation it is possible to calculate a set of theoretical diffusion coefficients (D_{calc}) (upper and lower limit), using the D_{exp} of any other assembly as a reference.

Moreover, from the diffusion coefficients, it is possible to obtain the so-called hydrodynamic radius, r_H, via the Stokes-Einstein equation (see eq 3), which, in turn, allows one to estimate the molecular volume.

$$r_H = \frac{kT}{6\pi\eta D} \qquad \textit{Eqn 3}$$

Although this equation has its drawbacks, it is widely used when comparing D-values involving data from differing solvents because it provides a correction for solvent viscosity, η.

The characterization of the 2+2 system supposed in our studies has been found to be difficult to accomplish with the traditional ^{1}H NMR spectroscopy.

More insight, the ordinary ^{1}H NMR spectra in $CDCl_3$ showed a broadened, upfield shifted resonances at ca 2 ppm for the bound 4,4'-bpy to ZnP1. Concomitantly, a broadening of the aromatic signals of ZnP1 receptor resulted upon complexation, indicating the formation of a more rigid structure. The presence of resonances of both free and bound species, in the presence of an excess of bypiridyl ligand, suggested the onset of a slow equilibrium within the NMR time scale. The free, unbound 4,4'-bpy protons resonated at 8.74 and 7.53 ppm, in $CDCl_3$.

In order to have more reliable information on the effective formation of this capsule we decided to carry out ^{1}H PGSE NMR diffusion studies with the aim to corroborate our hypothesis.

In Fig. 1.27 the DOSY spectra of the free ZnP1 and capsule formed with 4,4'-bpy are reported.

The calculated diffusion coefficients for the free ZnP1 and 4,4'-bpy, in d_2-TCE and 3% CD_3OD at 298 K, have been found to be 2.1 (±0.1) x 10^{-10} m^2s^{-1} and

3.7 x 10^{-10} m^2s^{-1}, respectively, whereas the relative capsule [ZnP1-4,4'-bpy]$_2$ featured D = 1.2 (±0.1) x 10^{-10} m^2s^{-1} in d_2-TCE

These values are indicative of a strong increase of molecular weight, in agreement to the capsule formation.

Based on the equation 2 we found that the ratio of the diffusion coefficients for the two species is 1.7 (±0.1), which is in fair agreement to that expected for an ellipsoidal (prolate) structure.

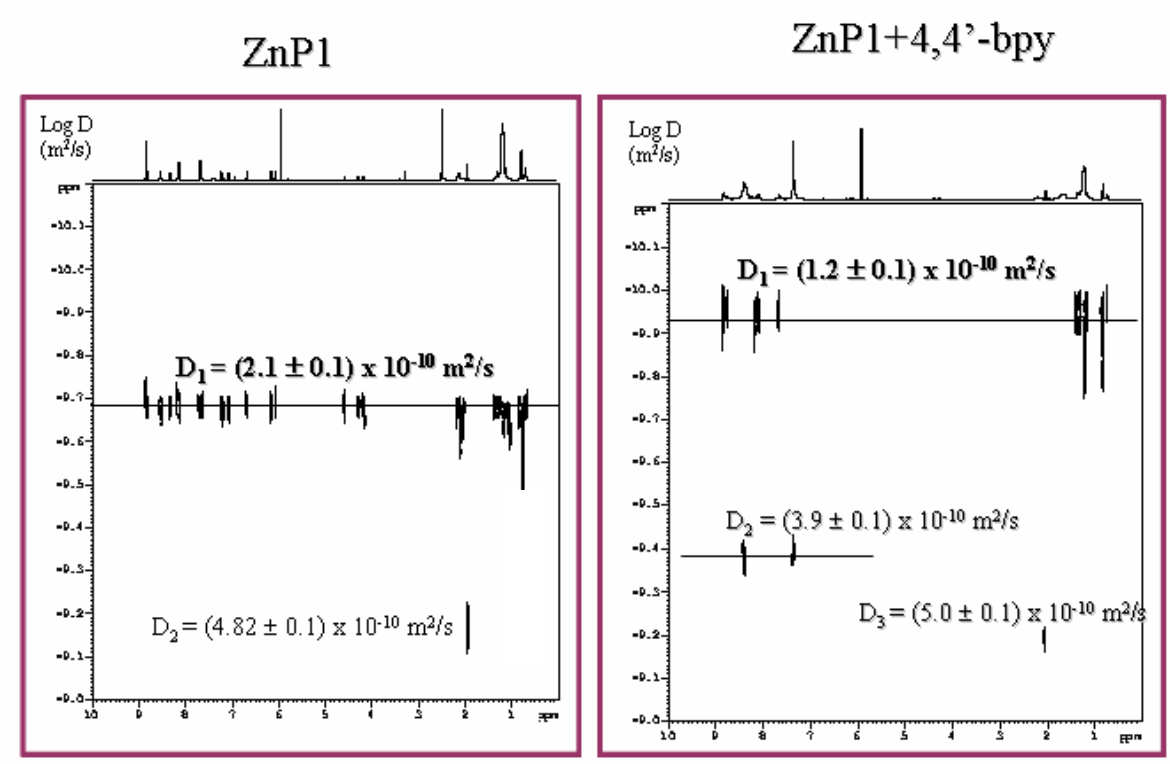

Fig. 1.27 *–The DOSY spectra of a solution of ZnP1 in d_2-TCE and 3% CD_3OD and capsule [ZnP1-4,4'-bpy]$_2$ in d_2-TCE. As expected, all the signals of ZnP1 have a lower diffusion coefficient in the capsule.*

1.5.4 Generation of a chiral capsule promoted by a chiral ligand coordination.

Prompted by the interesting results achieved in the case of coordination of 4,4'-bypiridyl to **ZnP1** conjugate we decided to extend the same approach to chiral bidentate guests, surmising that it should infer to such formed cavities elements of chirality. This aspect would of importance for a stereoselective host-guest molecular recognition and sensing.

We choose two ligands of the class of cinchona alkaloids, namely (+)-Cinchonine and (-)-Cinchonidine (**(+)-Chnn** and **(-)-Chdn**, respectively), possessing a quinolinic group, prone to bind to Zn atom, and a quinuclidine end that would constitute an effective hook for the aromatic cavity of the receptor, so resulting in a cooperative binding.

Related "adamantane-like" structures are well known to feature a high affinity for aromatic cavities, as shown by Rebeck and co-workers in recent reports[28], in which the high affinity of cavitand-porphyrin conjugates toward adamantyl-pyridine guests has been clearly demonstrated. Moreover it has been recently reported that cinchona alkaloids coordinate to transition metal exclusively through the quinoline aza-group[34].

Also in the case of chiral guests, the binding with receptor **ZnP1** occurred with an increase of about two orders of magnitude, with respect to ZnTPP, again indicating the likely formation of a supramolecular 2+2 capsule (see Table 1.3). Noteworthy, the binding of these chiral ligands results in the formation of a chiral cavity. This was clearly witnessed by CD spectroscopy that showed the presence of an evident bisignate spectral pattern, due to an excitonic coupling between the two porphyrin macrocycles held in a chiral conformation.

The interaction of **ZnP1** with **(+)-Chnn** resulted in a positive Cotton effect (λ_{max} = (-)435; (+)426 nm), whereas the binding to **(-)-Chdn** stereoisomer

resulted in a negative Cotton effect (λ_{max} = (+)433; (-)424 nm), indicating an opposite handedness of the resulting chiral cavity.

This opens the possibility of a modulation of the asymmetry of the formed cage upon chiral guest binding. Expectedly, the binding of **4,4'-bpy**, an achiral ligand, did not result in any chiroptical feature, indicating the formation of a symmetric cavity. The results are graphically reported in Fig. 1.28.

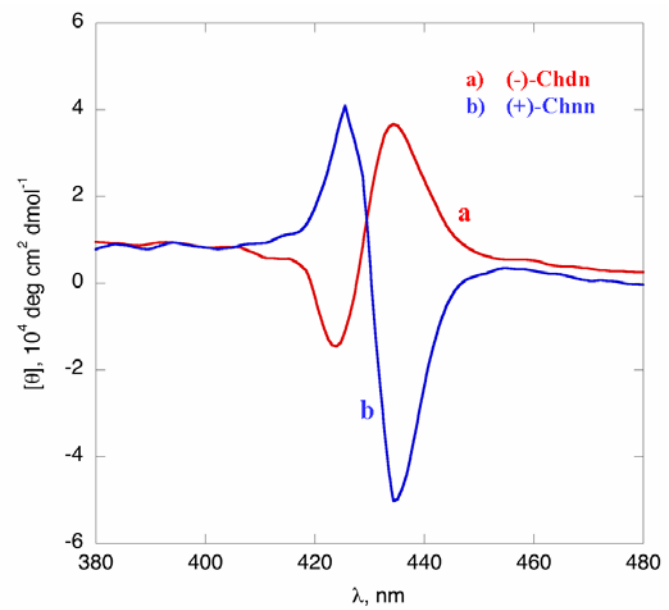

Fig. 1.28 *– CD spectra of supramolecular capsule formed by ZnP1 with: a) (-)-Chdn and b) (+)-Chnn.*

On the other hand, the interaction of these ligands to **ZnTPP** resulted in an induced CD spectra (ICD) featuring a dichroic, not excitonically coupled band in the Soret region, as expected in the case of a simple induction of chirality.

The binding with the different alkaloids resulted in an opposite sign, as expected for an interaction with alkaloids of different stereochemical configurations (λ_{max} = (-)427 nm for Chdn; (+)425 nm for Chnn). The intensity of the bands were somewhat lower, with respect to those observed in the case of the "caged" structures (for Chnn(+): $[\theta]_{427}$= 19000 (ZnTPP), $[\theta]_{435}$= -55000 (ZnP1); for Chdn(-): $[\theta]_{425}$= -10000 (ZnTPP), $[\theta]_{433}$= 36.400 (ZnP1)).

Remarkably, addition of a strong excess of ligand to a solution of receptor ZnP1 dramatically affected the relative chiroptical features, as reported in Fig. 1.29.

In the case of addition of a strong excess of (+)Chnn (≥ 250 fold) to a ZnP1 solution (6 μM), for example, the negative, bisignate CD band gradually evolved into a new positive, not coupled band, with λ_{max} 438 nm, reaching a maximum of intensity at ca 6 x 10^{-3} M of (+)Chnn.

This effect can be probably inferred to the formation of a "configurationally stable" linear porphyrin arrays with a head-to-tail arrangement, in which the handedness of the supramolecular structures are driven by the chirality of the cinchona ligands.

It is important to note that the reference, monotopic ZnTPP, presented ICD bands with alike sign, but shifted at different λ_{max} (Fig. 1.30). These different spectral features should corroborate the formation of linear array, rather than the formation of 1:1 ZnP1-(+)-Chnn complexes.

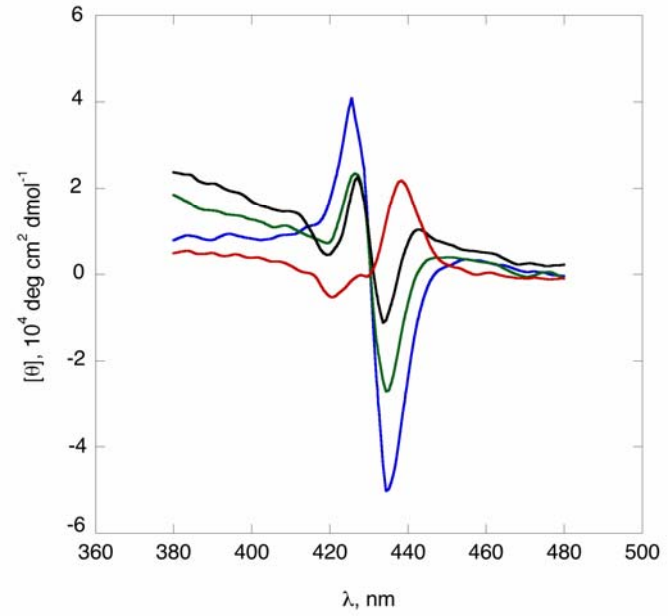

Fig. 1.29 *– Evolution of bisignate CD band of [ZnP1-(+)-Chnn]$_2$ capsule with the addition of a strong excess of (+)-Chnn.*

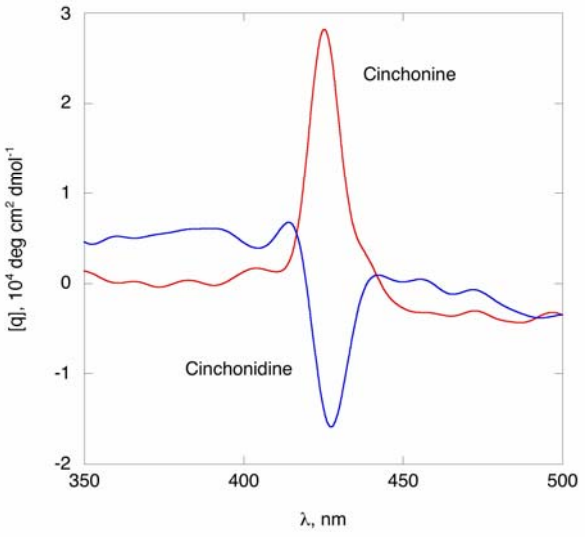

Fig. 1.30 *– CD spectra of ZnTPP bound to (+)-Chnn (red line) and (-)-Chdn (blue line).*

Analogous results have been obtained in the case of addition of strong molar excess of (-)Chdn. In this latter case, the spectral features generated by the chiral (2:2) capsule, evolved toward the growth of a new, not excitonically coupled, negative band, with λ_{max} at 427 nm.

Interestingly, the interaction of cinchona derivatives with the more rigid receptor **ZnP2**, did not result in any cooperative binding.

This would be explained in terms of a restricted cavity that hampers the optimal inclusion of the quinuclidine group within the aromatic bowl.

Finally, MM calculations afforded the following energy-minimized structure in which the two porphyrin macrocycles are close to each others and the bound alkaloids direct the quinuclidine end towards the aromatic cavity (Fig. 1.31). Although this structure is only an hypothetical spatial arrangement, it could account for the intense excitonic coupling observed by CD spectra,

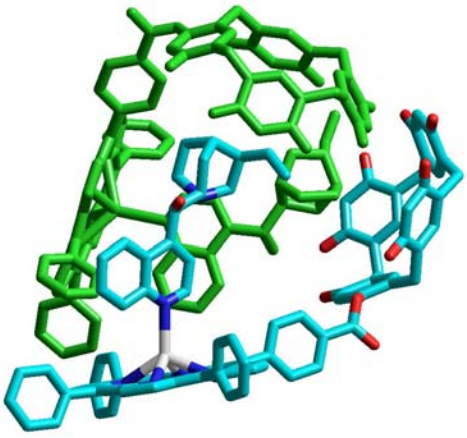

Fig. 1.31 *–Energy-minimized structure of [ZnP1-(-)Chdn]$_2$ (MMFF94 Spartan 02).*

1.6 Testing of Resorcinarene-Metalloporphyrin conjugates as sensitive materials for chemical sensors

A general requirement on sensors for artificial olfaction systems is the mutual orthogonality, namely, although unselective, each sensor should capture different aspects of the chemical richness of a complex sample. This can be in general accomplished by increasing number of sensors of the array modulating the chemical structures of the sensing layer. From this point of view, organic materials are the more versatile materials, offering many options for chemical modifications and huge flexibility in tailoring molecular recognition sites by controlled organic synthesis and through supramolecular interactions.

In recent years metalloporphyrins[35] and molecular containers[36] as resorcinarenes have been demonstrated to have very promising properties of sensing and have been widely employed in sensors applications.

Our laboratory developed in recent year an ***electronic nose*** (Fig. 1.32), whose performances have been demonstrated very successful in molecular recognition and discrimination of different classes of volatile organic compounds (VOCs).

Fig. 1.32 *– The electronic nose used in these studies.*

This device is an array of individual sensors based on metalloporphyrins, different one each other but globally selective according to the principle that each sensor senses more compounds and each compound is sensed by more sensors.

We used this analytical device to investigate the recognition properties of the ditopic material constituted by metalloporphyrin and resorcinarene (MP1), surmising that the presence of both metalloporphyrin platform and resorcinarene aromatic cavity would result in synergistic interactions useful for molecular recognition of organic molecules. Eventually, we expected that the new molecular system have higher sensitivities than the separated moieties.

We deposited the sensing subunits metalloporphyrins, cavitand, and ditopic receptors on 20 MHz AT-cut quartz microbalances (QMB) by spray casting technique to test the sensing properties of the new molecular material compared to the separated subunits.

In total, five sensors were tested: two coated with layers of ditopic receptors MP1 ***3a*** and ***5a*** (M= Zn, Mn) and three with the individual subunit MTPP (M=Zn, Mn) and CavBr (a methylene-bridged tetrabromocavitand), used as references.

The sensors were tested with different volatile organic compounds, in particular ***ethanol*** and ***triethylamine*** as representative of two classes of analytes largely occurring in many practical applications.

In particular the three-dimensional structure of the ditopic receptor suggested the possibility to offer to a single analyte a twice, cooperative, binding site. In order to exploit this feature a bidentate analyte, such ***ethanolamine***, was also tested.

Sensors were exposed to different analytes in a range of concentrations of 2-15 % of saturated pressure due to the different boiling temperature of tested compounds; it corresponds to different ranges for absolute concentration.

A simple and efficient way to summarize and compare informations in complex signals is to apply Partial Least Square (PLS) algorithm to the sensors responses (frequencies shifts in this case), in order to highlight the different contributions of sensing materials. Fig. 1.33 shows the first two Latent Variables of the whole set of measures which explain about 73% of the original information. This plot (Scores Plot) shows the classification of the considered molecules for the different tested concentrations. The Scores Plot addresses the correlation of the classification with the source of the QMB signals. In this graphic, scores that are 100% correlated with a measuring condition lie in the same direction, while perpendicularly oriented elements are not correlated: this figure shows a perfect separation between the three compounds, with a good orthogonality, indicating different contribution of sensing layers. Moreover, the system shows a good capability to recognize the exact amount of each analyte.

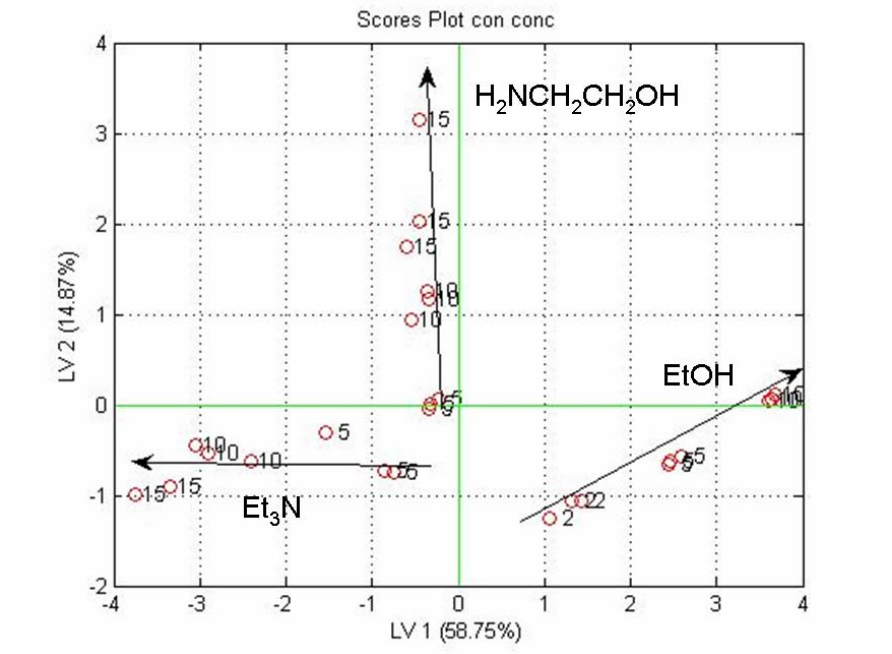

***Fig. 1.33** – Plot of the first two latent variables of the PLS model aimed at classifying the three different VOCs. About 73% of the total variance of the data is explained in this plot.*

The sensitivity of each sensors towards the various compounds was evaluated from response curves. Sensors coated with the ditopic receptor exhibited a large sensitivity in all the investigated cases. In Fig. 1.34 a sensitivity comparison for the bidentate compound (ethanolamine) is shown.

Sensitivity enhancement was not constant for all the ditopic receptors and for all the compounds.

In Fig. 1.35 the ratios of sensitivity of sensors coated with the ditopic compound and the correspondent metalloporphyrin are shown. It is worth to remark that since the resorcinarene counterpart of the composed receptors is the same we evaluated the sensitivity improvement with respect to the metalloporphyrin.

The largest sensitivity gain is obtained for ***ethanolamine***. The sensitivity of the sensors coated with the ditopic structure is 6-10 times greater of the sensitivity of the sensors coated with the correspondent subunits. For ethanol and triethylamine no meaningful differences are found.

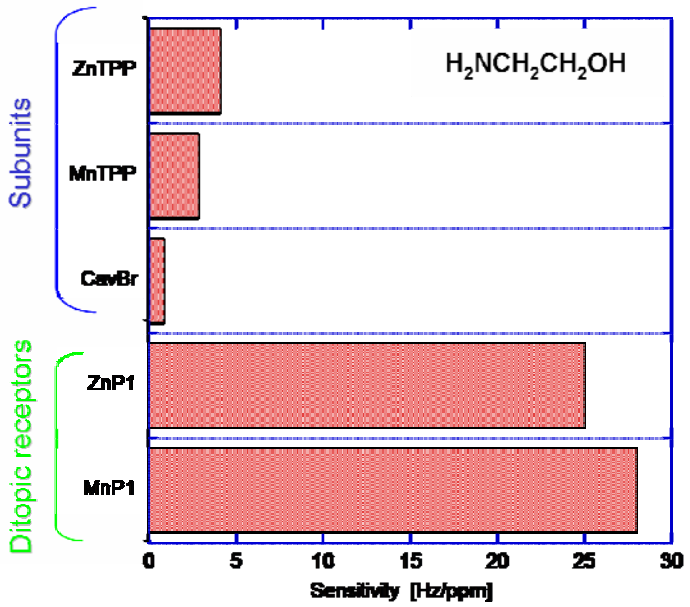

Fig. 1.34 *– Sensitivity of each sensor tested toward ethanolamine.*

The large gain of sensitivity observed for ethanolamine, a bidentate ligand with a OH and a NH_2 groups kept separated by an ethylene unit, corroborates the initial assumption which seems to emphasize, in a single molecular recognition center, the yet brilliant properties of cavitands and metalloporphyrins.

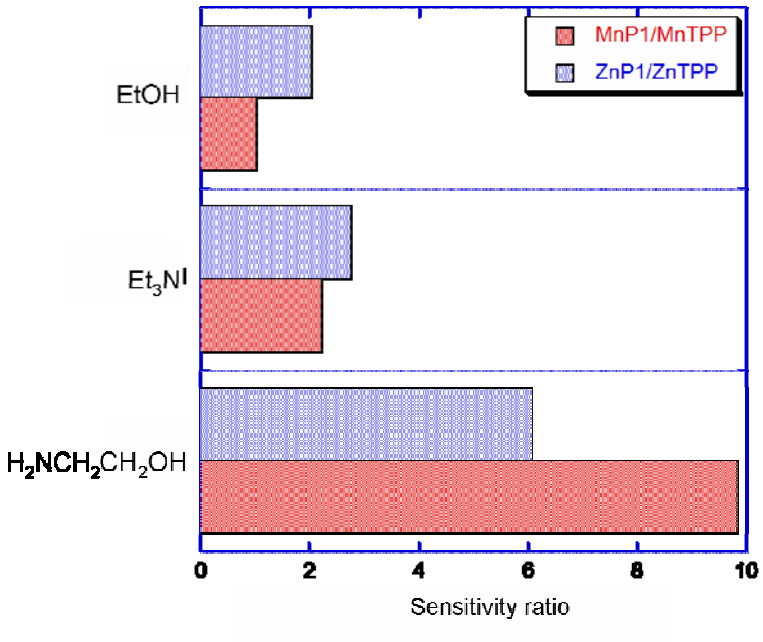

Fig. 1.35 *– Ratios of sensitivity of sensors coated with the ditopic receptors and the correspondent metalloporphyrin.*

Experimental Section

➢ *Reagents and materials*

Reagents and solvents (Sigma-Aldrich, Fluka and Carlo Erba Reagenti) were of the highest grade available and were used without further purification.

Solvents employed in the spectroscopic studies are of spectroscopic grade and used as received.

Silica gel 60 (70 -230 mesh) and alumina neutral (Brockmann Grade III). were used for column chromatography

Silica gel 60 (Merck) and neutral alumina 60 F_{254}, both on aluminium support, were used for TLC.

➢ *Instruments*

^{1}H NMR spectra were recorded with a Bruker AM400 (400 MHz) spectrometer, using $CDCl_3$ as solvent. Chemical shifts are given in ppm relative to tetramethylsilane (TMS).

^{1}H PGSE NMR diffusion studies were recorded with a Brucker Avance AQS 600 (600, 13 MHz) spectrometer, probe BB reverse with z-gradient, using d_2-TCE and CD_3OD as solvents.

Routine UV/Vis spectra were recorded in $CHCl_3$ on a Varian Cary 50 Spectrophotometer. whereas more delicate measurements were performed on a Perkin Elmer λ18 Spectrophotometer equipped with a temperature-controlled cell holder.

CD spectra have been performed on a JASCO J-600, equipped with a thermo stated cell holder, and purged with ultra-pure nitrogen gas.

Mass spectra (FAB) were recorded on a VG Quattro Spectrometer using m-nitrobenzyl alcohol (NBA, Aldrich) as a matrix in the positive-ion mode.

- ***List of acronyms***

DMF = *N*,*N*'-dimethylformamide
THF = tetrahydrofuran
TFA = trifluoroacetic acid
d_2-TCE= 1,1,2,2-tetrachloroethane
HOBT = 1-hydroxy-1*H*-benzotriazole
EDC-HCl = 1-[3-(dimethyl-amino)propyl)-3-ethylcarbodiimide hydrochloride

1.7 Synthesis of meso-arylporphyrins

*1.7.1 Synthesis of 5-(4'-Carboxymethylphenyl)-10,15,20-triphenylporphyrin (**1a**)*

A solution of pyrrole (5.32 g, 79 mmol) in acetic acid (50 mL) was added dropwise to a solution of methyl 4-formylbenzoate (1.30 g, 7.9 mmol) and benzaldehyde (8.42 g, 79 mmol) in refluxing acetic acid (400 mL), over a period of 30 minutes. The reaction mixture was stirred at reflux temperature for an additional 3 h, then cooled to room temperature and left standing overnight. The crystalline residue, separated from the bulk solution, was collected by filtration, washed with CH_3OH and then purified by chromatography on SiO_2, first eluting with a hexanes/CH_2Cl_2 mixture (1:2) to separate H_2TPP, then with CH_2Cl_2 to

elute the desired product as a purple band. The fractions containing H_2TPP were collected and evaporated to give 1.8 g (26%). Another crop of porphyrin *1a* was obtained from the mother liquor as follows: the solvent was evaporated under reduce pressure and the residue dissolved in 150 mL of CH_2Cl_2. A saturated solution of aqueous $NaHCO_3$ was added to the mixture and left stirring until the evolution of gas ceased. The separated organic layer was washed with aqueous $NaHCO_3$ solution (3x150 mL); the washings were collected and dried on anhydrous Na_2SO_4 and the solvent was evaporated under reduced pressure to give a red solid that was purified by column chromatography (SiO_2, CH_2Cl_2). The combined product was crystallized from CH_3OH to afford 0.65 g of the pure porphyrin (overall yield 12%) as a purple solid.

*1.7.2 Synthesis of 5-(4-Carboxyphenyl)-10,15,20-triphenylporphyrin (**2a**)*

Porphyrin (*1a*) (0.25 g, 0.37 mmol) was dissolved in 100 mL of 95% EtOH and NaOH (1 g) was added. The mixture was stirred at reflux temperature for 3 h, then cooled to room temperature and filtered, washing the precipitate several times with distilled H_2O. The residue was then redissolved with a mixture of $CHCl_3$ and CH_3OH, and the solution evaporated under reduce pressure. The purple solid was dissolved in 100 mL of $CHCl_3$ and washed with a saturated solution of aqueous NH_4Cl. The organic phase was then dried on Na_2SO_4 anhydrous and the solvent was reduced to a small volume. The addition of the same volume of hexanes afford pure porphyrin (0,2 g, 82%) as a purple solid.

The spectroscopic data obtained for the title compound are in agreement with those in the literature; FAB-MS give the parent ion peak at m/z 658; 'H-NMR ($CDCl_3$) d ppm: 8.86 (s,6H), 8.80 (d, 2H), 8.48 (d, 2H), 8.32 (d, 2H), 8.22 (d, 6H), and 7.77 ppm (m, 9H). UV/vis ($CHCl_3$) λ_{max}: 419 nm, Q bands at 516, 551, 590 and 647 nm.

1.8 Synthesis of Resorcinarene-ZnPorphyrin Conjugates

1.8.1 Synthesis of ZnP1 (**3a**)

All manipulations were carried out under an inert atmosphere by using standard Schlenk techniques. Porphyrin *2a* (0.2 g, 0.3 mmol) was dissolved in dry and distilled $CHCl_3$ (20 mL) in a 100 mL two-necked round-bottomed flask. An excess of a 2 M oxalyl chloride solution in CH_2Cl_2 (12 mL, 24 mmol) was added to the reaction mixture under stirring. After 2 h the solvent was evaporated in vacuo to give a dark brown residue, which was then dissolved in dry $CHCl_3$(20 mL). A solution of Res-$C_{10}H_{21}$ prepared by following published procedure[19] (0.33 g, 0.3 mmol) in dry THF (8 mL) was rapidly added along with two drops of anhydrous pyridine. The mixture was left stirring overnight. The solvent was then stripped off in vacuo, and the residue dissolved in $CHCl_3$, washed with brine and dried on anhydrous Na_2SO_4. A TLC run (SiO_2/3% MeOH/$CHCl_3$ solvent mixture) showed two main spots corresponding to the unreacted porphyrin *2a* and a more polar compound, with a lower R_f, corresponding to the desired product of coupling. The solvent was reduced to a small volume and an excess (2.5 mL) of a saturated methanolic solution of $Zn(AcO)_2$ was added. The progress of the reaction was monitored by UV-visible spectroscopy (Soret and Q visible bands changes). After 2 h, the solvent was removed in vacuo to give a cherry-purple solid which was dissolved in 50 mL of $CHCl_3$ and washed (3x 50 mL) with brine. The organic phase was dried on Na_2SO_4 anhydrous, reduced to a small volume and then chromatographed (SiO_2) eluting first with a 3% MeOH/$CHCl_3$ solvent mixture to recover the unreacted porphyrin *2a* and then with a 5% MeOH/$CHCl_3$ solvent mixture to give 0,17 g, of the desired conjugate *3a* (32%) as a bright cherry-red crystals.

*1.8.2 Synthesis of ZnP2 (**4a**)*

To a slurry of *3a* (50 mg, 0.03 mmol) and K_2CO_3 (55 mg, 0.4 mmol) in dry DMF (10 mL) was added $BrCH_2Cl$ (40 μL, 0.6 mmol) and the mixture was stirred at 65°C for 24 h under N_2, then more $BrCH_2Cl$ (10 μL ,0,15 mmol) was added and stirring was carried out for 24 h. The DMF was removed in vacuo to give a violet residue. It was dissolved in CH_2Cl_2 (20 mL) and 2 M HCl (20 mL) was added while strirring. The aqueous phase was separated and extracted with more CH_2Cl_2. The combined organic layers were washed with water, saturated brine, then dried on Na_2SO_4 anhydrous. Evaporation of the solvent gave a violet residue which was dissolved in CH_2Cl_2 and subjected to column chromatography (SiO_2) eluting with CH_2Cl_2. The first violet band was collected to afford 15 mg of the desired conjugate (28%) as a bright cherry-purple crystals.

*1.8.3 Synthesis of MnP1 (**5a**)*

Compound *3a* (25 mg, 0.015 mmol) was dissolved in $CHCl_3$ (10mL) and few drops of TFA were added. The mixture was stirred for 10 min at room temperature and then washed with a saturated solution of aqueous Na_2CO_3. The control by UV-vis spectroscopy helps to evaluate the complete demetallation of the starting compounds: the blue-shift of the Soret band and the concomitant appearance of the four characteristic Q-bands reveal the presence of the porphyrin free base. The organic phase was then dried on Na_2SO_4 and the solvent was removed under reduced pressure. The violet residue was then dissolved in DMF (5mL) and an excess of $Mn(AcO)_2$ was added. The reaction was stirred at reflux temperature for 3 h, monitoring by UV-vis the metal insertion process. After cooling at to room temperature, distilled H_2O was added. The resulting green precipitate was then filtered, and washed several times with distilled H_2O.

The residue was dissolved in a small amount of $CHCl_3$ and then chromatographed (SiO_2) eluting with a 8% MeOH/$CHCl_3$ solvent mixture. 16 mg of the desired product was obtained (67%) as green crystals.

1.9 Spectroscopic investigations: UV-visible titration, CD spectra and ^{1}H PGSE NMR diffusion studies.

UV-vis spectroscopic studies: Binding constant values (*K*) were determined by monitoring the spectroscopic spectral changes of porphyrin receptors (Soret band maxima), upon addition of proper aliquots of a ditopic ligand solution. Titrating nitrogen-base solutions, prepared by dissolving the required amount of the guests ($1x10^{-2}\div1x10^{-4}$ M) in a freshly prepared solution of the free receptor **ZnP1** or **ZnP2** ($5x10^{-6}$ M), were added to a 2.5 mL of the receptor solution (1 cm quartz cell, 25.0 ± 0.1 °C). This procedure ensures a constant value of the concentration of receptor trhoughout the titration procedure.

The absorbance variation (Soret band, 419 nm) was monitored at different concentration of added guest.

The stability constants (*K*) were calculated by using a standard equation for a 1:1 complexation:

$$\Delta A = \frac{\Delta\varepsilon[\mathrm{ZnP1}]K[\mathrm{G}]}{1+K[\mathrm{G}]}$$

where $\Delta A=A_0-A_i$; $\Delta\varepsilon=e_0-e_\infty$; [**G**] is the concentration of the added guest. The computer aided non-linear least square fitting analyses, to give *K* and Δε have been performed with the program Kaleidagraph® with data of 8-10 measurements. The results have run in duplicate and are reproducible within the range of 5÷10%, unless otherwise indicated.

CD spectroscopic studies: CD spectra were recorded in $CHCl_3$ at 25.0 ± 0.1 °C in 1 cm quartz cell following the same protocol employed for UV-vis studies.

^{1}H PGSE NMR diffusion studies: preparation of samples was accomplished as follows: ~ 2 mg of ZnP1 were dissolved in 1.5 mL of d_2-TCE and ~ 1 mL of this solution was added to 3.5 mg of 4,4'-bpy content into a 5 mm NMR tube.

^{1}H NMR spectra of ZnP1 was performed in similar concentration, but using a CD_3OD/ d_2-TCE (3:97) solvent mixture, in order to avoid the spontaneous formation of aggregates.

^{1}H NMR spectra were measured using a probe BB reverse with z-gradient in conjunction with a Brucker Avance AQS 600 (600, 13 MHz) spectrometer.

All ^{1}H free induction decays (FIDs) were acquired at 300 K with a spectral width from 9.352 to 8.927 ppm. Experiments were performed with a relaxion delay of 1.5 s, a diffusion delay, Δ, of 0.2 s, a gradient pulse duration, δ, of 3 ms, a delay between gradient pulses, τ, of 1.2 ms, and an eddy current delay time, T_e, of 15 ms. Gradient amplitudes were varied from 0.69 to 32.8 $G \cdot cm^{-1}$.

Individual FIDs were processed by routine program of Brucker spectrophotometer.

Diffusion coefficients were extracted from nonlinear least.squares fits of Eqn 1 (see text) to the measured integrated resonance intensity using SigmaPlot.

The reported diffusion coefficients are the average of 3 experimental trials performed in replicate on the same sample. The reported error is the larger of either the exponential fitting error or the standard deviation of the three trials.

References

1. Lehn, J.M.; In *Supramolecula Chemistry Concepts and Perspectives;* VCH Ed.; Weinheim Bundesrepublik Deutschland **1995**, 1.
2. Vriezema, D.M; Comellas Aragones, M.; Elemans, J.A.A.W.; Cornelissen, J.J.L.M.; Rowan, A.E.; Nolte R.J.M. *Chem. Rev.,* **2005**, *105*, 1445.
3. Breslow, R.; Dong, S.D. *Chem. Rev.,* **1998**, *98*, 1997.
4. a) Rebek, J.Jr *Chem. Soc. Rev.,* **1996**, *25*, 255. b) Conn, M.M.; Rebek, J.Jr *Chem. Rev.,* **1997**, *97*, 1647. c) Rebek, J.Jr. *Acc. Chem. Res.,* **1999**, *32*, 278.
5. Branda, N.; Wyler, R.; Rebek, J.Jr *Science*, **1994**, *263*, 1267.
6. Rivera, J.M.; Martin, T.; Rebek, J.Jr *J. Am. Chem. Soc.*, **2001**, *123*, 5213.
7. Kang, J.; Santamaria, J.; Hilmersson, G.; Rebek, J.Jr *J. Am. Chem. Soc.*, **1998**, *120*, 7389.
8. a) Holliday, B.A.; Mirkin, C.A. *Angew. Chem. Int. Ed. Engl.*, **2001**, *40*, 2022. b) Seidel, S.R.; Stang, P.J. *Acc. Chem. Res.,* **2002**, *35*, 972. c) Pinalli, R.; Cristini, V.; Sottili, V.; Geremia, S.; Campagnolo, M.; Caneschi, A.; Dal canale, E. *J. Am. Chem. Soc.*, **2004**, *126*, 6516.
9. Fujita, M. *Chem. Soc. Rev.,* **1998**, *27*, 417.
10. a) Kusukawa, T.; Fujita, M. *J. Am. Chem. Soc.,* **1999**, *121*, 1397. b) Kusukawa, T.; Fujita, M. *Angew. Chem. Int. Ed. Engl.*, **2001**, *40*, 1879. c) Kusukawa, T.; Fujita, M. *J. Am. Chem. Soc.,* **2002**, *124*, 13876. d) Ito, H; Kusikawa, T. *Chem. Lett.*, **2000**, 598.
11. Menozzi, E.; Pinalli, R.; Speets, E.; Ravoo, B.J.; Dalcanale, E.; Reinhoudt, D.N. *Chem. Eur. J.*, **2004**, *10*, 2199.
12. Hof, F.; Craig, S.L.; Nuckolls, C.; Rebek, J.Jr. *Angew. Chem. Int. Ed. Engl.*, **2002**, *41*, 1488.
13. Castellano, R.K.; Rebek, J.Jr. *J. Am. Chem. Soc.,* **1998**, *120*, 3657.

14. Castellano, R.K.; Kim, B.H.; Rebek, J.Jr. *J. Am. Chem. Soc.*, **1997**, *119*, 12671.
15. Tokunaga, Y.; Rebek, J.Jr. *J. Am. Chem. Soc.*, **1998**, *120*, 66.
16. a) Rivera, J.M.; Martin, T.; Rebek, J.Jr. *Science.*, **1998**, *279*, 1021. b) Rivera, J.M.; Martin, T.; Rebek, J.Jr. *J. Am. Chem. Soc.*, **2001**, *123*, 5213.
17. Steed, J.W.; Atwood, J.L.; In *Supramolecular Chemistry*; Wiley Ed.; **2000**, 304.
18. Timmerman, P.; Verboom, W.; Reinhoudt, D.N. *Tetrahedron*, **1996**, *52*, 2663.
19. Tunstad, L.M.; Tucker, J.A.; Dalcanale, E.; Weiser, J.; Bryant, J.A.; Sherman, J.C.; helgeson, R.C.; Knobler, C.B.; Cram, D.J. *J. Org. Chem.*, **1989**, *54*, 1305.
20. Erdtman, H.; Hŏgberg, A.G.S.; Abrahamsson, S.; Nilsson, B. *Tetrahedron Lett.*, **1968**, 1679.
21. Hŏgberg, A.G.S. *J. Am. Chem. Soc.*, **1980**, *102*, 6046.
22. Botta, B.; Di Giovanni, C.; Delle Monache, G.; De Rosa, M.C.; Gacg-Baitz, E.; Botta, M.; Corelli, F.; Tafi, A.; Santini, A., Benedetti, E.; Pedone, C.; Misiti, D. *J. Org. Chem.*, **1994**, *59*, 1532.
23. Falena, O.M.; Al-Farhan, E.; Keehn, P.M.; Stevenson, R. *Tetrahedron Lett.*, **1994**, 35, 65.
24. Cram, D.J.; Cram, J.M.; In *Container Molecules and Their Guests*; The Royal Society of Chemistry Ed.; Cambridge **1994**, 85.
25. Moran, J.R., Karbach, S.; Cram, D.J. *J. Am. Chem. Soc.*, **1982**, *104*, 5826.
26. Grigg, R. In *The Porphyrins*; Dolphin, D., Ed.; Academy Press: New York, **1978**, Vol. II.
27. Lindsey, J.S. In *The Porphyrin Handbook*, Kadish, K.M., Smith, K.M., Guilard, R., Eds.; Academic Press: New York; **2000**, Vol. 1.
28. Starnes, S.D.; Rudkevich, D.M.; Rebek, J.Jr. *J. Am. Chem. Soc.*, **2001**, *123*, 4659.

29. Nakazawa, J.; Hagiwara, J.; Mizuki, M.; Shimazaki, Y.; Tani, F.; Naruta, Y. *Angew. Chem. Int. Ed. Engl.*, **2005**, *117*, 2.
30. Nakazawa, J.; Mizuki, M.; Shimazaki, Y.; Tani, F.; Naruta, Y. *Org. Lett.*, **2006**, *8*, 4275.
31. a) Love, J.C.; Estroff, L.A.; Kriebel, J.K.; Nuzzo, R.J.; Whitesides, J.N. *Chem. Rev.,* **2005**, *105*, 1103. b) Corbellini, F.; Mulder, A.; Sartori, A.; Ludden, M.J.M.; Casnati, A.; Ungaro, R.; Huskens, J.; Crego-Calama, M.; Reinhoudt, D.N. *J. Am. Chem. Soc.,* **2004**, *126*, 17050.
32. Pinalli, R.; Nachtingell, F.F.; Uguzzoli, F.; Dalcanale, E. *Angew. Chem. Int. Ed. Engl.*, **1999**, *38*, 2377.
33. a) Pregosin, P.G.; Kumar, A.; Fernandez, I. *Chem. Rev*., **2005**, **105**, 2977. b) Timmerman, P.; Weidmann, J.L.; Jolliffe, K.A.; Prins, L.J.; Reinhoudt, D.N.; Shinkai, S.; Frish, L.; Cohen, Y. *J. Chem. Soc. Pertkin Trans. 2*, **2000**, 2077
34. Skórska, A.; Stadnika, K.; Oleksyn, B.J. *Chirality*, **2005**, *17*, 73.
35. Di Natale, C.; Paolesse, R.; D'Amico, A. *Sens. And Act. B*, **2006**, in press.
36. Dickert, F.L.; Baumler, U.P.A.; Stathopoulos, H. *Anal. Chem.*, **1997**, *69*, 1000.

Chapter 2

Aggregation Chemistry of Porphyrins and Related Macrocycles

Introduction

2.1 Noncovalent Synthesis of Supramolecular Systems[1]

In the last 30 years the way chemists think about synthesis has been strongly influenced by supramolecular concepts: molecules are not mainly collections of atoms connected by a continuous network of kinetically stable chemical bonds, but structures deriving from multiple, weak and non-covalent interactions of different nature, such as electrostatic and van der Waals forces or hydrophobic effects, π- π stacking interactions, metal coordination and hydrogen bonding. This new philosophy basically draws inspiration from biological systems, in which such interactions lead to the specific form and function of proteins and other biological macromolecules and are responsible for many biological events, like the transduction of signals, the selective transport of ions and small molecules across membranes, enzymatic reactions or the formation of larger aggregates.

In chemistry, such weak non covalent interactions determine the physical properties of molecules, like the ones of liquids, the solubility of solids or the organization of amphiphilic molecules in larger aggregates such as membranes, micelles , vescicles and liposomes.

Although the preparation of a molecular unit involves the formation of covalent bonds, the objective of the synthesis is the molecular information that this unit displays, useful for a specific recognition function (binding and selection). The understanding of the individual interactions that govern the molecular recognition process enable to use supramolecular chemistry as a tool

for noncovalent synthesis. Cooperative, weak interactions are used for the spontaneous and reversible formation of large aggregates that have well-defined structures, as helicates, grids, molecular containers, capsules and alike under thermodynamic equilibrium , with the possibility of error correction and without undesired side products. Furthermore, it does not require chemical reagents or harsh conditions.

It is important to note that those interactions should be sufficiently strong (of the order of kT) to provide sufficient stability, but not so strong that first contacts are irreversibly trapped: the self-optimization of the structures relies on the reversibility and the potential exploration of competing structural and energy states[2].

This new approach results a good alternative for the chemical assembly of nanostructures[1]. Large scale nanometer fabrication will be a requirement for future molecular electronic devices, high-density data storage or drug delivery. Covalent synthesis affords compounds with molecular weights in the range of 100 to 3000 Da, but there are no simple covalent strategies for the synthesis of pure molecules that have molecular weights between 10^4 and 10^6 kDa. Noncovalent systems have dimensions between 3 to 20 nm and fill the gap between small molecules and larger nano-objects that are now accessible by physical fabrication methods, mainly based on lithography. This is also the size range where quantum confinement influences the electronic and optical properties of matter.

In biosynthesis, chemical transformations are highly stereoselective with only one of the many possible stereoisomers being formed. With the current state of chemical synthesis a comparable stereocontrol over covalent bond formation is possible for many types of reaction as well. In the synthesis of noncovalent systems, this control over stereochemistry is much more difficult, because bonds between the individual components are kinetically labile and are continuosly broken and formed. However, in noncovalent synthesis, the stereochemistry of

reaction products (regioselectivity, diastereoselectivity and enantioselectivity) must also be controlled. Rebek et al. have demonstrated that certain symmetrical molecules dimerize through hydrogen bonding to form molecular capsules with dissymmetrical cavities. In the presence of symmetrical guest, the capsule exists as an equal (racemic) mixture of two mirror-image forms (enantiomers). Nevertheless, with the presence of a chiral guest inside the cavity, these noncovalent assemblies preferentially form one of the two possible diastereomeric complexes[3]. More interestingly these systems also exhibit amplification of chirality[4]. Thus, the achiral components "follow" the helicity induced by the chiral components even when the chiral molecules are present in very small fractions, far less than equimolar amounts. From a philosophical point of view this amplification of chirality is also regarded as essential for the explanation of homochirality in nature (i.e. only L-aminoacids and D-sugars)[5].

2.2 Porphyrin Aggregates

The aggregation of porphyrins and metalloporphyrins has been studied for several decades[6]. Although most of the early works were devoted to the naturally occurring iron porphyrins and easily obtained derivatives, in the last 10 years a large number of investigations about the aggregation properties of the porphyrins were carried out.

In 1937, Alexander studied monomolecular layers of a variety of porphyrins on the surface of water, concluding that the protoporphyrin molecules are packed face to face and oriented vertically. In this manner, the polar carboxylic acid groups are in the water, while the vinyl groups are far from water. Afterwards similar results were found by other groups, leading to the formulation of a basic assumption in virtually all the aggregation studies for both porphyrins and metalloporphyrins, that is the "face-to-face", ring stacking, "sandwich" or "stack

of pancakes" model. The classification of the different geometries presented by porphyrin aggregates and the understanding of the intermolecular forces responsible of the aggregation process have been exploited at later term.

2.2.1 Classification of Porphyrin Aggregates[7]

Porphyrins, as other related cromophores may be arranged in different ways in an aggregate structure, because of the strong electrostatic interactions between the electronic clouds of different macrocycles. The aggregates are usually classified into three types:

- J-aggregates that are "edge-to-edge" structures;
- H-aggregates that are "face-to face" structures;
- non-specific aggregates, having middle features between J and H types.

Recently theoretical studies have shown that the simple picture of a π-system as a sandwich of the positively charged σ-framework between two negatively charged π-electron clouds accounts well for the observed interactions between π-systems. It is a π-σ attraction rather than a π- π electronic interaction which leads to favourable interactions, that determine, together with van der Waals forces, the preferential cofacial arrangement of porphyrins both in solution and crystals, as shown in Fig. 2.1. The presence of a metal atom coordinated into the inner core of the macrocycle does not alter the geometry of the aggregate and enhances the magnitude of the π-π interaction: the greater the intramolecular polarization between the porphyrin and the metal, the stronger is the π-π interaction between two porphyrins, while coordination of the metal by a ligand reduces the magnitude of the π- π interaction in metalloporphyrins and generally leads to disaggregation.

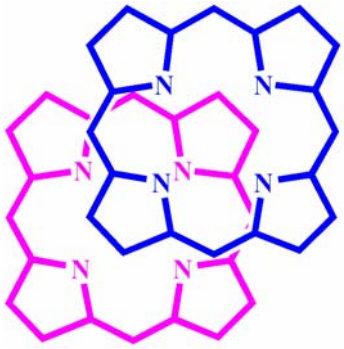

Fig. 2.1 *– Preferential cofacial arrangement of porphyrins.*

The aggregation phenomena are often accompanied by UV-vis spectral shifts, such as hypsocromicity, bathochromicity and broadening of the starting band or the appearance of new spectral bands due to the excitonic interactions between the cromophores (Fig. 2.2).

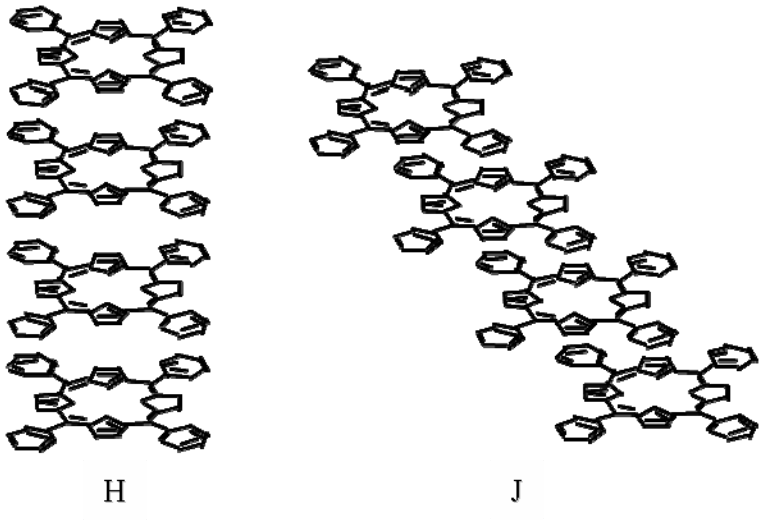

Fig. 2.2 *– J- and H-type aggregates of porphyrins.*

These changes can be explained and visualized using a vectorial picture and considering the interactions between the electrostatic dipole moments of the molecules. In Fig. 2.3 and 2.4 are depicted two extreme cases, where the

interaction is between two monomeric units having dipole moments lying along the molecular plane.

For ***H-aggregates*** two types of alignments are possible. The "orientation mode" A corresponds to the transition at higher energy because the dipoles coupling provides for this event an alignment "in-phase", determining repulsion between partial charges of the same sign: the resulting vectorial sum is not equal to zero.

The "orientation mode" B provides a more favourable coupling (that is at lower energy), but dipole moments cancel each other, resulting in a virtually "zero" dipole moment vector. The ΔE_{tran} is larger for the dimer resulting form the aggregation compared to the monomer, because the arrangement of the dipole moments of monomers within the dimeric system is energetically unfavourable. This leads to the *blue-shift* of the Soret band of the aggregate compared to the one of the monomeric unit.

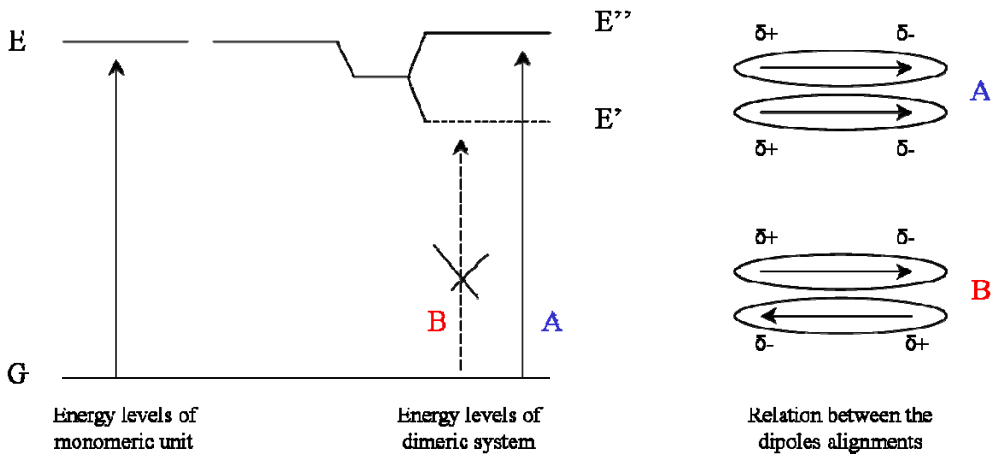

Fig. 2.3 – *Orientation of dipole moments of two porphyrins forming H-aggregate.*

An opposite situation concerns ***J-aggregates*** because the dipole moments of the monomers are parallel and lie along the line joining the molecular centres.

Again, two types of alignments are possible for the transition dipoles (Fig. 2.4). The "aggregation mode" A corresponds to the transition at higher energy because the dipoles coupling provides for this event an alignment determining repulsion between partial charges of the same sign: the resulting vectorial sum is zero. In the orientation B this vectorial sum is not zero and coupling results energetically more favourable (that is at lower energy). The ΔE_{tran} is smaller for the dimer resulting form the aggregation compared to the monomer and leads to a *red-shift* of the Soret band of the aggregate compared to the single unit of porphyrin.

With respect to intermediate geometries featuring by non-specific aggregates both transitions can be partially allowed so that the electronic spectrum is characterized by the presence of two bands simultaneously, the former at a blue-shifted wavelength and the latter at a red-shifted wavelength in the aggregate relative to the monomer, or a general, less specific, broadening of the strarting band resulting from the aggregation.

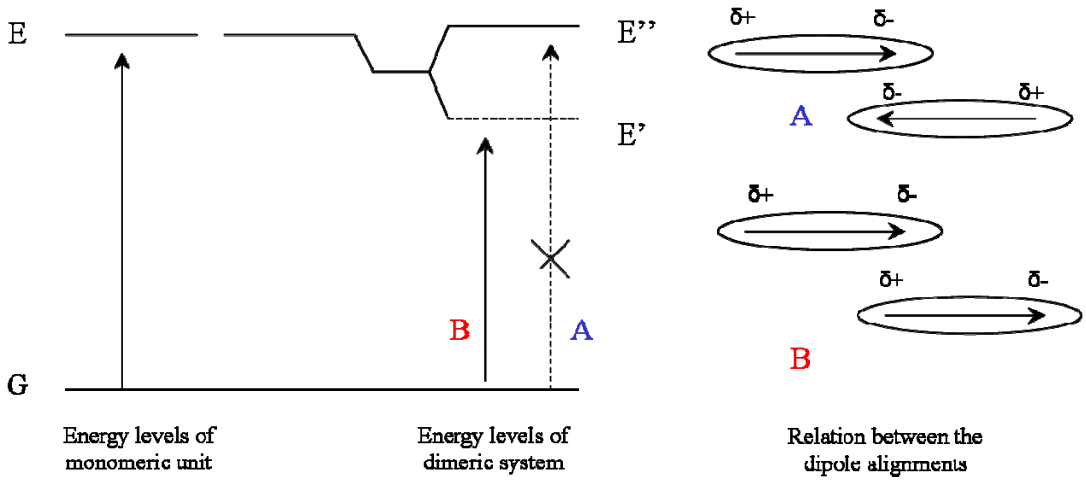

Fig. 2.4 *– Orientation of dipole moments of two porphyrins forming J-aggregate.*

2.2.2 *Spectroscopic techniques for the characterization of Porphyrin Aggregates: Fluorescence, CD and RLS.*

The changes of the spectroscopic pattern can give some information on the geometry and the morphology of the porphyrin aggregates. More insight, they can be given by means of other addressed spectroscopic techniques such as fluorescence, resonance light scattering (RLS) and circular dichroism (CD).

- **Fluorescence[8]**

Luminescence is the emission of photons from electronically excited states. Luminescence is divided into two types, depending upon the nature of the ground and the excited states. In a singlet excited state, the electron in the higher-energy orbital has the opposite spin orientation as the second electron in the lower orbital. These two electrons are said to be paired. In a triplet state these electrons are unpaired, that is, their spins have the same orientation. Return to the ground state from an excited singlet state does not require an electron to change its spin orientation. A change in spin orientation is needed for a triplet state to return to the singlet ground state. Fluorescence is the emission which results from the return to the lower orbital of the paired electron. Such transitions are quantum mechanically "allowed" and the emissive rates are typically near 10^8 sec^{-1}. These high emissive rates result in fluorescence lifetimes near 10^{-8} sec or 10 nsec. The lifetime is the average period of time a fluorophore remains in the excited state. Phosphorescence is the emission which results from transition between states of different multiplicity, generally a triplet excited state returning to a singlet ground state. Such transitions are not allowed and the emissive rates are slow. Typical phosphorescent lifetimes range from milliseconds to seconds, depending primarily upon the importance of deactivation processes other than emission.

Fluorescence spectral data are generally presented as emission spectra. A fluorescence emission spectrum is a plot of the fluorescence intensity versus wavelength (in nanometers) or wave numbers (in cm^{-1}). Emission spectra vary widely and are dependent upon the chemical structure of the fluorophore and the solvent in which it is dissolved.

A typical fluorescence emission spectrum of a common porphyrin is shown in Fig. 2.5.

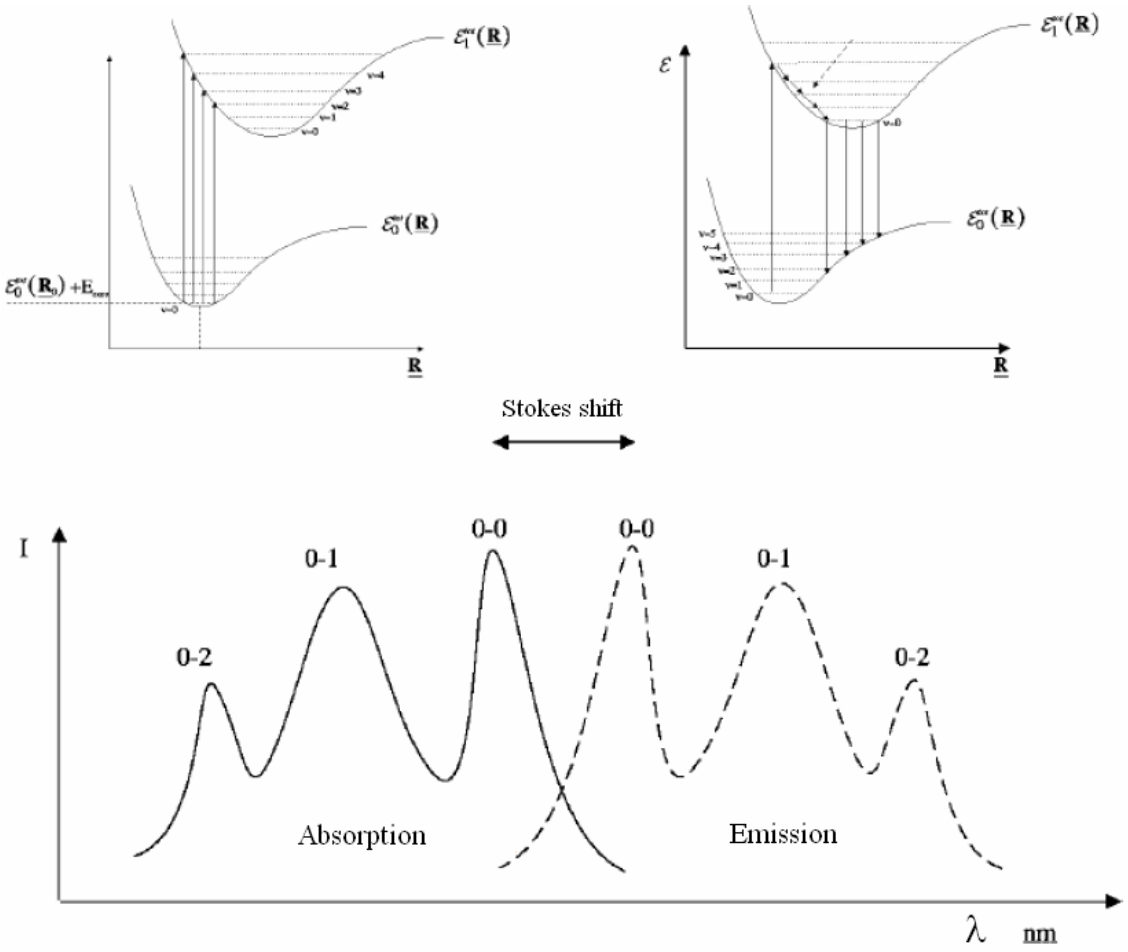

Fig. 2.5 – *Absorption and emission spectra of porphyrins.*

The absorption and emission of light is nicely illustrated by the energy level diagram suggested by A. Jablonski (Fig.2.6).

Excitation from the ground state S_0 to any singlet exited state S_x leads to very fast radiationless decay to the lowest excited singlet S_1 in times ~ 10^{-12} -10^{-13} sec. From S_1 the molecule can emit fluorescence radiation $S_1 \rightarrow S_0$ with rate k_f, can radiationlessly decay $S_1 \rightsquigarrow S_0$ with rate k_1, or can internally convert to the lowest triplet $S_1 \rightsquigarrow T_1$ with rate k_2. (We here use straight arrows to denote radiative transitions and wavy arrows to denote radiationless transitions). S_1 decays over times between $10^{-12}$and 10^{-7} sec, after which, if the system is still excited, it exists in the lowest triplet T_1. From T_1 the molecule can emit phosphorescence radiation $T_1 \rightarrow S_0$ with rate k_p, can radiationless decay $T_1 \rightsquigarrow S_0$ whit rate k_3, or can be reexcited to the first excited singlet $T_1 \rightarrow S_1$ whit rate k_{-2}. Such repopulation of S_1 can lead to delayed fluorescence. It requires an input of energy to T_1, which can occur in one of two ways: thermal repopulation (*E*-type delayed fluorescence) or triplet-triplet collisions (*P*-type delayed fluorescence).

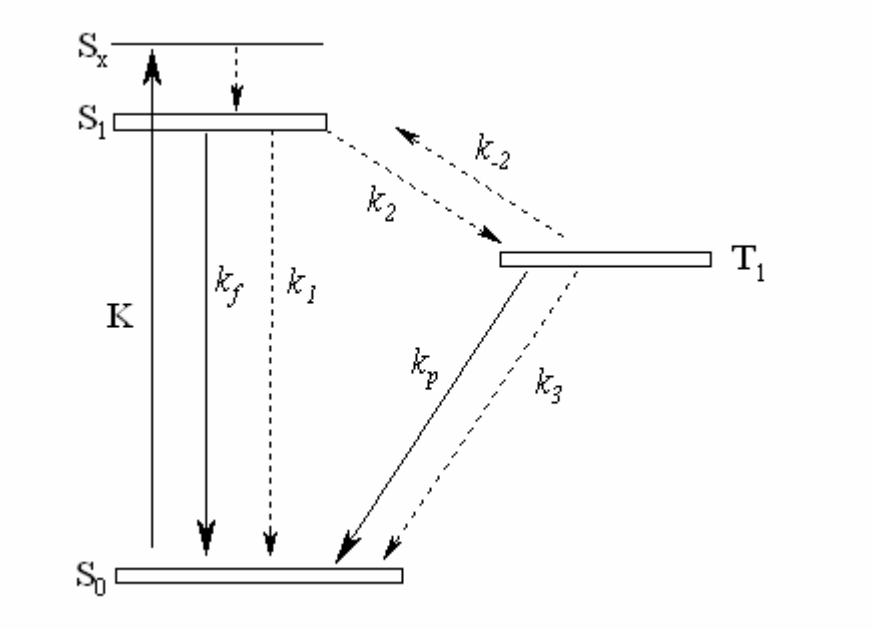

Fig. 2.6 – *Jablonski diagram.*

Fluorophores preferentially absorb photons whose electric vectors are aligned parallel to the transition moment of the fluorophore. The transition moment has a defined orientation in the fluorophore. In an isotropic solution,

fluorophores are molecules oriented randomly. Upon excitation with polarized light, one selectively excites those fluorophore molecules whose absorption transition dipole is parallel to the electric vector of the excitation. This selective excitation of a partially oriented population of fluorophores results in partially polarized fluorescence emission. The transition moments for absorption and emission have fixed orientations within each fluorophore, and the relative ngle between these moments determines the maximum measured anisotropy. The ***fluorescence anisotropy (r)*** is defined by

$$r = \frac{I_{||} - I_{\perp}}{I_{||} + 2\,I_{\perp}}$$

where $I_{||}$ and $I_{\perp}$ are the fluorescence intensities of the vertically ($||$) and horizontally ($\perp$) polarized emission, when the sample is excited with vertically polarized light. Several phenomena can decrease the measured anisotropy to values lower than the maximum values. The most common is rotational diffusion occurring during the lifetime of the excited state and then displacing the emission dipole of the fluorophore. Measurement of this parameter provides information about the relative angular displacement of the fluorophore between absorption and emission. Being very sensitive to any factors which affects the rate of rotational diffusion, measurements of fluorescence anisotropy are widely used to study the hydrodynamic properties of macromolecules or large aggregates in general.

- **Resonance Light Scattering (RLS)[9]**

Light scattering is a common event of our daily life: rainbows, sunrises and sunsets originate from scattered rays of photons interacting with particles such as dust, cloud and smog in the medium like air. Scattered light can emit in all

directions except that of the incident light beams propagated and are strongly related to the inhomogeneity of the medium. Depending on the size of the photon-interacted particles (d) and the wavelength of incident light beam (λ_0), light scattering can be classified in Mie ($d >> \lambda_0$), Tyndall ($d \cong \lambda_0$), and Rayleigh scattering ($d \leq 0{,}05\ \lambda_0$) and it can be divided also in elastic scattering and quasi-elastic scattering. The next one results from the Brownian movement of the scatters and can be named as dynamic light scattering.

These light scattering phenomena, if coupled with laser technique, have been extensively applied to polymer, colloidal and pharmaceutical sciences, including measurements of the size and distributions of polymer particles, colloids, drug powders and self-assemblies of biopolymers. Nevertheless in those cases this optical method was only marginally successful; in these experiments in fact the absorbing species did not form aggregates with good electronic coupling among the chromophores under any of the experimental conditions.

Recently Pasternack et al. found that this spectroscopic technique could be successfully applied in aggregation experiments for chromophores like porphyrins and chlorins. They showed in fact that it not only meets sensitivity and selectivity criteria but offers the additional benefits of versatility and simplicity, basically requiring an ordinary double-monochromator fluorimeter and a software control.

For a better understanding of the scattering phenomena here will be reported the basic theory of RLS.

In general, two processes occur when light passes through a solution of aggregates. If the solvent itself is nonabsorbing , then energy is removed from the incident light through absorption and scattering by the aggregates. The light scattering component is a consequence of differences in polarizability between aggregates and the solvent. The incident electromagnetic wave induces on oscillating dipole in the assembly, which radiates light in all directions. The ratio

of the rate of energy absorption from the incident beam to the intensity of the incident beam is called the *absorption cross section*, C_{abs}. The ratio of the rate of energy scattering out of the incident beam (in all directions) to the intensity of the incident beam is called the *scattering cross section*, C_{sca}. If the induced dipole can be considered ideal- which is usually a valid assumption if the size of the aggregate is small compared to the wavelength of the light in the solvent, λ_m-

$$C_{abs} = k_m \alpha_i$$

both cross sections are related to the polarizability of the aggregates in simple ways:

$$C_{sca} = \frac{k^4_m}{6\pi} |\alpha|^2 = \frac{k^4_m}{6\pi} (\alpha_r^2 + \alpha_i^2)$$

where k_m is the wave vector of light in the solvent ($k_m=2\pi/\lambda_m$), and α_r and α_i are the real and the imaginary parts of the polarizability of the aggregates, respectively.

Absorption at a certain wavelength band by a solution of aggregates can be understood as the result of a maximum in the imaginary part of the polarizability in that region of the spectrum; the absorbance A of a sample of thickness L is

$$A = 2.3^{-1} \left(\frac{N}{V} \right) C_{abs} L$$

where N/V is the number of aggregates per unit volume. The real and imaginary parts of α are related to each other, so that when α_i is maximized in some wavelength range, α_r also behaves anomalously in this region; hence, $|\alpha|^2$ is at a maximum in the absorption band, which also results in increased scattering.

Under normal conditions this increased scattering is difficult or impossible to detect because of the increased absorption and the weakness of the enhanced

scattering effect. However, when this effect is investigated for aggregates of chromophores such as porphyrins, the enhanced RLS scattering can be enormous. For a solution of a fixed concentration of the aggregating component the absorption, depending on the first power of polarizability, which in turns depends linearly on the volume of the aggregate will exhibit no change in A as aggregation occurs, because the product of N/V and α_i remains constant. On the contrary, the amount of scattering depends on the square of the volume of the aggregate, and thus it increases as a consequence of aggregation phenomena; RLS is therefore extremely sensitive to even low concentrations of extended aggregates. This effect is observed at or very near the wavelength of absorption of an aggregated molecular specie and is can be enhanced by several orders of magnitude when strong electronic coupling exists among the chromophores. In addition, the wavelength dependence of this technique allows for selective observation of aggregates, even in multicomponent systems that include a large fraction of monomers or other aggregates.

- **Circular Dichroism (CD)**

Circular dichroism[10] is a spectroscopic technique useful for the determination in solution of the structure of different molecular aggregates, as proteins, polypeptides and porphyrin aggregates. It measures the optical activity of molecules in solution and its variation can be related to aggregation mode, providing crucial information about the interactions between monomers in the larger structure. It's a quick and non destructive technique that doesn't require large amounts of samples and extensive data processing. It can be used to survey with accuracy a large number of solvent conditions, varying pH, temperature, ionic strength and presence of various cofactors.

Circular dichroism is observed when the molecules in solution absorb the left- and right-handed circularly polarized light in a different way. As a result, the

recombination of the two components doesn't give linearly polarized light (Fig.2.7a), but elliptically polarized (Fig.2.7b).

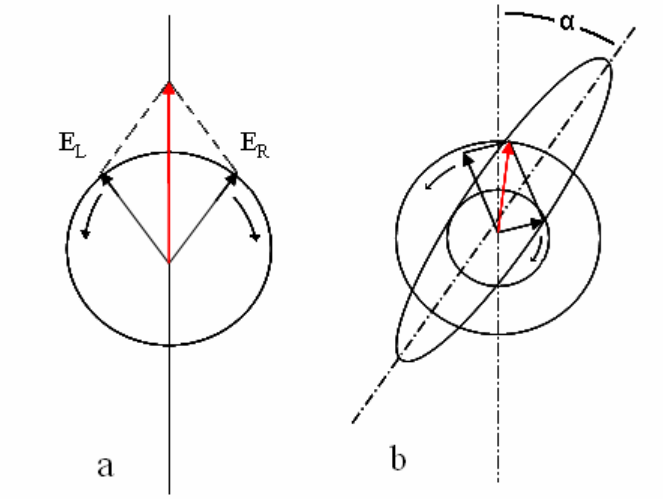

Fig. 2.7 *– Schematic description of the basic concepts of circular dichroism.*

At a given wavelength,

$$\Delta A = A_L - A_R$$

where ΔA is the difference between absorbance of left circularly polarized (LCP) and right circularly polarized (RCP) light (this is what is usually measured). It can also be expressed, by applying Beer's law, as:

$$\Delta A = (\varepsilon_L - \varepsilon_R)Cl$$

where ε_L and ε_R are the molar extinction coefficients for RCP and LCP light, where *C* is the molar concentration and l is the path length in centimeters (cm). Then

$$\Delta\varepsilon = \varepsilon_L - \varepsilon_R$$

is the molar circular dichroism. This is what is usually meant by the circular dichroism of the substance. Although ΔA is usually measured, for historical reasons most measurements are reported in degrees of ellipticity. Molar circular dichroism and molar ellipticity, [θ], are readily interconverted by the equation:

$$[\theta] = 3298\Delta\varepsilon$$

In general circular dichroism is exhibited in absorption bands of any optically active molecule. This activity is commonly related to molecular dissymmetry: as a consequence, many biological molecules display this phenomenon, because of the dextrorotary (e.g. some sugars) and levorotary (e.g. some amino acids) molecules they contain. Noteworthy, a supramolecular arrangement of molecules can also impart a distinct CD signal, even if they are symmetric. In this case they may also present supramolecular chirality by

- forming intrinsically chiral assemblies;
- aggregating onto chiral polymeric templates, as nucleic acids or peptides (extrinsic chirality);

The latter case leads to induced circular dichroism bands (ICD) which, having a conformational origin (i.e. , arising from self-organization of the achiral monomer by chiral templates), modify or disappear following matrix conformational transition. The intensity of the resulting CD signals depends both on the features of the assembled chromophores and the geometrical organization of the whole aggregate.

In particular, in large, dense and chiral aggregates the excitation can be delocalized throughout the entire particle[11]. The extent of the delocalization depends in turn on the strength of the coupling among chromophores. This coupling is determined by the extinction coefficient of the isolated chromophores, their density in the aggregate, their spatial relationships in space, their spatial extension, the dimensionality of the aggregates, and the degree to which the long-range chirality of the aggregate matches the wavelength of the incident light. When the requirements for delocalization are met, the aggregate reacts as a single entity, via a series of a *collective* modes of excitation; the delocalization can extend to dimensions comparable to the size of the whole aggregate. If the packing of the aggregate is chiral, certain collective modes can

be preferentially excited by one circular polarization over the other, giving rise to preferential absorption (CD) signals.

Moreover aggregates with a low chromophore density can still display strong delocalization if the individual chromophores possess large extinction coefficients. This is because the chromophore interaction and therefore the efficiency of delocalization is proportional roughly to the square of the extinction coefficient of the chromophores. Similarly, a highly structured chromophore organization can compensate for a low extinction coefficient of the chromophores or a somewhat smaller size of the aggregate.

In conclusion a conjunction of two effects - high values of extinction coefficients and an ordered spatial arrangement of the dyes in the aggregate – could afford very intense CD signals.

2.2.3 Applications of Porphyrin Assemblies

The controlled organization of functional cromophores into highly ordered self-assembled arrays is an area of research[12] with great potentials in many different fields such as materials science, the construction of systems mimicking biological functions or sensors applications. These sophisticated architectures yield, in general, new materials that exhibit unique photophysical and (opto)electronic properties as a result of excitonic interactions between adjacent dye units useful for a specific application.

Over the last decade a large number of studies has been devoted to creating artificial, highly ordered arrays of chromophores with the final goal to construct devices that can usefully capture light and utilize the excitation energy to realize a long-range vectorial transfer to a specific acceptor point. Among the innumerable investigations on ***biomimetic systems*** "inspired" by Nature, important studies were performed on the chlorosomes, unique organelles evolved

by green photosynthetic bacteria, that can efficiently capture sunligt through a collection of densely packed chromophores, such as bacteriochlorophylls (BChls) *c*, *d* or *e* and carotenoids. In this organelle BChl molecules self-organize without the use of proteinaceous scaffolding. In effect, the chlorosome is the most efficient antenna known. This is in part due to the large size of its structure and the large number of pigment molecules inside, tipically 10^5 BChl molecules. These molecular units self-assemble into large suprastructures, which exhibit exitation energy transfer without significant quenching of fluorescence. Perhaps because of the large size and the unusual organization compared to the majority of photosynthetic systems, no crystals of chlorosomes or aggregated BChls have been obtained until recently and only several models were proposed on the basis of freeze-fracture electron microscopy and spectroscopic constraints.

Pšenčik and co-workers[13] recently have obtained the first high-resolution images of chlorosomes from the green sulphur bacterium *Chlorobium tepidum* by cryoelectron microscopy. The model proposed described a simple lamellar organization of pigments molecules, in contrast with previous models in which BChls were aggregated into rod-like elements.

In the same period Balaban and co-workers[14] reported several model compounds constituted by various zinc porphyrins containing hydroxyl and acetyl substituents (Fig 2.8) and investigated the ability of such systems to mimic the self-assembly ability of BChls *c*, *d* or *e*. The synthetic molecules they studied possessed features essential for the self-assembly algorithm to be able to operate, that are:

- the ligation of the central magnesium atom by the 3'-hydroxy group of another molecule;
- cooperative hydrogen bonding of the same OH group to the 13'-carbonyl group of a third BChl *c* molecule;

- π-π interactions between the chlorine macrocycles, which are organized into stacks.

In nonpolar solvents, the molecules investigated self-assemble: the UV-vis spectra are severely broadened and a nonzero absorption coefficient is found between 400 and 700 nm, which is beneficial for light harvesting over a broad spectral range. The degree of aggregation is controlled by peripheral substituents on the porphyrin macrocycles. Highly untypical for aggregated chromophores, the fluorescence of the systems investigated is not quenched and intense emission is observed both in solution and in a solid film, which is attributed to the high ordering and the absence of coordination quenching.

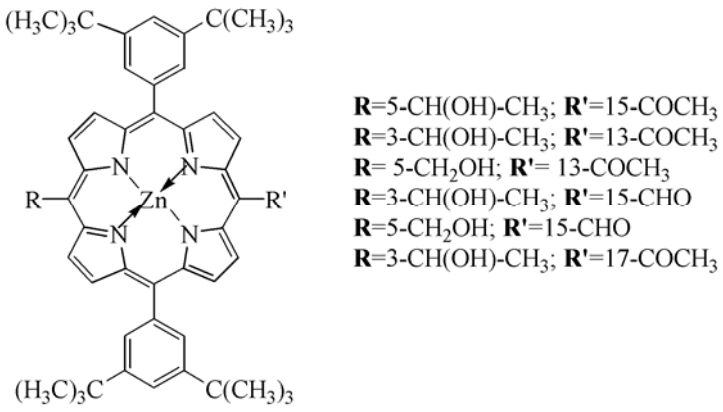

Fig. 2.8 *– Synthetic mimics for the natural BChls reported bt Balaban and co-workers.*

In these assemblies extensive π-π stacking of the macrocycles are the dominant interactions, being no evidence of hydrogen bonding between stacks, that is probably prevented by either the interaction of the CO group with the zinc atom or cohesive forces between the porphyrin and the surrounding cyclohexane solvent, or a combination of both.

The intense signals of fluorescence observed for these aggregates also in a film cast allowed photosensitization of a wide band semiconductor, such as TiO_2 nanoparticles. Self-assembled zinc porphyrins onto this inorganic substrate

afforded bright spots proving that fluorescence was coming out from the porphyrin aggregates. This excellent fluorescence properties of these assemblies made them interesting and cheap candidates for applications in solar cells.

Moreover the exploration of porphyrins, metalloporphyrins and their assemblies afforded a large number of ***nanomaterials*** featuring various electronic and structural characteristics, like rods, rings, particles, sheets, wires and tubes. Those structures have been prepared with or without templates, rather than formed by virtue of J-aggregation due to intermolecular π-π interactions of planar porphyrins and metalloporphyrins.

Metalloporphyrins-based functional materials have been represented by porous materials reported by Suslick and co-workers[15], consisting of Co(III)(porphyrin)-Co(II) trinuclear clusters, which exhibited selective and reversible absorption properties toward various organic compounds.

In order to create various shape and size of assemblies very recently Kojima[16] and co-workers choose a different type of building block other than the usual planar porphyrin, focusing on a saddle-distorted metalloporphyrin, Mo(V)-dodecaphenylporhyrinato complex [Mo^{V}(DPP)(O)(OMe)], which could provided in principle a "curved surface" useful to give tubular nanostructures via non covalent self-assembly. The slow cristallization of this complex gave the porphyrin nanotube that has a nanosized *hydrophilic* environment in its inside which facilitates inclusion of hydrophilic entities such as Mo-oxo clusters inside of *hydrophobic* porphyrin aggregates.

The tubular assembly is derived from intermolecular π-π interactions of alternatively inserted peripheral phenyl groups and intermolecular hydrogen bonding with tetranuclear Mo(VI)-oxo clusters: probably they could be formed and protected in accordance with the porphyrin aggregation in the hydrophilic cavity, and they could also act as templates for the tube stabilization. Schematic description of the porphyrin nanotube formation is given in Fig. 2.9.

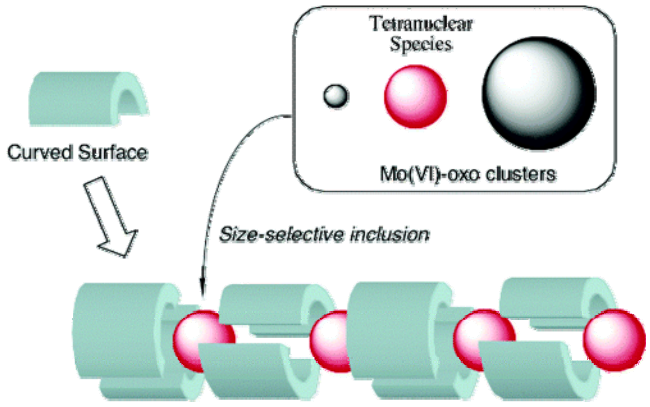

Fig. 2.9 *– Schematic description of the nanotube formation with curved surface concomitant with the size-selective inclusion of Mo(IV)-oxo clusters..*

A remarkable feature of this tubular structure is the formation of the hydrophilic isolated inner sphere in the hydrophobic porphyrin supramolecule.

The peculiar features exhibited by porphyrins and the assemblies they form concerning molecular recognition make them also excellent candidates as sensitive materials for ***sensors applications***[17]. In this particular field of research is required the transduction of the recognition event to an external signal (optical, electrical, etc.). One of the most used and simple ways of signal transduction is obtained by monitoring fluorescence, mainly because it's a powerful visual phenomenon, its sensitivity is several orders of magnitude higher than that of absorption spectroscopy and a spectrofluorimeter is a piece of equipment commonly available in many scientific laboratories. As a consequence, a large number of fluorescent sensors based on porphyrin aggregates for pH measurement or metal ions detection have recently been designed and developed by means of a non-covalent strategy.

Purrello and co-workers reported that water-soluble tetraanionic mesotetrakis(4-sulfonatophenyl)porphine (H_2TPPS) and some its metalloderivatives, whose structures are reported in Fig. 2.10, interacts with a polymeric matrix of polylysine, leading, under appropriate experimental

conditions, to the formation of supramolecular aggregates[18]. Even if many processes contribute to the polymer-induced self-aggregation of the porphyrins, the very first recognition event is primarily driven by electrostatic interactions: those between the negatively charged peripheral groups of the porphyrins and the protonated side chains of the matrices and those among porphyrins themselves.

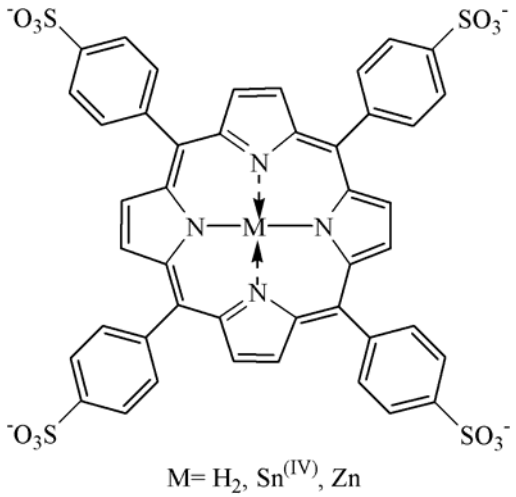

Fig. 2.10 *– Molecular structures of meso-tetrakis(sulfonatophenyl)-porphine and the relative metal complexes.*

As occurs commonly in aggregation process, the fluorescence owned by chromophores in the monomeric form is quenched by aggregation. Since it's possible to control porphyrin fluorescence and hence by varying pH by modulating the interactions between the anionic porphyrins and the protonated polylysine, such a self-assembled system can behave as a supramolecular fluorescent "pH-sensor".

In particular the stability toward pH of these supramolecular aggregates seems to be related to their size, which can be finely tuned by changing:

- the polylysine to porphyrin ratio;
- the pH;

- the steric features of porphyrins (e.g. the central metal ion), which mainly affect the lateral distribution of the porphyrins along the polymer matrix and hence the quenching.

Spectrofluorimetric pH-titrations show that, in the absence of polylysine, the fluorescence intensity of H_2TPPS does not change in the investigated pH range (5 ÷11.5) (Fig. 2.11). On the other hand, in the presence of polylysine, the profile of the fluorescence intensity vs pH shows a sigmoidal shape (Figure 2.11). Back-titrations with HCl show that these aggregation processes are fully reversible. Therefore, it turns out that such sigmoidal shape must be due to the equilibrium between aggregated and free anionic porphyrins.

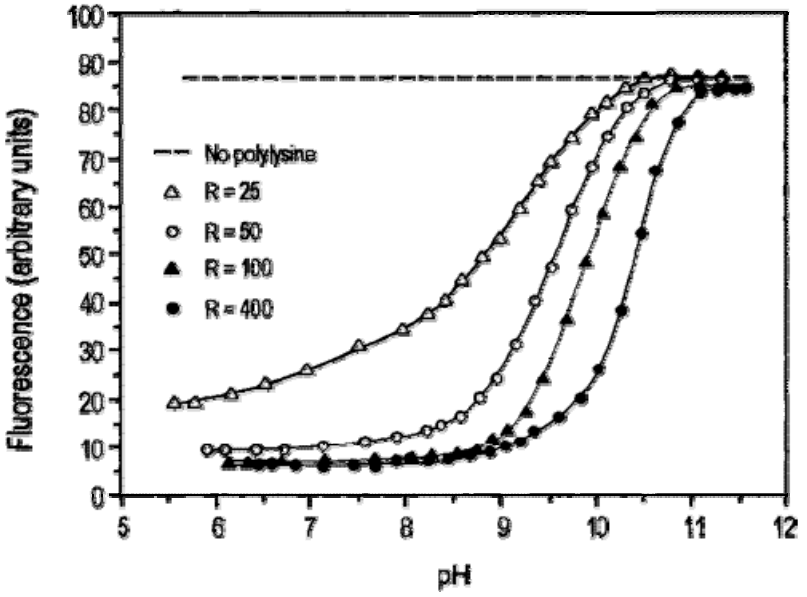

Fig. 2.11 *– pH dependence of the fluorescence emission (λ_{ex} = 405nm, λ_{em} = 640 nm) of H_2TPPS (1 μM) in the presence (continuous lines) and in the absence (dotted line) of polylysine.*

Here, fluorescence variations report only the porphyrins aggregation state, and the pH dependence of the equilibrium indicates that the formation of the supramolecular species is triggered by the presence of positively charged amino groups of polylysine. Thus, at low pHs (≤7), where polylysine is extensively protonated, the equilibrium is shifted toward binding and concomitant

aggregation (strong fluorescence quenching in Fig. 2.11). Here, only the bound porphyrins in aggregated form (dimers, trimers, ...) contribute to the emission quenching. At pHs higher than 9-10 the porphyrins tend to dissociate from the polylysine matrix and eventually exist as monomers in solution (no fluorescence quenching in Fig. 2.11).

Interestingly, the authors observed that the molecular recognition process leading to the formation of these aggregates can be modulated by using porphyrins containing different central metal ions with particular coordination geometry.

The same experiments achieved on a hexacoordinated Sn^{IV}TPPS-Polylysine system afforded different results. The spectral variations are much less pronounced than those observed for the analogous system with the free-porphyrin and Sn^{IV}TPPS fluorescence is only slightly quenched in the presence of the matrix, confirming that the quenching observed for the H_2TPPS-polylysine system must be mainly due to the short range porphyrin-porphyrin interactions, as those occurring in self-assembled structures.

The spectrofluorimetric titrations of the ZnTPPS-polylysine system are similar to those described for H_2TPPS, but in this case small aggregates pertain a series of subsequent equilibria which leads to high apparent pK values. Moreover, at pH between 7 and 8 an additional fluorescence inflection in the tritations, probably due to the deprotonation of the axially bound water to the zinc., appears.

It's important to underline that in this case the term sensor is not used to indicate a device, but rather a chemical system able to recognize a species and to report its recognition (e.g. by spectroscopic variations).

Another example of chemical sensor based on amphiphilic porphyrin aggregates was reported very recently by Monti and co-workers[19]. In a previous study[20] they observed that the deposition of an aqueous solution (H_2O/EtOH 9:1 v:v) of the amphiphilic porphyrin derivative reported in Fig.2.12 occurred

spontaneously on silanised glass surfaces, in a controlled J-type aggregation fashion, giving solid films presenting, beside a good mechanical stability, an appreciable fluorescence emission.

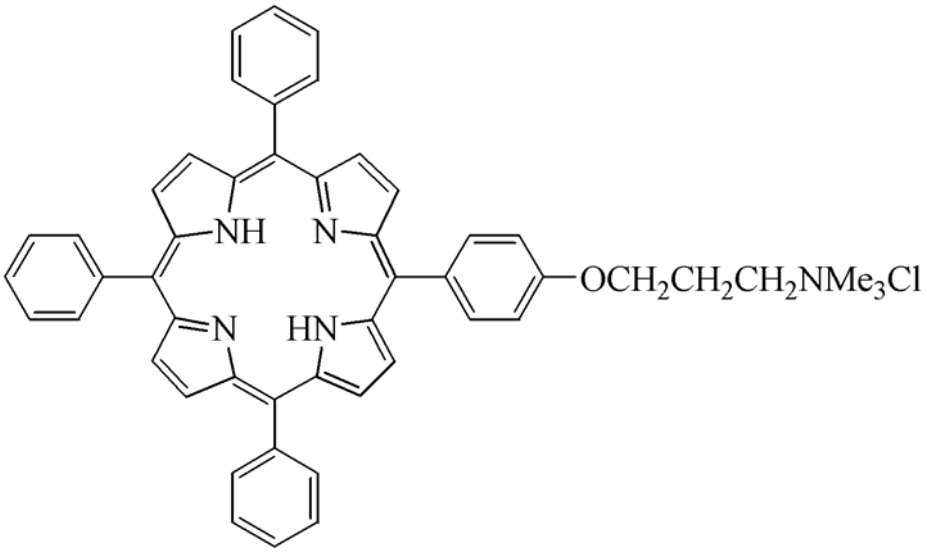

Fig. 2.12 *– Molecular structure of the cationic amphiphilic porphyrin prepared by Monti and co-workers.*

This property can be a crucial feature in the sensing of heavy and transition metal ions that typically quench the luminescence, often via deactivation to the triplet state by heavy metal atom effect. On the basis of these interesting results they investigated the potentialities of these simple systems for the construction of an efficient and specific luminescent solid-state chemosensor for the selective detection of Hg^{2+} ions in water.

They observed that the porphyrin emission was strongly quenched by simply dipping the porphyrin layered glass slides into diluted solutions of heavy metal salts, as reported in Fig. 2.13 that depicts the efficient quenching of fluorescence emission of layered porphyrins by simple immersion into a solution of Hg^{2+} 1.0×10^{-5}M (Fig. 2.13, trace d). Moreover the initial intensity could be

restored by washing with a solution of *N,N,N',N'*-tetrakis(2-pyridilmethyl)ethylenediammine (TPEN) with no loss of efficiency.

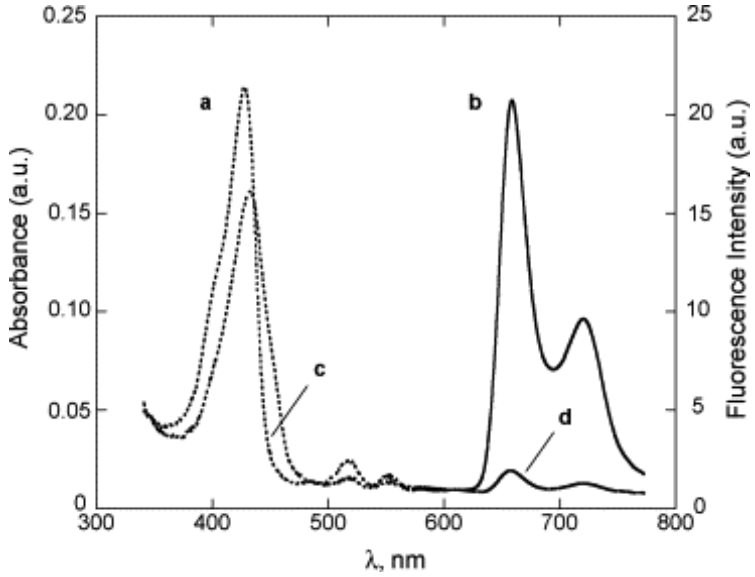

Fig. 2.13 *– Absorption (dashed lines) and emission (solid lines, λ_{ex} 420 nm, λ_{em} 654, 720 nm) of porphyrin layers at different Hg^{2+} concentrations.(a and b) $[Hg^{2+}] = 0.0$ M; (c and d) $[Hg^{2+}] = 1.0\times10^{-5}$ M.*

A consistent quenching was also observed in the case of lower Hg^{2+} activity, as low as 1μM concentration, pointing out the appreciable sensitivity of the investigated system. The concomitant examination of the UV–vis spectral pattern changes revealed the occurrence of a bathochromic shift of the porphyrin chromophores upon metal ion interaction, indicating the onset of coordinative interactions between the porphyrin core and the mercuric ion.

To test the reversibility and the stability of the system in operative conditions OFF/ON cycles (i.e. quenching with Hg^{2+}, restoring in a TPEN solution) were also performed. The results are graphically reported in Fig. 2.14 and show that a cycle can be repeated several times, with no appreciable loss of sensitivity, and dissolution of the film.

Moreover the authors extended this protocol to a flow-trough device.

To study this issue, a porphyrin coated flow-through quartz cell was used and the fluorescence emission responses, upon passage of Hg^{2+} solutions, analysed. Also in this case, a quenching of fluorescence was observed, when a solution of Hg^{2+} passed through the cell. The fluorescence change was found to be dependent on the ion concentration.

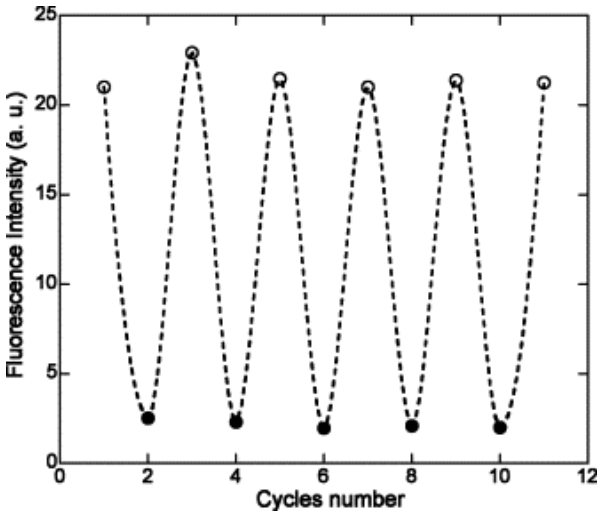

Fig. 2.14 *–ON/Off cycles of porphyrin layers in different aqueous solutions.*

More interestingly a good selectivity of the porphyrin layer responses with respect to other transition and post-transition metal ions, such as Cd^{2+}, Pb^{2+} and Cu^{2+} was observed. Appreciable quenching of fluorescence, in fact, resulted only in the presence of more concentrated solution (mM range) of the corresponding ions, as shown in Fig.2.15.

Competition experiments revealed negligible interferences by the other metal cations. The spectroscopic changes featured in the presence of Hg^{2+} 1×10^{-5}M remained unaffected by further addition of Cd^{2+}, Cu^{2+} and Pb^{2+} up to 100 μM.

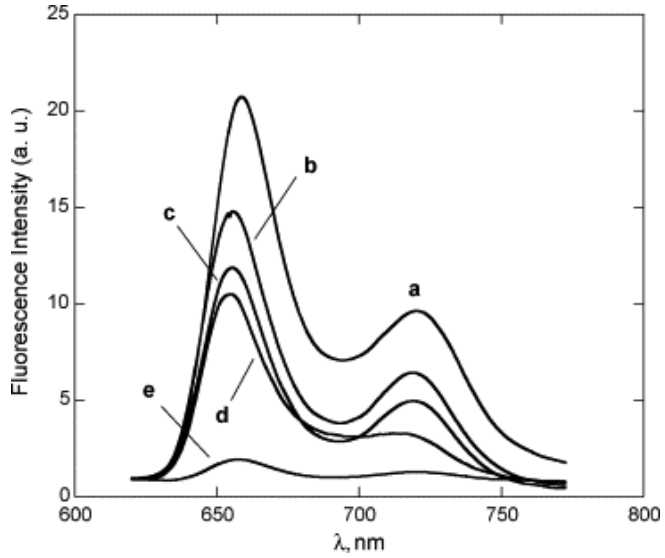

Fig. 2.15 *– Fluorescence emission (λ_{ex} 420 nm) of porphyrin layers in different solutions. (a) H_20, (b) Cd^{2+} (saturated solution), (c) Cu^{2+} (1.0×10^{-3} M), (d) Pb^{2+}(1.0×10^{-3} M) and (e) Hg^{2+} (1.0×10^{-5} M).*

Conversely, a quenching effect could be observed upon addition of Hg^{2+} (10μM) to a still emissing solution of the other cations (≥100μM). The inspection of the UV–vis spectra upon addition of cations other than Hg^{2+} did not reveal evident perturbation of the porphyrin electronic states. The Soret band remained, in fact, virtually unchanged either at high concentration of added Cd, Cu or Pb cations. This finding safely rules out, in these latter cases, the occurrence of metal co-ordination.

2.3 Chiral Porphyrin Aggregates

The control and tuning of the spatial disposition of atoms and molecules is a field of ever growing interest because it can have dramatic consequences in chemical systems[21]. For example some enzymes only catalyze the reaction of one enantiomer leaving the other enantiomer unchanged. Also in materials science, chirality has great effects: the use of one enantiomer instead of the racemic

mixture increases the second-order non linear optical (NLO) susceptibility about 30 times. Since it's accepted that aggregation and self-assembly play an important role in the origin of life, it's easy to understand the great attention devoted to chiral aggregates. They in fact could be used as models for the symmetry-breaking processes that lead to optically active systems in primitive biosphere models. Furthermore, the optical properties of the aggregates of these dyes suggest potential applications for their chiral phases. However, in noncovalent sysnthesis the formation of chiral self-assembled aggregates is still in its infancy, due to the highly dynamic character of noncovalent interactions. Despite of this inconvenient feature in the last decade a large number of investigations has been carried out on this topic.

Among the main objects of these studies porphyrins attracted great attention: the control of chirality in porphyrin-based self-assembling architectures in fact constitutes a mandatory step for the construction of systems mimicking biological functions, such as, for example, cytochrome P-450 activity[22] or antenna systems of phosynthetic bacteria[14]. Moreover the achievement of solid-state porphyrin systems possessing elements of supramolecular chirality would be also of important application in the field of sensors and molecular materials.

2.3.1 Supramolecular chirality of porphyrin assemblies: concepts[21].

It is well known that chirality at the *molecular level* is displayed when the atoms of a molecule are arranged in one unique manner in space. This different arrangement is due to the presence of a chiral centre or the absence of planes of symmetry.

Similarly chirality is also expressed at the *supramolecular level*. Supramolecular chirality involves the nonsymmetric arrangement of molecules in

a noncovalent assembly. This can be initiated by the properties of the components, i.e. one or more of the components are asymmetric, or the achiral components associate in such a way that the assembly has no elements of symmetry.

It should be emphasized that chirality at molecular level is not a prerequisite to observe chirality at the macroscopic level, that is, it is not essential to have chiral molecules as building blocks.

All the assemblies that have an asymmetric arrangement of their building blocks are chiral. The general method to control the supramolecular chirality is the introduction of chiral centers in the components (asymmetric induction). In this way, the resulting chiral assemblies exist as two different species that have a diastereomeric relationship. This approach is called "induction of chirality" or "diastereoselective noncovalent synthesis".

Thanks to the peculiar electronic and optical properties of porphyrins, the formation of a chiral aggregate based on this macrocycle is very convenient to follow by spectrophotometric methods. Their aggregation performed under certain conditions give rise to an asymmetric perturbation of the chromophore which can be traced as a circular dichroism (CD) band in its UV-absorbing region. Such induced CD (ICD) spectra in general can be observed in a number of situations where aggregation between chiral and achiral partners takes place, when the conditions are such that the effect from the perturbation can be studied by CD. In particular chiral porphyrin aggregates reported in literature were generated using different methods.

The straightforward way to achieve a supramolecular assembly espressing elements of chirality is the introduction of a chiral functionality on the porphyrin periphery that is transferred to the macroscopic superstructure during the aggregation event[23]. A very common way to generate a chiral assembly consists in aggregating porphyrins onto chiral templates[24], like aminoacids, polypeptides,

DNA or biomembranes. In this case, the achiral components (porphyrins) "follow" the templated helicity of chiral components (biological matrices).

Recently some papers reported that completely achiral porphyrin could possibly lead to chiral assemblies[25], by a simple physical treatment, like stirring and annealing.

In the next paragraph all these modes will be discussed in details.

2.3.2 The main methods of generating chiral porphyrin assemblies

- **Self-aggregation of a chiral porphyin**

The simplest method to generate a chiral aggregate was the introduction of a chiral center into the porphyrin structure and a nice example was very recently reported by Monti and co-workers[23]. They prepared an amphiphilic tetraarylporphyrin possessing a chiral cationic functionality on a pheripheral phenyl group, namely (L)-prolinium moiety, whose chemical structure is reported in Fig. 2.16.

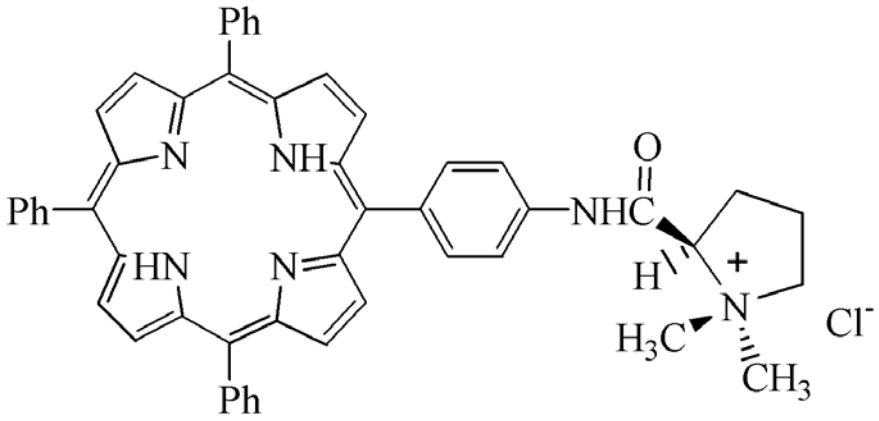

Fig. 2.16 *– Structure of the chiral amphiphilic porphyrin prepared by Monti and co-workers..*

They showed that this macrocycle not only can aggregate in larger structures exhibiting chiral features, but especially pointed out the possibility of tuning the morphology, and then the supramolecular chirality, of these porphyrin aggregates by simple changes of solvent composition. In fact the medium effect and solvent interactions with the molecular components of whole systems can play a key role in such association processes, thus influencing stereochemistry and consequently the degree of induced chirality of the assembly.

In literature a large number of examples of the solvent effect on the asyemmetry transfer were reported and recently a rational investigation of this *"solvodichroic effect"* was reported by Borovkov and co-workers[26] about a supramolecular chiral zinc porphyrin system.

Monti and co-wokers performed the aggregation experiments in mixed water-ethanol solvent mixtures. While in the composition range of 100% to 50% ethanol (v:v) the macrocycle is in monomeric form, the increase of water proportion in the solution promotes the self-aggregation process, as witnessed by the broadening and bathochromic shift of the Soret band (Fig. 2.17b). CD and UV-vis spectroscopies revealed that the aggregation of these chiral units induces the formation of large chiral superstructures, steered by the presence of the appended chiral functionality. Remarkably, the organisation and the resulting chirality of the aggregates are strongly controlled by the composition of the solvent, as indicated in Fig. 2.17a.

In fact, the aggregation promoted in 75% H_2O results in the formation of porphyrin superstructures featuring CD signals of 1-2 orders of magnitude larger than those obtained at a higher water proportion (90% H_2O). This can be explained in terms of the rate of the aggregation: in water/ethanol (90:10 v:v)

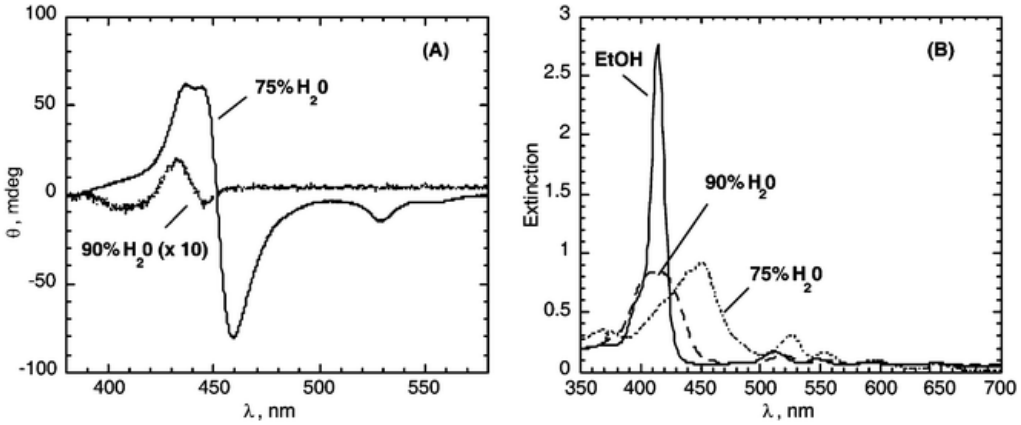

Fig. 2.17 *– a) CD spectra of chiral porphyrin in different aqueous solvents. b) Extinction spectra of chiral porphyrin in different media: EtOH (—); H_2O–EtOH 75:25 (v:v) (……); H_2O–EtOH 90:10 (v:v) (- - - -).*

porphyrins aggregate completely within the time of mixing, affording aggregates with poorly defined structure; on the contrary, at higher ethanol proportions (75% H_2O), a slower aggregation process is onset, resulting in the formation of probably J-type structures indicated by the red shifted Soret band with λ_{max} at 460 nm (Fig.2.17b).

Moreover, RLS experiments indicated that solvent composition also strongly influences the size of the porphyrin aggregates: in H_2O-EtOH 75:25 (v:v) the relative scattering signals are markedly more intense (up to two-fold) than those observed in the case of aggregation in H_2O-EtOH 90:10 (v:v). In this latter experiment, the onset of less specific π-π stacking or other hydrophobic interactions becomes overwhelming, promoting the formation of less structured, smaller porphyrin aggregates in a faster process.

- **Aggregation of achiral porphyins on chiral templates**

Another simple strategy for "building" tailored supramolecular chiral species consists of aggregation of achiral porphyrins on biopolymeric, then chiral, matrixes. All the works concerning this type of systems have been inspired by the seminal studies carried out by Pasternack, in which cationic

meso-substituted porphyrins and their metalloderivatives were employed as probes of nucleic acid structure and dynamics[11]". Under appropriate conditions of concentrations and ionic strength, some of these macrocycles aggregated extensively in water and bound to both condensed and noncondensed DNA or helical polypeptides to produce intense bisignate circular dichroism spectra whose profile revealed the helical sense of the biopolymer, which served as a template for the aggregation process.

Later, a very large number of investigations on this topic were carried out, since these systems can be useful for many biomedical and technological applications.

Binary systems "porphyrin-chiral polymeric matrix" carrying opposite charges have been extensively investigated and characterized [24d], but recently a great interest was addressed to ternary systems constituted by cationic and anionic porphyrins aggregating onto a polymeric charged template in a specific mode.

Purrello and co-workers[27] reported the formation of chiral ternary heteroaggregates in which cationic porphyrins acted as "spacers" between an anionic chiral polymeric matrix and anionic porphyrins. In particular they used some metal derivatives of meso-tetrakis(N-methylpyridinium-4-yl)porphine (MT4) as cationic porphyrins having peculiar steric and electronic properties, the meso-tetrakis(4-sulfonatophenyl)porphine (H_2TPPS) as anionic porphyrin and polyglutamic acid as a matrix. Using ZnT4 as cationic porphyrin they obtained very interesting results. Fig.2.18 shows the absorption spectrum (curve a) of a solution of H_2TPPS (5μM) at pH 2.9 in the presence of poly-L-glutamate (50 μM) and ZnT4 (5 μM).

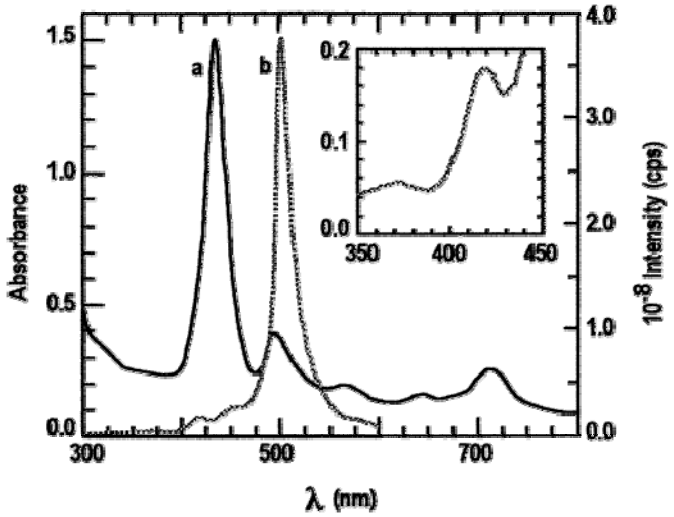

Fig. 2.18 *– Absorption (a) andRLS (b) spectra at pH 2.9 of H_2TPPS (5μM) in the presence of ZnT4 (5μM) and poly-L-glutamate (50 μM).*

Together with the expected band at 436 nm (due to the absorption of both ZnT4 and H_4TPPS) there are two additional bands at about 490 nm and 700 nm. In addition, the RLS spectrum (Fig.2.18, curve b) shows a very intense band at about 500 nm and a smaller signal at about 720 nm (not shown). The RLS and absorption bands observed around 500 and 700 nm are diagnostic of the presence of H_2TPPS J-aggregates. In the RLS spectrum, a feature at 420 nm (inset of Fig.2.18) have been also observed, which might be assigned to the formation of H-type aggregates.

The presence of the cationic porphyrin ZnT4 was essential, in that experimental conditions, for the formation of H_2TPPS aggregates. In fact, in the absence of ZnT4, none of the spectroscopic features associated with aggregation of the protonated form of H_2TPPS has been observed. Surprisingly they observed that using the same concentrations of H_2TPPS and poly-L-glutamate and one-fifth of the stoichiometric amount of ZnT4, the intensity of the CD bands was reduced only by 30%. This observation indicated that anionic and cationic porphyrins were not forming the 1:1 heteroaggregates and suggested that ZnT4 served as a "spacer" to minimize the repulsion between the two negative

components. ZnT4 most likely was monodispersed on the matrix, shielding the negative charges: this allowed the anionic porphyrins to approach the (partially) anionic chiral polypeptide and gain chirality. Moreover, when poly-D-glutamatic acid was used, they observed the mirror image of the CD features, confirming that the aggregates of the anionic porphyrin can be able to read out chirality of the polypeptide matrix even though they interact with it only indirectly, "through" the cationic porphyrin. The same authors also investigated a very similar ternary system, using almost the same components, but adding the anionic porphyrin H_2TPPS to a solution of a preformed binary complex between α-helical polyglutamate and the cationic porphyrin CuT4[28]. In the pH range 3.2-4.0 the latter compound interacts with poly-L-glutamate forming a kinetically labile chiral binary complex. The addition of H_2TPPS (in the same pH range) to such species induces drastic changes in the absorption, fluorescence and CD spectra, indicating the formation of chiral ternary complexes. In particular, both the shape (bisignate) and the unusually high intensity of the induced CD feature (Fig.2.19, curve a) strongly indicated that both porphyrins are extensively aggregated onto the matrix. When H_2TPPS was added to a preformed CuT4-poly-D-glutamate complex, the mirror images of the CD signals observed with the L-isomer have been obtained (Fig.2.19, curve b), indicating that the chirality of these assemblies follows the matrix chirality.

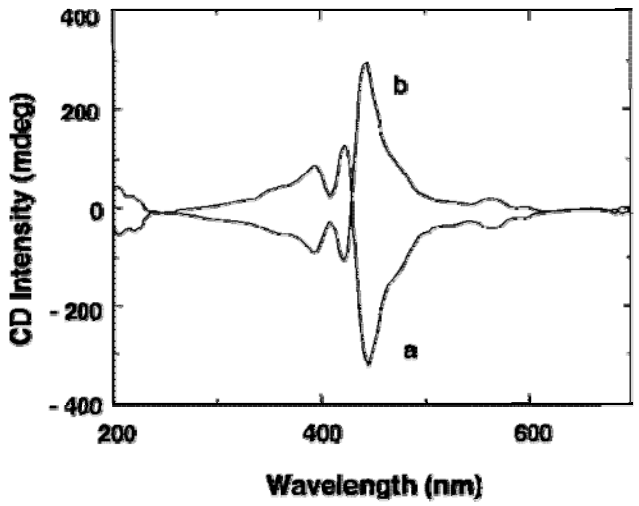

Fig. 2.19 *– CD spectra of a solution of CuT4 (4 μM) in the presence of(a) poly-L-glutamate (200 μM) and (b) poly-D glutamate (200 μM) after the addition of H_2TPPS* (4 μM).

Interestingly, these ternary complexes resulted kinetically inert compared to the parent CuT4-polyglutamate binary species. Their inertia has been clearly revealed by the lack of inversion of the induced CD bands after the addition of an excess of poly-L-glutamate to the ternary complexes "built" on the poly-D-glutamate. Another evidence of this inertia was given by the stability vs pH as well. In fact, once the ternary complexes were formed, no significant variations of the ICD spectra have been monitored by raising to ~ 12 the pH of the solution.

Recalling that at this pH polyglutamate is in a "random-coil" conformation, this finding strongly indicated that these porphyrin assemblies retained their "original" chirality, even when the matrix loses it. The role of the template is crucial only in the very first step of the formation of these ternary chiral species. In fact, once formed, these aggregates seem to have a "life" independent from the matrix but retain ***"memory"*** of the shape of the "mold" used for their formation. The aggregation of pophyrins H_2TPPS and CuT4 have been also carried out in the presence of chiral aggregates of L- or D-aromatic amino acids, leading to a simple but smart chemical system capable of autonomous growth. In particular the simultaneous aggregation of these two macrocycles onto chiral phenylalanine (Phe) clusters afforded chiral imprinted aggregates that retained the memory of the mold even after Phe removal. The formation of these inert systems was explained as a correlated sequence of induction, memory and ***amplification*** of chirality, involving only noncovalent interactions between polyanions and polycations. However, their synergism gives rise to interactions which are by no means weak. The strength of these forces is the key factor for the *memory* and *amplification* of the chiral structures.

- **Aggregation of achiral porphyrins by symmetry breakage**

Chiral supramolecular assemblies can also be formed from achiral molecules without any chiral template. The appearance of such kind of chirality

could be due to the chiral symmetry breakage. So far, the chiral symmetry breakage are usually reported in those systems such as spontaneous precipitation of enantiomorphically enriched sodium chlorate crystals,[29] chiral symmetry breakage in stirred crystallization of supercooled melt,[30] and the formation of chiral domains in liquid crystals.[31] Also in solution the spontaneous generation of enantiomerically enriched J-aggregates from achiral monomers through stirring the solution had been reported by Hada et al.[32] Recently Liu and co-workers [25a] reported one of the fewer examples of the fabrication of chiral Langmuir-Schaefer films from an achiral porphyrin (H_2TPPS) and different amphiphiles (CTAB, ODA, DOAB). The complex monolayers formed with these compounds (pH 3.1) were transferred onto quartz substrates and the spectroscopic variations of the UV-vis absorption spectra of the LS films showed that H_2TPPS can be incorporated into the LS film as a J-aggregate or H-aggregate.

Moreover those complex LS films showed also chirality. CD measurements have been obtained by rotating the film during acquisition in order to delete the contribution of the linear dichroism (LD) that can affect the CD signal in the case of LS films. Those measures revealed strong CD signals in all the LS films, even if the H_2TPPS solution didn't have in the same experimental conditions. The signal could be detected only when J-aggregate was formed and it could be either positive or negative in different deposition batch. Thes CD features clearly indicated that the complex films were chiral although both H_2TPPS and the amphiphiles are achiral. The random appearance of the CD signal excluded out the existence of any chiral impurity in the LS films. The fact that CD signals were only detected in the J-aggregate clearly indicated that chirality of the film came from the J-aggregate of the H_2TPPS in the LS film.

Remarkably, the chirality of the film was formed spontaneously, probably because of the helical (right or left-hand) alignment of the molecular plane. In fact, if the latter ones were distorted in a certain degree in one direction, then a chiral J-aggregate could be formed. Although the chance of H_2TPPS to form

right-hand or left-handed chiral J-aggregate are equal, the balance can be broken in the surface monolayer formation and/or during the film transfer and thus resulted in the chiral LS films.

In a more recent work[33], the same authors have reported that the supramolecular chirality of porphyrin assemblies from an achiral porphyrin derivative can be further amplified via thermal annealing. The formation of LS films constituted by an uncharged and achiral porphyrin, namely 5,10,15,20-tetrakis(4-methoxyphenyl)-21*H*,23*H*-porphine (TPPOMe) was performed both at 20°C and 120°C; while weak CD signals were observed in the former case, a great increase (amplification about 8.5 times) of the CD intensity for the TPPOMe films was detected after the annealing, indicating a high supramolecular chirality amplification. This can be explained as follows: for TPPOMe, π-π stacking predominates in the assembly, giving the rise to a scarcely ordered structure. Thus, weak CD intensity from its freshly deposited LS films was observed. Upon annealing, TPPOMe forms a more ordered aggregate, as showed from the AFM images reported in Fig.X. Again, a weak CD signal is detected, which indicates that only some of the porphyrins form chiral supramolecular assemblies by stochastically spontaneous symmetry breaking in the Langmuir films floating at the air/water interface. However, during the annealing process, these small amounts of chiral assemblies can induce the other molecules to follow their chirality in the same manner, which follows the so-called ***" sergeants and soldiers"*** principle, by which a small amount of chiral units (sergeants) incorporated within the achiral units (soldiers), can dictate the helical sense of a suprastructure.

A spontaneous symmetry-breaking process can be also caused by physical forces. Recently Ribò and co-workers identified one of the effects that can induce chirality during the homoassociation of diprotonated porphyrins as the vortex direction of stirring[25d]. Even if a direct correlation between vortex direction and

chirality sign of the obtained assemblies is not easy to assess, this work showed the possibility that weak stirring forces may influence the weak cooperative forces at molecular level, causing energy differences between enantiomers and preferred growth directions. In particular, this vortex effect can be attributed to the enhancement of the chirality fluctuations that originate in the diffusion-limited aggregation to high molecular-weight homoassociates. In this sense, the phenomenon could be general for supramolecular systems that are obtained under kinetic control, and its detection would be possible when inherent chiral chromophores were being generated in the association process.

Results and Discussion

2.4 Templated heteroaggregation of chiral porphyrin derivatives

The control of molecular organisation in porphyrin-based self-assembled architectures constitutes a mandatory step for the construction of systems mimicking, among others, the antenna systems of photosynthetic bacteria. This topic can be also of deep impact in the area of research devoted to the bottom-up approach to molecular materials, and for sensors applications[12], as largely described in the introduction of this chapter. In particular, the genesis and the tuning of the chirality in self-assembling architectures are a key task for the development of even more sophisticated functional materials such as nano-sized molecular machinery, data storage, and optical devices.

During the course of the studies on porphyrin derivatives carried out by our group as Cytochrome P450 mimics[34] or sensitive material for sensor applications[20], we found that the presence of a charged chiral, functionality on the porphyrin periphery steers the self-aggregation process toward the formation of large porphyrin aggregates featuring supramolecular chirality.

Moreover, we also found that the chiroptic features of the resulting assembled systems can be deeply affected by the solvent composition, being higher in less polar (i.e. less water rich) media.

Prompted by these results we decided to perform some detailed spectroscopic studies (UV-Visible, CD, and RLS) on the heteroaggregation of

amphiphilic chiral cationic porphyrin derivatives **PL(+)** carried out in the presence of chiral aggregates of the anionic, i.e. negatively charged, chiral counterpart **PL(-)**. The molecular structures of the porphyrin derivatives used in these studies are reported in Fig. 2.20.

The results obtained show that the electrostatic-templated aggregation induces a remarkable amplification of the chirality of the final porphyrin suprastructure. This can be of importance, inter alia, for the construction of complex hetero-porphyrin architectures in which the supramolecular chirality can be tuned *ad hoc*.

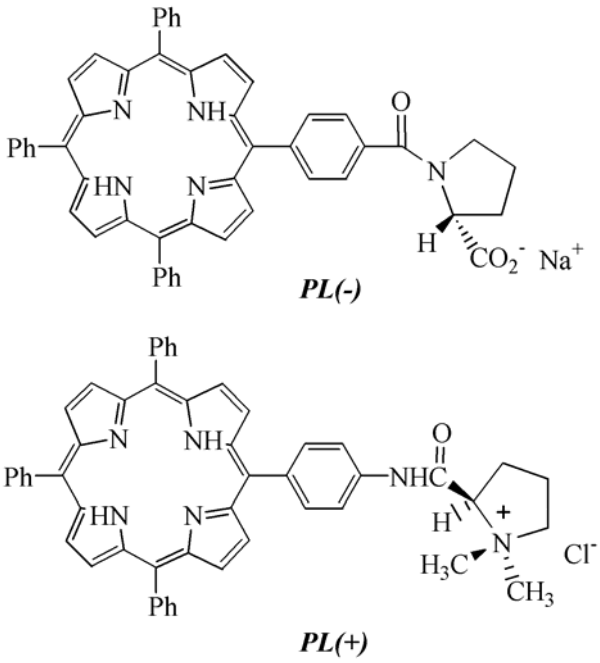

Fig. 2.20 *– Molecular structures of porphyrins used in the aggregation studies.*

2.4.1 Self-aggregation of charged chiral porphyrin derivatives: generation of PL(-) and PL(+) chiral aggregates

Synthesis of chiral porphyrin derivatives were carried out by following a straightforward synthetic procedure.

The cationic derivative **PL(+)** ***4b*** was obtained in four main steps. Tetraphenylporphyrin ***1b*** was synthesized according to the Adler method by acid catalysed condensation of pyrrole and benzaldehyde. The subsequent nitration with $NaNO_2$ in TFA in the required molar ratio afforded the mononitro derivative that was reduced by $SnCl_2$/HCl system, giving the *p*-aminophenyl porphyrin ***2b*** (Scheme 2.1)[34].

Then, this compound has been functionalised with N-methyl-(L)-proline by EDC-HOBT mediated coupling to give porphyrin ***3b***. Finally the subsequent nitrogen quaternisation afforded the desired cationic chiral compound ***4b*** (Scheme 2.2).

The related, negatively charged, chiral macrocycle **PL(-)** has been prepared following published procedure[35a], by EDC-HOBT coupling of the parent *p*-carboxyphenyl derivative with (L)-proline tertbuthylester, followed by alkaline hydrolysis of the protecting group.

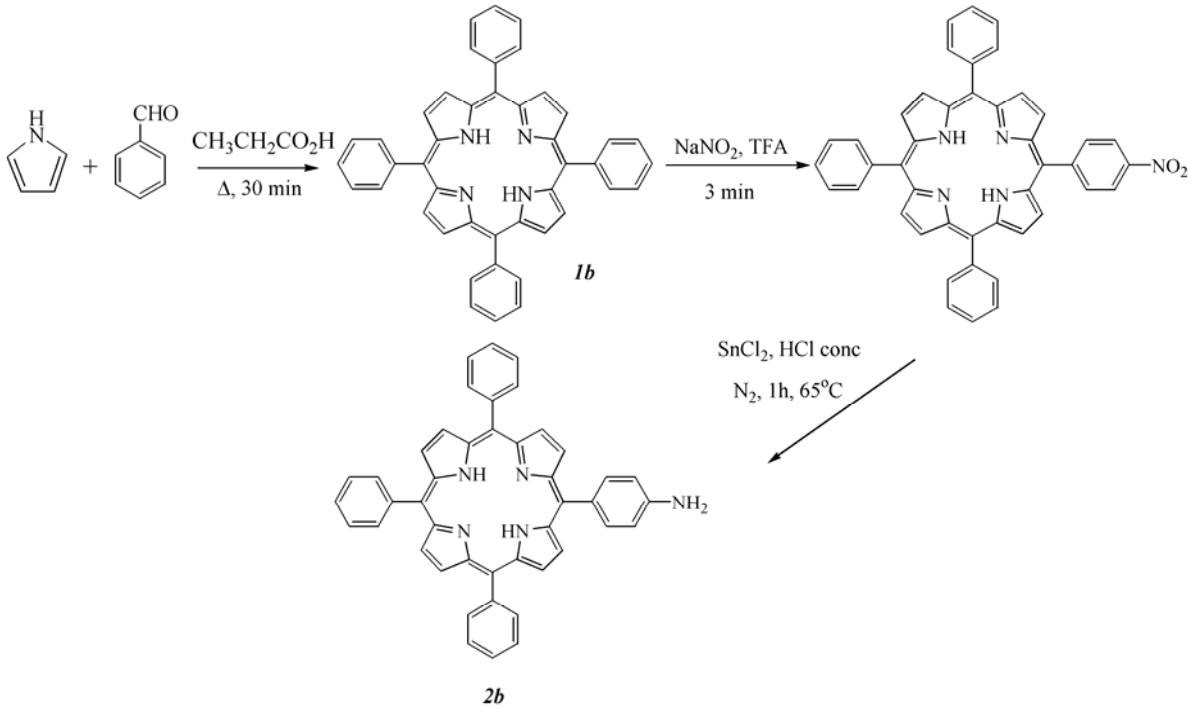

Scheme 2.1 *– Synthesis of porphyrin derivatives* ***1b*** *and* ***2b****.*

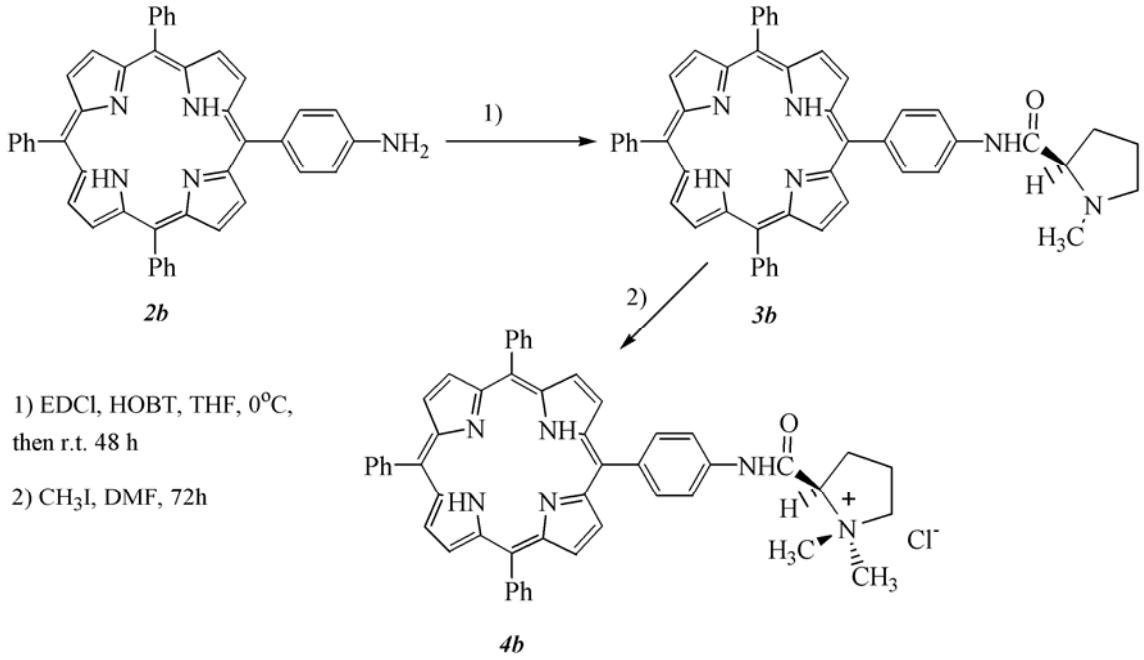

Scheme 2.2 *– Synthesis of porphyrin derivatives* ***3b*** *and* ***4b****.*

Aggregation experiments on **PL(+)**, at micromolar porphyrin concentration, were carried out in water/ethanol 75-25 (v:v) mixtures. It was found that this bulk composition promotes efficient porphyrin self-aggregation process, as witnessed by the broadening and bathochromic shift of the relative Soret band (Fig. 2.21).

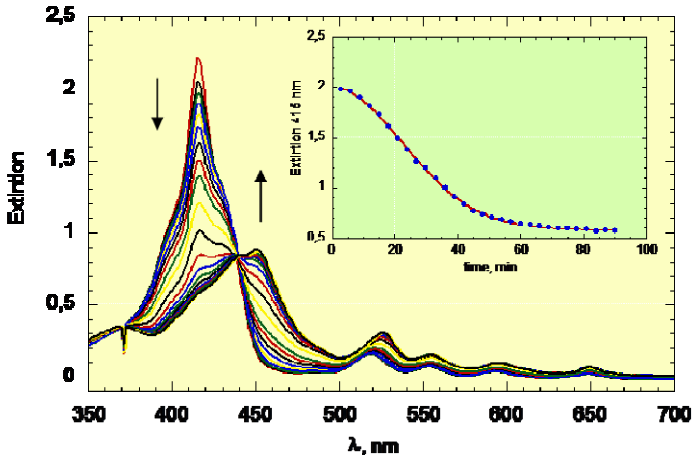

Fig. 2.21 *– UV-vis spectral changes of PL(+) in H_2O-EtOH (75:25 v:v) with time. In the inset is reported the fit of the experimental data points by Eqn1.*

Kinetic data were analysed using the following equation which showed that the aggregation follows a fractal-type kinetic:

$$E=E_{inf} + (E_0-E_{inf})\exp[-(kt)^{n+1}/(n+1)] \qquad \textit{Eqn.1}$$

where E, E_0, E_{inf} are the extinction values at time t, initially, and equilibrium, respectively, n is the ‘‘aggregate growth rate’’ parameter, and k is the kinetic constant.

This equation is a reduced form of a more general nonconventional equation that is widely used in fractal-type aggregation of porphyrins and other related macrocycles. The ‘‘fractal-type’’ equation reduces to Eqn.1 in the limiting case of m = 1 (m is a parameter determining the size of aggregation nuclei, i.e. the dimension, in terms of number of aggregated monomers, of a new nucleation point for a further aggregation growth). Indeed, in the present case, a fit with the ‘‘fractal-type’’ equation gave m values very close to 1 (i.e. 0.95–1.1) together with a poorer adherence of the calculated profiles to the experimental data points.

Some preliminary Atomic Force Microscopy (AFM) studies corroborate the given hypothesis on the fractal nature of the aggregated species. The corresponding topographic picture is ported in Fig. 2.22. The picture represents the topographic image of a hydrogenated silicon surface covered by a layered film of porphyrin **PL(+)** aggregates obtained upon spontaneous deposition from a proper water/ethanol mixture solution. The image of the adlayer shows peculiar, uniform, clear gorgonian-like structures, which are reminiscent to that surmised in solution, in the case of fractal-type aggregates. The height profile (inset of Fig. 2.22), calculated along the line marked in the picture, shows peaks with intensity of about 6-8 nm, with constant periodicity of about 110 nm, and 30 nm wide (at half height of the peak). Geometry optimisation of a basic tetraphenylporphyrin

structure ***1b***, obtained by hybrid density-functional theory optimisation, carried out at B3LYP/6-31G(d) level[36] gave 17.8 and 4.0 Å, for the length and height, respectively. This would indicate, for example, a numbered of a stacked platform of about 18, in height, extending uniformly over an area of tens of squared micrometers. These dimension are in good agreement to that evidenced by RLS techniques, which, according to the intensities reported, indicate the formation of self-assembled structures formed by 10^4-10^5 porphyrin units[23].

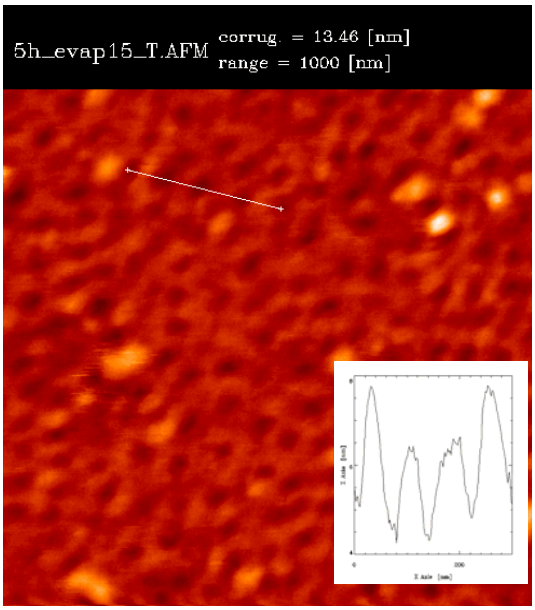

Fig. 2.22 *– AFM image of a hydrogenated silicon surface covered by a layered film of PL(+) aggregates.*

Moreover circular dichroism spectroscopy revealed that the aggregation of **PL(+)** promotes the formation of large chiral suprastructures, steered by the presence of the appended chiral functionality (Fig. 2.23).

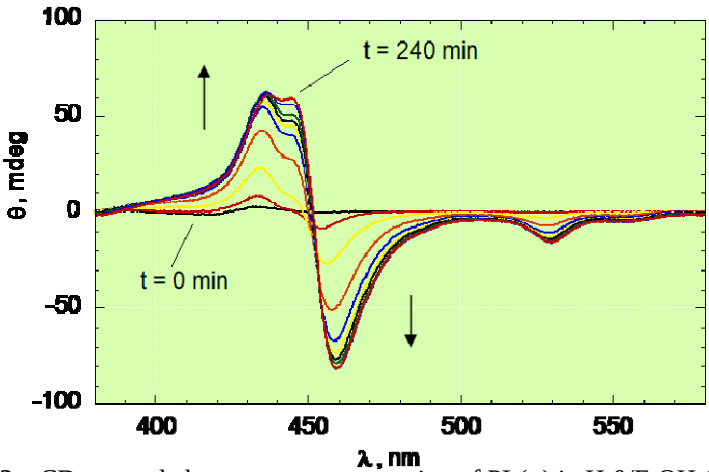

Fig. 2.23 – CD spectral changes upon aggregation of PL(+) in H_20/EtOH (75:25 v:v)

It is worth of noting that in nonaggregative conditions porphyrin solutions result to be CD silent in the Soret band region. Moreover, aggregates of related cationic or anionic, achiral, amphiphilic porphyrin derivatives are CD silent. This should safely rule out the effect of the scattering in the observed phenomenon. The supramolecular aggregates of the anionic derivatives **PL(-)** showed a somewhat higher ellipticity with respect to the cationic derivatives, probably as a consequence of a stronger intermolecular π-π stacking. This can be due to a higher degree of hydrophobicity featured by the anionic derivative, as witnessed by its very fast kinetic of aggregation, which is complete within the time of mixing in the window of concentration examined.

2.4.2 Chiral imprinted aggregation of PL(+) on PL(-) aggregates

The evolution of chiral porphyrin systems, at a supramolecular level relies on the aggregation of achiral porphyrin platforms on chiral templates, such as DNA, RNA, and other natural or synthetic polymers. We decided to perform the aggregation of a the chiral cation porphyrin **PL(+)** on a “unusual” chiral template constituted by preformed chiral supramolecular aggregates of **PL(-)**.

Interesting features are evidenced by these binary systems. If the self-aggregation of **PL(+)** is carried out in the presence of preformed chiral aggregates of **PL(-)**, the aggregation still occurs in a chiral fashion as witnessed by CD spectral changes upon heteroaggregation (Fig. 2.23) and more insight, a dramatic amplification of the resulting supramolecular aggregates, of about twenty-fold, is observed (Fig. 2.24).

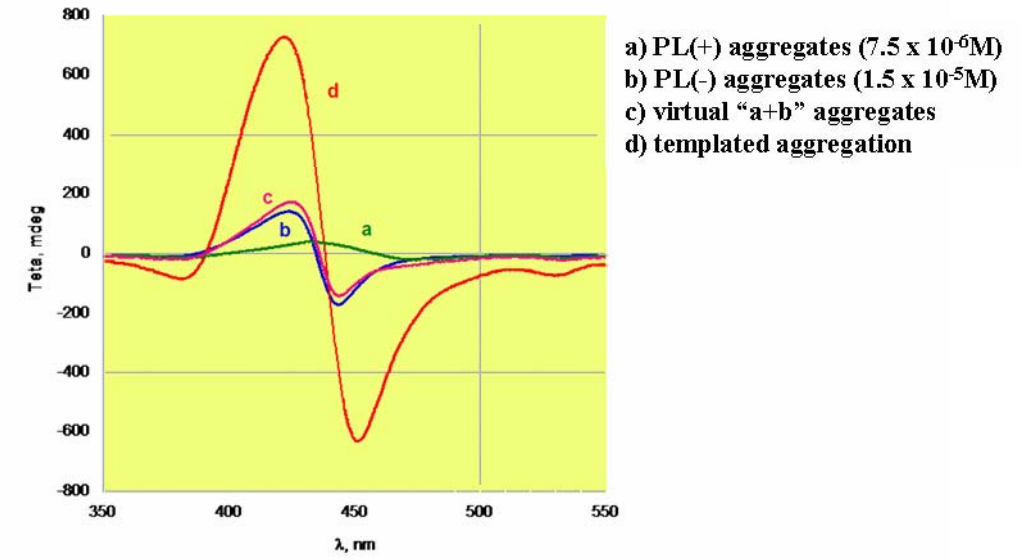

***Fig. 2.24** – Amplification of CD signal (line d) for templated aggregation compared to both individual chiral aggregates (lines a and b) and their virtual sum (line c).*

The ellipticity of the resulting heteroaggregates is higher compared to the one of the virtual sum "a+b" aggregates. This should indicate a strong template effect exerted by the presence of the anionic assemblies, reasonably onset by electrostatic forces. The presence of the template has a profound effect also in the kinetic of aggregation.

In the absence of the template, the aggregation follows a fractal-type kinetic, whereas the templated aggregation features a coupled first order kinetic, which can be described by the following equation:

$$E=E_{inf} + (E_0-E_{inf})_1[\exp(-k_1 t)] + E'_{inf}[\exp(-k_2 t)] \qquad Eqn.2$$

in which the faster rate constant k_1 refers to the aggregation step, while the slower rate k_2 can be safely related to a concomitant deposition phenomenon of porphyrin solid layer onto the cuvette walls. The results are graphically reported in Fig. 2.25. This is reminiscent to that formerly reported by our group, in which

the spontaneous deposition of cationic amphiphilic porphyrin derivatives on glass surfaces has been demonstrated.

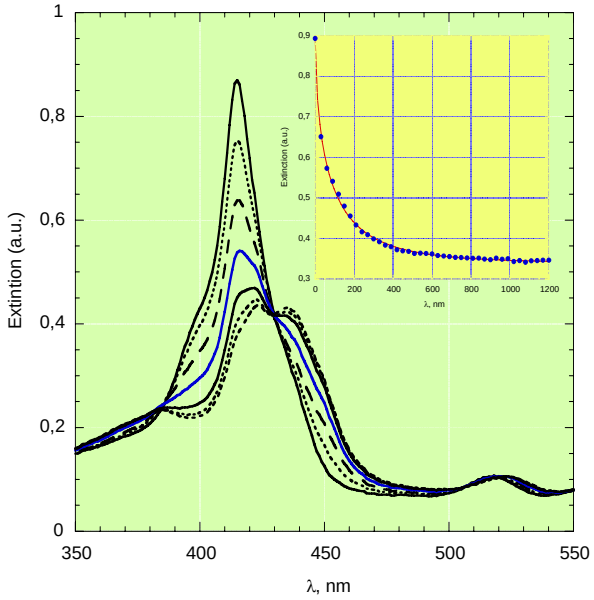

Fig. 2.25 *– CD spectral changes upon heteroaggregation of PL(+) on preformed PL(-) chiral aggregates in H_20/EtOH (75:25 v:v).*

The calculated values for the first order rate constants are k_1 = 6.9 x 10^{-2}, and k_2 = 6.3 x 10^{-3} min^{-1}, respectively, at a 7.5 μM concentration of **PL(+),** and 15 μM whole concentration of templating **PL(-)**. It is worth of noting that the rate of aggregation is increased by one order of magnitude, the untemplated aggregation being 6.0 x 10^{-3} min^{-1} at the same porphyrin bulk concentration[23].

Beside the increased aggregation rates, the effect of the electrostatic template shows itself also in an increasing of the stability of the final suprastructures. Remarkably, the CD intensity of such templated aggregates is satisfactorily retained in the presence of added achiral *p*-carboxylate porphyrin derivative (15 μM), which should act as an "electrostatic competitor". The corresponding CD intensity in fact decreases of about 30%, with respect to the initial value, after prolonged standing. Conversely, the CD intensity of not-templated chiral aggregates of **PL(+)** is virtually extinguished upon addition of aggregates of *p*-carboxylate porphyirin derivative, within the time of mixing (data not shown).

This dramatic change should imply a "*sergeant-soldier*" effect exerted by the chiral, negatively charged, porphyrin aggregates.

Resonance Light Scattering spectroscopy studies corroborates the occurrence of the porphyrin aggregation phenomenon. Interestingly, the intensity of the RLS emissions of the **PL(+)** templated aggregates corresponds to the superposition of the virtual "sum" of the independently aggregated structures, as reported in Fig. 2.26.

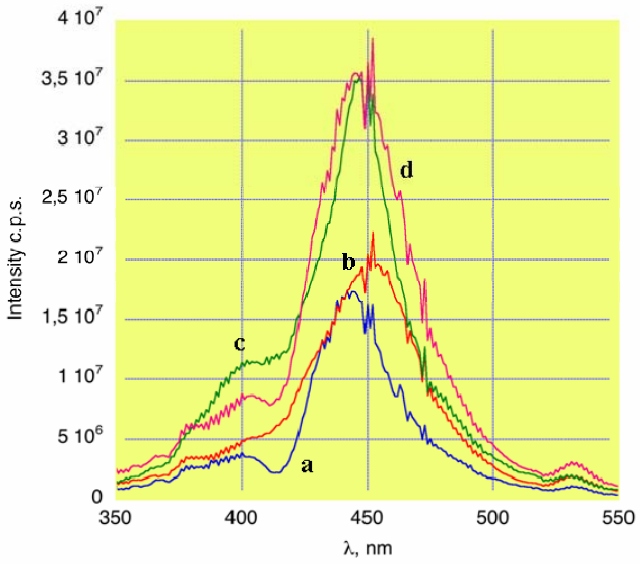

a) I PL(+)
b) I PL(-)
c) I templated aggregates
d) I tot

Fig. 2.26 *– RLS emissions of the PL(+) templated aggregates.*

This should safely rule out the occurrence of an extended electronic coupling between the cationic and the anionic structures, ruling out the formation of intercalated species.

In summary, the results obtained in the case of the templated aggregation open interesting perspectives for the achievement of new porphyrin-based supramolecular species bearing attractive properties for the construction of stereoselective sensor systems or supramolecular devices.

2.5 Current developments and future perspectives: self-aggregation of amphiphilic corrole derivatives

The spontaneous self-aggregation of tetrapyrrolic macrocycles as porphyrins and chlorins to form molecular assemblies have been largely reported in the literature, while corroles have not ever been investigated so far.

Prompted by the results so far obtained in the case of the above described amphiphilic porphyrin derivatives, we extended this philosophy to related corrole derivatives, with the aim to investigate the aggregation properties of such class of macrocycles. The exploitation of the above described strategy to the case of corroles, may open important perspectives for the achievement of new supramolecular materials, owing to the peculiar properties of this class of molecules, such as, for example, their ability to coordinate transition metal cations, in non conventional, "hypervalent", oxidation states.

2.5.1 Synthesis of amphiphilic corroles Corr (+) and Corr(-)

Corroles are "one carbon shorter" analogues of porphyrins, whose chemical and physical properties will be discussed in details in chapter 3.

The transfer of the same approach adopted for the aggregation studies of chiral porphyrin derivatives implied that mono-substituted corroles has to be obtained, through an efficient synthetic method.

Very recently, a new procedure for the preparation of A_3 and A_2B-corroles has been reported by Gryko and Koszarna[37], improving reaction yields from 15-20% to 15-55%.

The inspiration for this work came from an intriguing paper by Král and co-workers[38] describing the synthesis of dipyrromethanes in water. The basic principle for the preparation of these compounds was represented by the

difference in water solubility between the substrates (aldehyde, pyrrole) and the product (dipyrromethane). By taking advantage of this solubility difference, it was possible to steer the reaction yield toward the selective formation of dipyrromethanes by using only a 6-fold excess of pyrrole.

Furthermore, Král and co-workers briefly found that the addition of MeOH to the reaction mixture led to a decrease in the yield of dipyrromethanes, probably due to the formation of higher oligocondensates. This could be attributed to the better solubility of dipyrromethanes in H_2O/MeOH mixtures, which permits further reaction.

According to these considerations, Gryko reasoned that careful optimization of the aldehyde/pyrrole ratio in conjunction with the amount of MeOH might be a perfect way for narrowing the distribution of oligocondensates and, thus, open the way to a more efficient synthesis of corroles.

Indeed they reported very successful results on the synthesis of A_3-corroles as well as *trans*-A_2B-corroles in an H_2O/MeOH mixture. Remarkably, the preparation of triphenylcorrole by following this protocol resulted in the highest yield (32%) reported to date.

The scope and limitations studied showed that this method was particularly efficient for moderately reactive aldehydes and those bearing electron-donating groups (yields 14-27%). Using these conditions, corroles bearing strongly electron-donating groups were obtained for the first time.

In addition, it was found that the reaction of unhindered dipyrromethanes with aldehydes under analogous conditions afforded *trans*-A_2B-corroles in very high yields (45-56%; 8-fold higher than previously reported) without scrambling.

In our studies, we entailed the synthesis of two triarylcorroles, bearing charged functional group on the peripheral positions capable to confer them amphiphilic features. In particular we decided to prepare an anionic triphenylcorrole, bearing a carboxyl group, and a cationic one functionalised by a trimethylammonium moiety.

It was first necessary to synthesize the relative precursors ***5b*** and ***6b***, which were obtained in very good yields (60% and 52% yields respectively) by following Gryko's method, as depicted in Scheme 2.3.

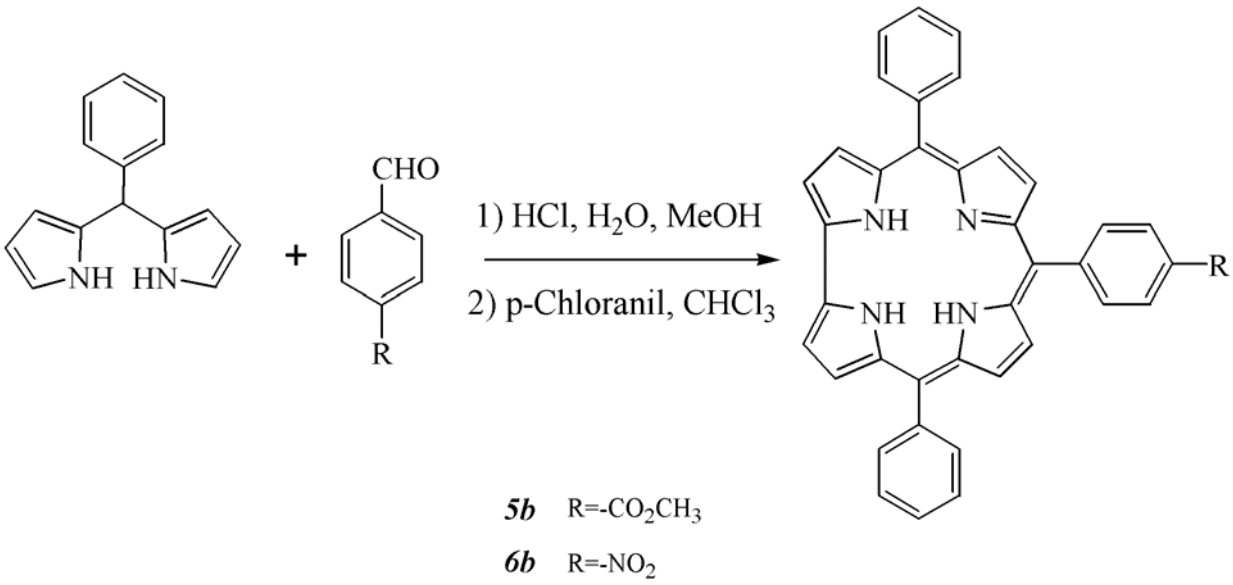

Scheme 2.3 *– Gryko method for the synthesis of trans-A_2Bcorroles.*

The cationic corrole **Corr(+)** ***8b*** has been prepared in two steps: the first was the reduction of corrole ***6b*** by $SnCl_2$/HCl system, giving the *p*-aminophenyl corrole derivative ***7b*** and the second one was the subsequent nitrogen quaternisation with CH_3I (Scheme 2.4).

The anionic corrole **Corr(-)** ***9b*** has been prepared by a simple alkaline hydrolysis of corrole ***5b*** (Scheme 2.5).

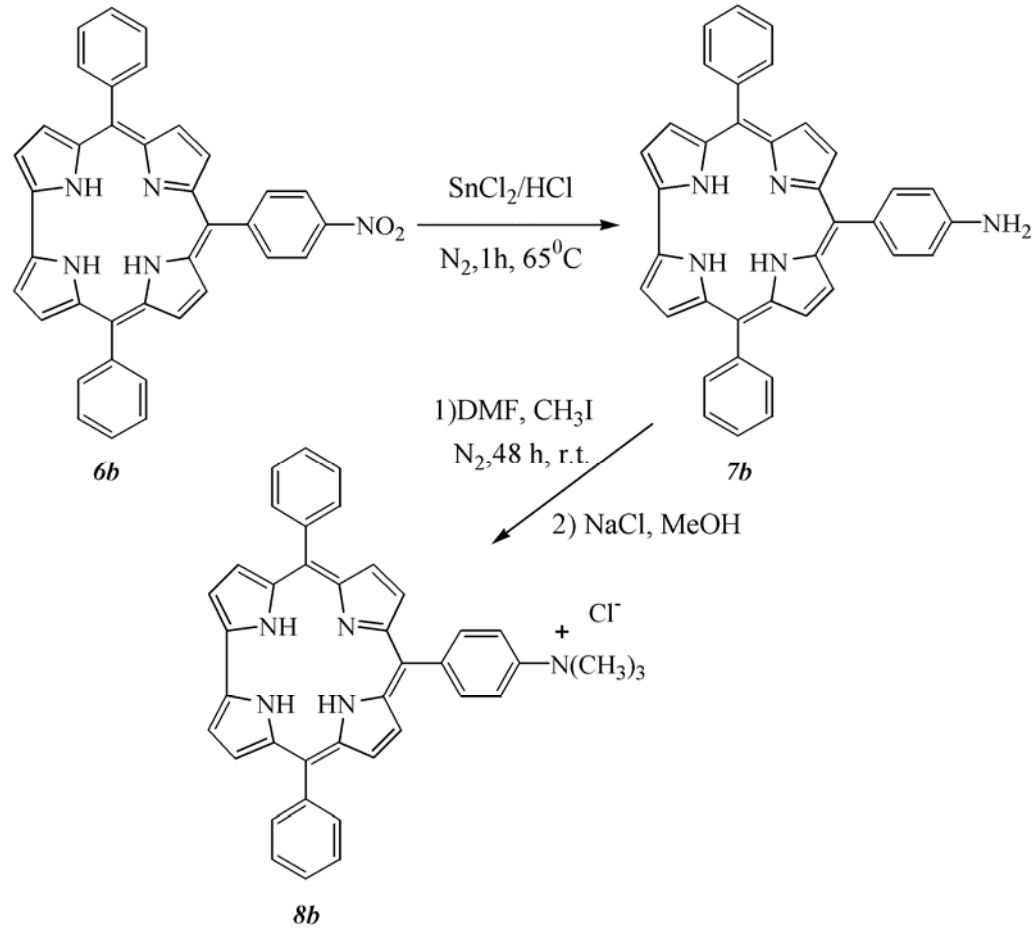

Scheme 2.4 *– Planned synthesis of Corr(+).*

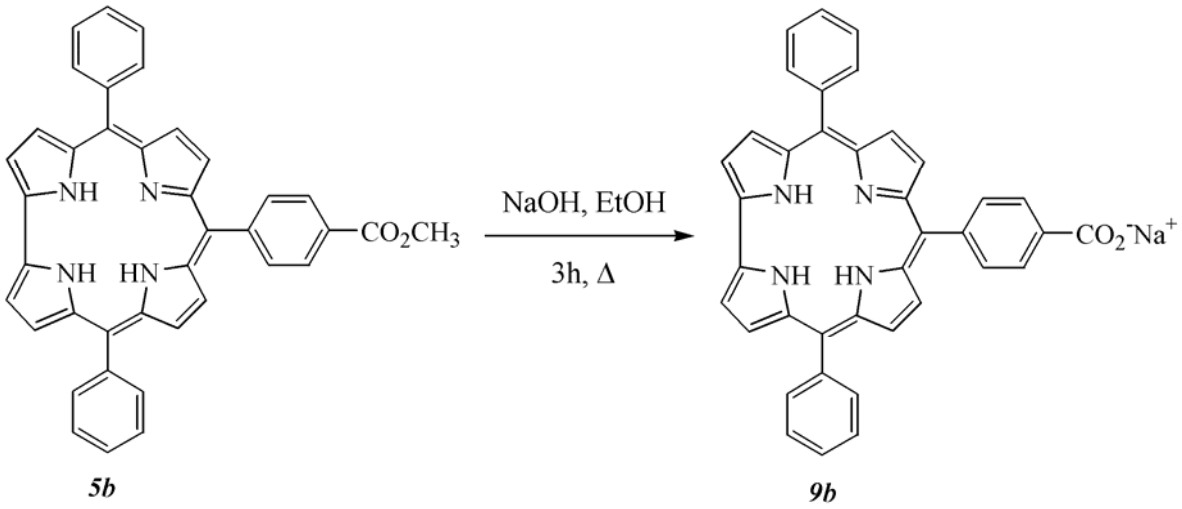

Scheme 2.5 *– Synthesis of Corr(-).*

2.5.2 Preliminary aggregation studies on amphiphilic corrole Corr (-)

Aggregation experiments of **Corr(-)** have been carried out in mixed water-ethanol solvent mixtures. In the composition range of 100% to 50% ethanol (v:v) the macrocycle is in monomeric form, as clearly evidenced by the shape of the Soret band positioned at *ca* 413 nm. Further increase of the water proportion promotes the aggregation process, steered by π–π interactions, as well as hydrogen bond, between the carboxylate group and the inner hydrogen atoms of the adjacent corrole core. This is witnessed by either the broadening, and a small hypsochromic shift of the Soret band.

It is interesting to note that the corresponding anionic porphyrin aggregates in similar conditions, resulting in the formation of J-type aggregates. This different behaviour featured by the anionic corrole examined may evidence a peculiar orientation of corrole macrocycles, consistent with a H-type (i.e. face-to-face) aggregation. Evidently, this can be accounted for by the different geometry inferred by the direct pyrrole-pyrrole bond. This structural constraint would drive the aggregation toward the formation of supramolecular species characterised by a different packing motif.

The self-aggregation profile driven by solvent composition is reported in the inset of Fig. 2.27.

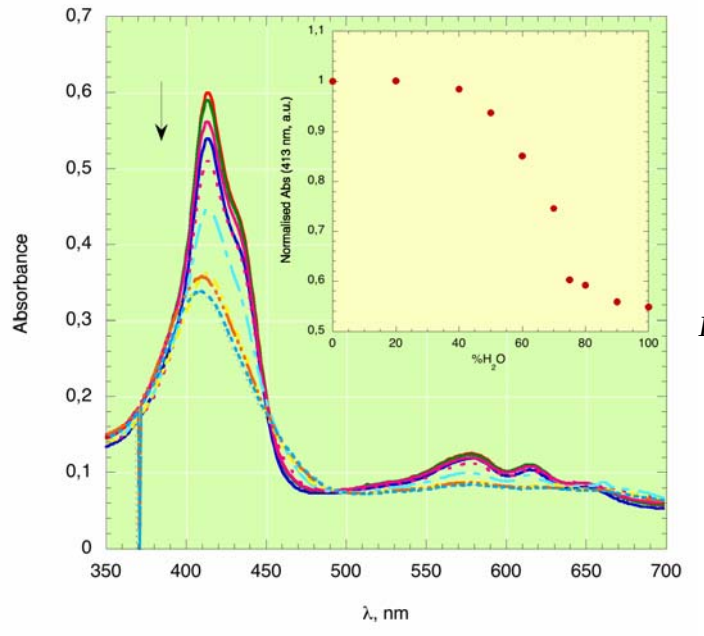

Fig. 2.27 *– Self-aggregation profile of corrole Corr(-) in H_20-EtOH 50:50 (v:v). The inset shows the aggregation behaviour upon solvent composition.*

Concomitant kinetic studies have been performed in water/ethanol 50/50 (v:v) composition. At this solvent composition the aggregation rate is negligibly small. Only marginal spectroscopic changes can be detected after one day of storage. The self-aggregation process is triggered by the addition of NaBr. It is well known that the increase of the ionic strength of the medium, promotes the aggregation process by hydrophobic effect, as reported in the case of templated aggregation of water-soluble porphyrin derivatives on DNA, RNA or other polymeric matrices[39]. We choose NaBr, as a salt, owing to its better solubility in mixed aqueous solvent mixtures, compared to the more hydrophilic NaCl counterpart.

Kinetic runs were carried out by following the decrease of the Soret band intensity (at 413 nm) with time. A typical absorbance *vs* time profile is reported in the Fig. 2.28. The presence of several isosbestic points indicates that the aggregation process occurs toward the formation of a narrow distribution of structurally similar species.

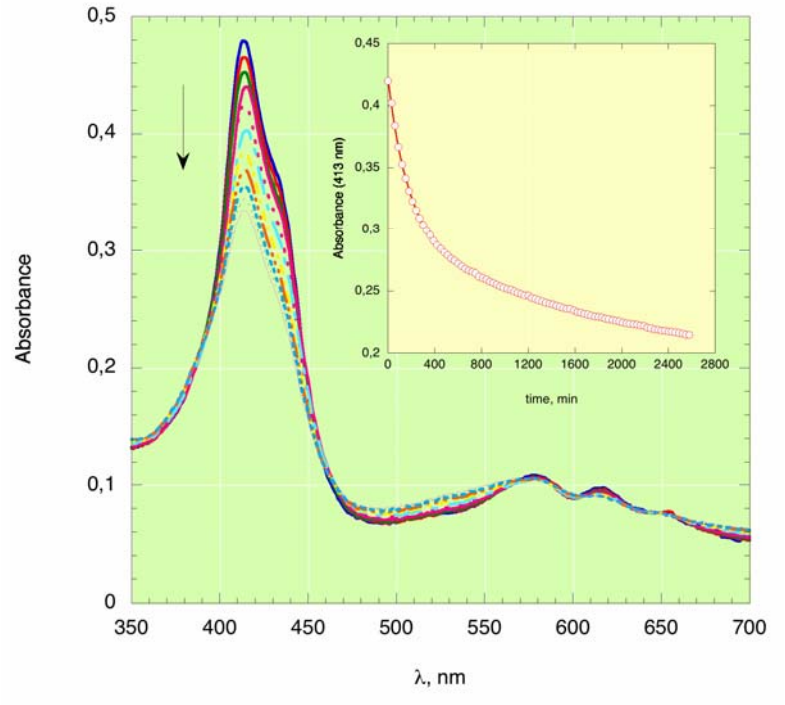

Fig. 2.28 *- Kinetic runs on Corr(-). The inset shows the close adherence of the calculated fit to the experimental values.*

The experimental decays can be excellently fitted by a coupled first order kinetic, which is described by the following Equation 3. This is reported in the Fig. 2.28, in which the close adherence of the calculated fit to the experimental values is emphasised.

$$E=E_{inf} + (E_0-E_{inf})_1[\exp(-k_1 t)] + E'_{inf}[\exp(-k_2 t)] \qquad Eqn.3$$

In this present case, differently from that evidenced in the case of related porphyrin derivatives, there is no evidence of deposition of a corrole film onto the walls of the reaction vessel. A different aggregation mechanism must be then operative in the observed phenomenon. A tentative hypothesis would concern the occurrence of a so-called Diffusion Limited Aggregation mechanism (DLA), in which large cluster are formed by interaction between initial smaller cluster (seeds) and monomers[40]. Notable examples are reported in the aggregation of charged cyanine dyes on charged polymeric templates, such as poly(vinylsulfonate)[41], or in an our very recent work, focused on the synthesis and aggregation properties of porphyrin-*C*-glycoside conjugates[42]. According to those literature reports, the faster rate constant k_1 can be referred to the formation of the initial corrole clusters, while the concomitant slower step (k_2) can be ascribed to the subsequent, growth of the final structures.

As expected, the rates have found to be dependent on the ionic strength of the solution, as pictorially reported in Fig. 2.29. The non-linearity effect on increasing NaBr concentration can be probably ascribed to Na^+ Br^- ion pairing effect that become increasingly important at higher salt concentration.

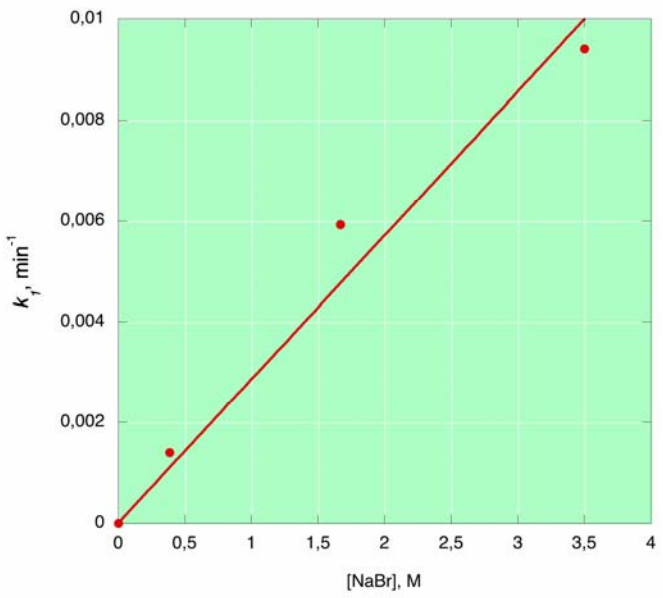

Fig. 2.29 *– Dependence of aggregation rate from ionic strength of solution.*

These preliminary results showed that amphiphilic corrole derivatives can be successfully achieved by straightforward synthetic procedures, in high yields. These molecules evidenced interesting properties in terms of self-aggregation process, toward the formation of specific supramolecular architectures, driven by the molecular information stored in the periphery of the tetrapyrrolic macrocycle. The extension to more elaborate structures, i.e. chiral charged groups, would made possible the achievement to final assemblies with interesting stereoselective features.

Experimental Section

➢ *Reagents and materials*

Reagents and solvents (Sigma-Aldrich, Fluka and Carlo Erba Reagenti) were of the highest grade available and were used without further purification.

Solvents employed in the spectroscopic studies are of spectroscopic grade and used as received. Milli-Q, Millipore, previously doubly distilled water, was used for the preparation of porphyrin aqueous solutions.

Silica gel 60 (70 -230 mesh) and neutral alumina (Brockmann Grade III). were used for column chromatography

Silica gel 60 (Merck) and neutral alumina 60 F_{254}, both on aluminium support, were used for TLC.

➢ *Instruments*

^{1}H NMR spectra were recorded with a Bruker AM400 (400 MHz) spectrometer, using $CDCl_3$ as solvent. Chemical shifts are given in ppm relative to tetramethylsilane (TMS).

Routine UV/Vis spectra were recordered in $CHCl_3$ on a Varian Cary 50 Spectrophotometer. whereas more delicate measurements were performed on a Perkin Elmer λ18 Spectrophotometer equipped with a temperature-controlled cell holder.

CD spectra have been performed on a JASCO J-600, equipped with a thermostated cell holder, and purged with ultra-pure nitrogen gas.

RLS experiments have been performed on a Spex Fluorolog Fluorimeter.

Mass spectra (FAB) were recorded on a VG Quattro Spectrometer using m-nitrobenzyl alcohol (NBA, Aldrich) as a matrix in the positive-ion mode.

- ***List of acronyms***

DMF = *N,N'*-dimethylformamide
THF = tetrahydrofuran
TFA = trifluoroacetic acid
HOBT = 1-hydroxy-1*H*-benzotriazole
EDC-HCl = 1-[3-(dimethyl-amino)propyl)-3-ethylcarbodiimide hydrochloride

2.6 Synthesis of meso-arylporphyrins

*2.6.1 Synthesis of 5,10,15,20-tetraphenylporphyrin (**1b**)*

In a 250 mL round bottomed flask, pyrrole (2.24 mL, 32 mmol) and benzaldehyde (3.2 mL, 32 mmol) were added to 120 mL of refluxing propionic acid. After refluxing for 30 min, the solution was cooled at room temperature and filtered. The filtrate was washed thoroughly with methanol and the resulting purple crystals were air dried to yeld 1.06 g (21%) of the desired product. The spectroscopic data obtained for the title compound are in agreement with those in the literature.

*2.6.2 Synthesis of 5-(4-Aminophenyl)-10,15,20-triphenylporphyrin (**2b**)*

To a solution of ***1*** (100 mg, 0.163 mmol) in TFA (10 mL) was added $NaNO_2$ (20 mg, 0.29 mmol). After 3 min stirring at room temperature, the reaction mixture was poured into water (100 mL) and extracted with CH_2Cl_2 (6x25 mL). The organic layer was washed with saturated aqueous $NaHCO_3$ and water as described above and then the solvent was removed under vacuum. The residue was purified on a plug of silica gel, eluting with CH_2Cl_2. After evaporation of the solvent, the residue was dissolved in concentrated HCl (10 mL) and, while stirring, $SnCl_2$(220 mg, 0.975 mmol) was carefully added. The final mixture was heated to 65 °C for 1 h under N_2 before being poured into cold water (100 mL). The aqueous solution was neutralized with NH_4OH until pH 8. The aqueous solution was extracted with CH_2Cl_2 until colorless. The organic layer was then concentrated under vacuum and the residue was purified on a plug of alumina using CH_2Cl_2 for elution. The final residue was recrystallized from methanol, yielding 55.3 mg (54%) of the desired porphyrin . The spectroscopic data obtained for the title compound are in agreement with those in the literature;[19] MS (MALDI) m/z 629.8 (Mþ); ^{1}H NMR ($CDCl_3$) d ppm: 22.75 (br, 2H), 4.02 (s, 2H), 7.07 (d, J=9.0 Hz, 2H), 7.75 (m, 9H), 7.98 (d,J=9.0 Hz, 2H), 8.20 (m, 6H), 8.84 (s, 6H), 8.96 (s, 2H). UV–Vis ($CHCl_3$) λ_{max}: 417.5 nm (1 315,800), 514 (28,900), 551 (20,600), 589 (15,600) and 645.5 (12,800).

*2.6.3 Synthesis of N-[5-(4-Aminophenyl)-10,15,20-triphenylporphyrinyl]-L-prolin(N-methyl)amide (**3b**)*

To a stirred solution of 0.4 g of **2** (0.635 mmol) in 50 mL of anhydrous THF kept at 0 °C, 0.082 g of N-methyl-Lproline monohydrate (0.635 mmol), 0.1 g of N-methyl-morpholine (0.80 mmol), and 0.086 g of HOBT (0.635 mmol)

were added. The reaction mixture was stirred under a nitrogen atmosphere for 1 hour at 0 °C. EDC-HCl (0.129 g, 0.667 mmol) was then added and the reaction mixture was stirred for additional 48 hours at room temperature. After that time a tlc run ($CHCl_3$-1% MeOH) showed no further progress of the reaction. The solvent was then removed under reduced pressure and the residue dissolved in 100 mL of $CHCl_3$and extracted with brine (3 x 100 mL). The organic layer was dried on Na_2SO_4 and the solvent evaporated to give a red solid that was applied to a short SiO_2 chromatographic column and eluted with a $CHCl_3/CH_3OH$ 9:1 v/v solvent mixture. The unreacted aminophenylporphyrin derivative was separated. The L-proline-porphyrin conjugate was subsequently separated by eluting with a $CHCl_3/CH_3OH$ 3:1 v/v solvent mixture. A 0.090 g crop (0.120 mmol; 18% yield) of the title porphyrin was recovered after solvent evaporation, and used without further purification in the subsequent reactions.

*2.6.4 Synthesis of N-[5-(4-Aminophenyl)-10,15,20-triphenylporphyrinyl]-L-(N,N-dimethyl)prolininium amide chloride (**4b**)*

In a 100 mL two-necked round bottomed flask, 0.06 g of porphyrin **3** (0.08 mmol) were dissolved in 50 mL of dry DMF. To this solution, stirred under an inert atmosphere, 600 mg of CH_3I (4 mmol) were added. The reaction mixture was stirred at room temperature for 3 days. After that time a tlc run ($CHCl_3$- 5% CH_3OH) showed no further progress of the reaction. Usual workup of the mixture gave, after column chromatography (SiO_2, $CHCl_3$-5% CH_3OH as eluant) gave a red microcrystalline solid. The product was subsequently dissolved in CH_3OH (25 mL) and stirred overnight with a large excess of solid NaCl (1 g). The mixture was then filtered and evaporated under reduced pressure. The red solid was then dissolved in the minimum amount of CH_2Cl_2, filtered and

crystallised by addition of *n*-pentane obtaining 0.05 g (0.065 mmol, 80% yield) of the desired porphyrin, as a bright purple crystalline solid.

UV-Vis ($CHCl_3$): λ_{max} (log ε) 419 (5.0), 514 (3.7), 546 (3.6), 586 (3.5), 645 (3.1). ^{1}H-NMR (CD_3OD), δ: 9.1-8.5 (brs, 8H, pyrrole β-Hs), 8.2 (m, 10H, Aromatics), 7.8 (m, 9H, Aromatics), 3.9 (m, 1H, proline δ-H), 3.7 (m, 1H, proline δ-H), 3.45 (d, *J* = 12 Hz, 6H, proline NMe), 2.7 (m, 2H, proline β-H), 2.4 (m, 2H, proline γ-H), -2.81 (brs, 2H, pyrrole NH) ppm. FAB-MS (NBA), *m/e*: 756 [M-Cl]+.

2.7 Synthesis of trans-A_2Bcorroles

*2.7.1 Synthesis of 10-(4-Rphenyl)-5,15-diphenylcorrole (**5b**), (**6b**)*

In a 250 mL round bottomed flask, phenyldipirromethane (1 mmol) and aldehyde (0.5 mmol) were dissolved in CH_3OH (50 mL). Subsequently, a solution of HCl_{aq} (36%, 2.5 mL) in H_2O (50 mL) was added, and the reaction was stirred at room temperature for 1 h. The mixture was extracted with $CHCl_3$, and the organic layer was washed twice with H_2O, dried on Na_2SO_4, filtered, and diluted to 250 mL with $CHCl_3$. *p*-Chloranil (1.5 mmol) was added, and the mixture was stirred overnight at room temperature. The reaction mixture was then concentrated to half the volume and passed over a silica column (SiO_2, CH_2Cl_2/hexanes, 2:1). All the fractions containing corrole were combined and evaporated to dryness. The resulting solid was suspended in boiling EtOH, cooled, and filtered to give the pure product as a violet crystalline solid.

Yield: 53% (***5b***), 58% (***6b***).

*2.7.2 Synthesis of 10-(4-Aminophenyl)-5,15-diphenylcorrole (**7b**)*

In a 250 mL round bottomed flask, corrole **5b** (150 mg, 0.26 mmol) was dissolved in concentrated HCl (10 mL) and, while stirring, $SnCl_2$(mg, x mmol) was carefully added. The final mixture was heated to 65 °C for 1 h under N_2 before being poured into cold water (100 mL). The aqueous solution was neutralized with NH_4OH until pH 8. The aqueous solution was extracted with CH_2Cl_2 until colorless. The organic layer was then concentrated under vacuum and the residue was purified on silica column (silica, $CHCl_3$). The first green band was the unreacted corrole **5b**, while the second one was the desired product. After crystallization from CH_2Cl_2/CH_3OH, 45 mg (32%) of pure compound was isolated. ^{1}H NMR (300 MHz, $CDCl_3$): δ -1.92 (br s, 3H), 1.92 (s, 12H), 2.60 (s, 6H), 3.91 (br s, 2H), 7.01 (d, J = 7.92 Hz, 2H), 7.25 (s, 4H), 7.93 (d, J = 7.92 Hz, 2H), 8.31 (d, J = 3.86 Hz, 2H), 8.47 (d, J = 4.52 Hz, 2H), 8.54 (d, J = 4.52 Hz, 2H), 8.88 (d, J = 3.86 Hz, 2H). UV-Vis (CH_2Cl_2): λ_{max}/nm ($10^{-3}\varepsilon$/mol^{-1} L cm^{-1}) 408 (92.9), 427 (69.7), 567 (14.3), 606 (10.4), 637 (6.9).

*2.7.3 Synthesis of 5,15-diphenyl-10-(4-Trimethylammoniumphenyl) corrole chloride (**8b**)*

In a 100 mL two-necked round bottomed flask, 100 mg of corrole **7b** (0.18 mmol) were dissolved in 50 mL of dry DMF. To this solution, stirred under an inert atmosphere, 1.28 g of CH_3I (9 mmol) were added. The reaction mixture was stirred at room temperature for 3 days. The solvent was then removed under reduced pressure and the residue purified on a silica column (SiO_2, $CHCl_3$-5% CH_3OH) giving a dark green solid. The product was subsequently dissolved in CH_3OH (25 mL) and stirred overnight with a large excess of solid NaCl (1 g). The mixture was then filtered and evaporated under reduced pressure. The green

solid was then dissolved in the minimum amount of CH_2Cl_2, filtered and crystallised by addition of *n*-pentane obtaining 84 g (0.135 mmol, 75% yield) of the desired corrole, as a dark green crystalline solid.

*2.7.4 Synthesis of sodium 5,15-diphenyl-10-(4-Carboxylatephenyl)-corrole (**9b**)*

In a 250 mL round bottomed flask corrole **6b** (100 mg, 0.17 mmol) was dissolved in 100 mL of 95% EtOH and NaOH (0.2 g) was added. The mixture was stirred at reflux temperature for 3 h, then cooled to 25°C and filtered, washing the precipitate several times with distilled H_2O. The residue was dried on air and then dissolved with a mixture of $CHCl_3$ and CH_3OH, and the solution evaporated under reduce pressure. The green solid was dissolved in 100 mL of $CHCl_3$ and washed with a saturated solution of aqueous ammonium chloride. The organic phase was then dried on Na_2SO_4 anhydrous and the solvent was reduced to a small volume. The reaction mixture was purified on silica column (silica, $CHCl_3$). All the fractions containing the desired corrole were collected, reduced to a small volume and washed with NaOH 0,1 M (3x100 mL). The crystallization from CH_2Cl_2/ n-pentane afforded 83 mg of the title corrole (0.14 mmol, 84% yield) as a dark green solid.

2.8 Spectroscopic studies: UV-visible, CD and RLS spectra.

*UV-vis spectroscopic studies: k*inetic experiments were performed by measuring the UV-Visible spectroscopic changes of porphyrin with time. Porphyrin aqueous solutions, suited for kinetic studies, were prepared as follows. Proper aliquots, of the cationic chiral porphyrin millimolar stock solution in ethanol (15÷150 μL), where added to a 1.0 mL of ethanol in an 8 mL glass vial.

To this solution 3.0 mL of water were then added and the resulting solution vigorously shaken. A 3 mL portion was then transferred in a quartz couvette and the relative UV-Visible spectra acquired. This procedure ensures a 75:25 H_2O/EtOH (v:v) final solvent composition, with a final porphyrin concentration spanning in the range of 1.5 to 9.0 x 10^{-5} M.

Values of *k* were obtained by analysing the absorbance (extintion) *vs*. time data points. The kinetic parameters were obtained by nonlinear least-squares regression fit (Kaleidagraph® program, Synergy Software, 2003) over hundreds of experimental data points.

A similar procedure has been used for the study of corrole aggregation.

A typical procedure for the preparation of a corrole solution, suitable for kinetic studies, is as follows: to a 2 ml of ethanol, containing the appropriate amount of corrole solution, a 2 ml of a NaBr solution is slowly added. This ensures a corrole concentration within 1 to 10 M, on the final solution. The resulting solution is then rapidly shaken to guarantee homogeneity, and immediately transferred into a 10 mm quartz cuvette. The relative spectra are recorded in a time-drive scan, by the computer aided routine program.

Data treatment has been accomplished following the same approach using for porphyrin aggregates.

CD and RLS studies: CD spectra have been performed on a JASCO J-600, equipped with a thermostated cell holder, and purged with ultra-pure nitrogen gas. RLS experiments have been performed on a Spex Fluorolog Fluorimeter. In this latter case spectra have been acquired, at 25 ± 0.5 °C, in a "synchronous scan" mode, in which the emission and excitation monochromators are pre-set to identical wavelengths.

In both cases solutions have been prepared by following the protocol used in the kinetic experiments.

References

1. Reinhoudt, D.N.; Crego-Calama, M. *Science.*, **2002**, *295*, 2403.
2. Antonietti, M; Gŏltner, C.G. *Angew. Chem. Int. Ed. Engl.*, **1997**, *36*, 910.
3. Rivera, J.M.; Martin, T.; Rebek, J.Jr. *Science.*, **1998**, *279*, 1021.
4. Prins, J.L.; Timmerman, P.; Reinhoudt, D.N. *J. Am. Chem. Soc.*, **2001**, *123*, 10153.
5. Buschmann, H.; Thede, R.; Heller, D *Angew. Chem. Int. Ed. Engl.*, **2000**, *39*, 4033.
6. White, W.I. In *The Porphyrins*; Dolphin, D., Ed.; Academy Press: New York, **1978**, Vol. V.
7. a) Hunter, C.A.; Sanders, J.K.M. *J. Am. Chem. Soc.*, **1990**, *112*, 5525. b) Kasha, M.; Rawls, H.R.; El Bayoumi, M.A. *Pure Appl. Chem.*, **1965**, *11*, 371.
8. Lakowicz, J.R. In *Principles of Fluorescence Spectroscopy;* Plenum Press: New York and London, **1983**, 1.
9. a) Huang, C.Z.; Li, Y.F. *Anal. Chim. Acta*, **2003**, *500*, 105. b) Pasternack, R.F.; Collings, P.J. *Science.*, **1995**, *269*, 935.
10. Cantor, C.R.; Schimmel, P.R. In *Biophysical Chemistry*, W.H. Freeman and Company Ed.; New York, **1980**, Vol. II.
11. Pasternack, R.F.; Bustamante, C.; Collings, P.J.; Giannetto, A.; Gibbs, E.J. *J. Am. Chem. Soc.*, **1993**, *115*, 5393.
12. Elemans, J.A.A.W; Van Hameren, R.; Nolte, R.J.M.; Rowan, A.E. *Adv. Mater.*, **2006**, *18*, 1251.
13. Pšenčik, J.; Ikonen, T.P.; Laurinmăki, P.; Merckel, M.C., Butcher, S.J.; Serimaa, R.E.; Tuma, R. *Biophys. J.*, **2004**, *87*, 1165.

14. Balaban, T.S.; Linke-Schaetzel, M.; Bhise, A.D.; Vanthuyne, N.; roussel, C.; Anson, C.E.; Buth, G.; Garab, G.; Javorfi, T.; Schimmel, T. *Chem. Eur. J.*, **2005**, *11*, 2275.
15. Suslick, K.S.; Bhyrappa, P.; Chou, J.H.; Kosal, M.E.; Nakagaki, S.; Smithenry, D.W.; Wilson, S.R. *Acc. Chem. Res.*, **2005**, *38*, 283.
16. Kojima, T.; Harada, R.; Nakanishi, T.; Kaneko, K.; Fukuzumi, S. *Chem. Mater.*, **2007**, *19*, 51.
17. Purrello, R.; Guerrieri, S.; Lauceri, R. *Coord. Chem. Rev.*, **1999**, *190-192*, 683.
18. Purrello, R..; Bellacchio, E.; Guerrieri, S.; Lauceri, R.; Raudino, A.; Monsù Scolaro, L.; Santoro, A.M. *J. Phys. Chem. B*, **1998**, *102*, 8852.
19. Monti, D. ; Venanzi, M. ; Russo, M.; Bussetti, G.; Goletti, C.; Montalti, M.; Zaccheroni, N.; Prodi, L.; Rella, R.; Manera, M.G.; Mancini, G.; Di Natale, C.; Paolesse, R. *New. J. Chem.*, **2004**, *28*, 1123.
20. Dolci, L.S.; Marzocchi, E.; Montalti, M.; Prodi, L.; Monti, D.; Di Natale, C.; D'Amico, A.; Paolesse, R. *Biosens. Bioelectron.*, **2006**, *22*, 399.
21. Mateos-Timoneda, M.A.; Crego-Calama, M.; Reinhoudt, D.N. *Chem. Soc. Rev.*, **2004**, *33*, 363.
22. Ortiz de Mantellano, P.R. In *Cytochrome P-450: Structure, Mechanism, and Biochemistry*; 2nd edn, Plenum New York, **1995**.
23. Monti, D.; Venanzi, M.; Mancini, G.; Di Natale, C.; Paolesse, R. *Chem. Commun.*, **2005**, 2471.
24. a) Bustamante, C.; Gurrieri, S.; Lauceri, R.; Pasternack, R.F.; Purrello, R.; Rizzarelli, E. *Biopolymers*, **1994**, *34*, 1099. b) Pasternack, R.F.; Guerrieri, S.; Lauceri, R., Purrello, R. *Inorg. Chim. Acta*, **1996**, *246*, 7. c) Chen, X.; Liu, M. *J. Inorg. Biochem.*, **2003**, *94*, 106. d) Lauceri, R.; Campagna, T.; Contino, A.; Purrello, R. *Angew. Chem. Int. Ed. Engl.*, **1996**, *35*, 215.
25. a) Zhang, L.; Lu, Q.; Liu, M. *J. Phys. Chem. B*, **2003**, *107*, 2565. b) Zhang, L.; Yuan, J.; Liu, M. *J. Phys. Chem. B*, **2003**, *107*, 12768. c) Jiang, S.; Liu,

M. *J. Phys. Chem. B*, **2004**, *108*, 2880. d) Rubires, R.; Farrera, J.A.; Ribò, J.M. *Chem. Eur. J.*, **2001**, *7*, 436.

26. Borokvov, V.V.; Hembury, G.A.; Inoue, Y. *Angew. Chem. Int. Ed. Engl.*, **2003**, *42*, 5310.
27. Purrello, R.; Monsù Scolaro, L.; Bellacchio, E.; Guerrieri, S.; Romeo, A. *Inorg. Chem.*, **1998**, *37*, 3647.
28. Lauceri, R.; Raudino, A.; Monsù Scolaro, L.; Micali, N.; Purrello, R. *J. Am. Chem. Soc.*, **2001**, *124*, 894.
29. Kondepudi, D.K.; Kaufman, R.J.; Siggh, N. *Science*, **1990**, *250*, 975.
30. Kondepudi, D.K.; Laudadio, J.; Asakura, *J. Am. Chem. Soc.*, **1999**, *121*, 1448.
31. Link, D.R.; Natale, G.; Shao, R.; Maclennan, J.E.; Clark, N.A.; Korblova, E.; Walba, D.M. *Science*, **1997**, *278*, 1924.
32. Honda, C.; Hada, H. *Tetrahedron Lett.*, **1976**, 177.
33. Chen, P.; Ma, X.; Duan, P.; Liu, M. *Chem. Phys. Chem.*, **2006**, *7*, 2419.
34. Luguya, R.; Jaquinod, L.; Fronczek, F.R.; Vicente, M.G.H.; Smith, K.M. *Tetrahedron*, **2004**, *60*, 2757.
35. a) Cantonetti, V.; Monti, D.; Venanzi, M.; Bombelli, C.; Ceccacci, F.; Mancini, G. *Tetrahedron: Asymmetry*, **2004**, *15*, 1969. b) Monti, D.; Pastorini, A.; Venanzi, M.; Borocci, S.; Mancini, G. *J. Porphyrins Phtalocyanines*, **2003**, *7*, 181.
36. Frisch, M.J. et al. Gaussian 03 Revision 8.01, Gaussian Inc., Wallinford CT, **2004**.
37. Koszarna, B.; Gryko, D.T. *J. Org. Chem.*, **2006**, *71*, 5942.
38. Král, V.; Vašek, P.; Dolenskỳ *Collect. Czech. Chem. Commun.*, **2004**, *69*, 1126.
39. Pasternack, R.F.; Goldsmith, J.I.; Szep, S.; Gibbs, E.J. *Biophys. J.*, **1998**, *75*, 1024.

40. Micali, N.; Mallamace, F.; Romeo, A.; Purrello, R.; Monsù Scolaro, L. *J. Phys. Chem. B*, **2000**, *104*, 5897.
41. Castriciano, M.A.; Romeo, A., Monsù Scolaro, L. *J. Porphyrins Phtalocyanines*, **2002**, *6*, 431.
42. Štepánek, P.; Monti, D.; Venanzi, M.; Dražar, P. *Org. Biomol. Chem.*, **2007**, in press.

Chapter 3

The Corroles Chemistry: novel aspects of their reactivity

Introduction

3.1 Corroles

The history of corroles began more than thirty years ago[1] as an outcome of Johnson's research devoted to the development of synthetic methods for the preparation of vitamin B_{12}. Johnson's idea was to use a corrole as the precursor of the corrin ring;[2] unfortunately this approach was unsuccessful and for a long time this macrocycle remained in the shadow of porphyrin chemistry, with its peculiar characteristic being that it was only the first example of a synthetic tetrapyrrolic macrocycle bearing a direct pyrrole-pyrrole link.

Corrole chemistry has recently received a new impetus, because of the discovery of some interesting and peculiar ligand properties of this macrocycle,[3] which impart upon the corrole a unique role, not necessarily related to the porphyrins. Furthermore the particular ligand behavior of corroles can be of interest for its application in several fields.

3.1.1 General properties of Corroles[3]

Because of its structure, corroles can be considered as intermediates between porphyrins and corrins (Figure 3.1). In fact, the molecular skeleton of corroles contains a direct pyrrole-pyrrole link, similar to corrins, but they retain an 18-π electron aromatic system in close resemblance to the porphyrins.

The numbering scheme of corroles has been derived from that of the porphyrins and, to retain a comparability, position 20 has been omitted with the inner core nitrogen atoms numbered from 21 to 24. In the corrole structure (Fig.

3.1) the position of the imino nitrogen atom is located at position 22, according to the calculations performed by Dyke et al.; more recently Ghosh and Jynge have reported a detailed theoretical study that suggested the presence of fast NH tautomerism in the corrole free base[4], with no significant energy difference between the possible tautomers.

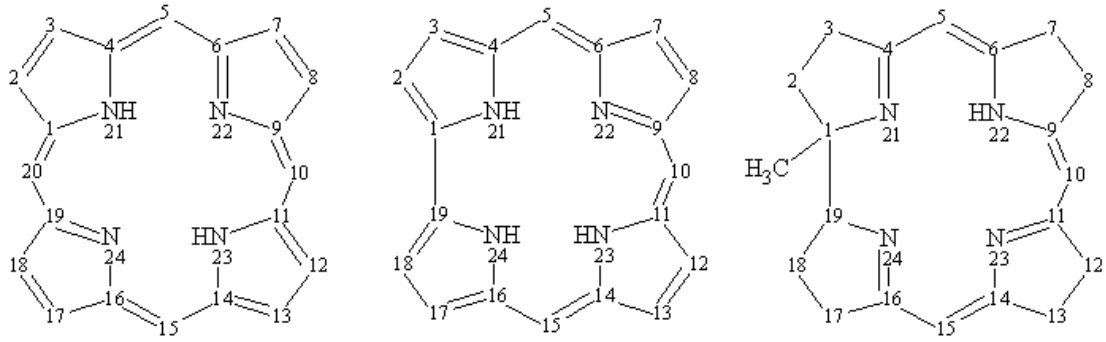

Fig. 3.1 *– Molecular structure of porphyrin, corrole and corrin.*

Spectral properties of corroles confirm their aromaticity; their UV-visible spectra show an intense absorption around 400 nm and weaker bands in the 500-600 nm region[1] (Fig. 3.2). These bands can be related to the B and the Q bands of the porphyrins and indicate the presence of an aromatic system. The corroles show an intense luminescence band around 600 nm, with a lifetime in the nanosecond region and a very short Stokes-shift. Furthermore, a diamagnetic ring current effect is also present in the NMR spectra of corroles and all resonances show significant shifts similar to those observed in the porphyrin analogues.

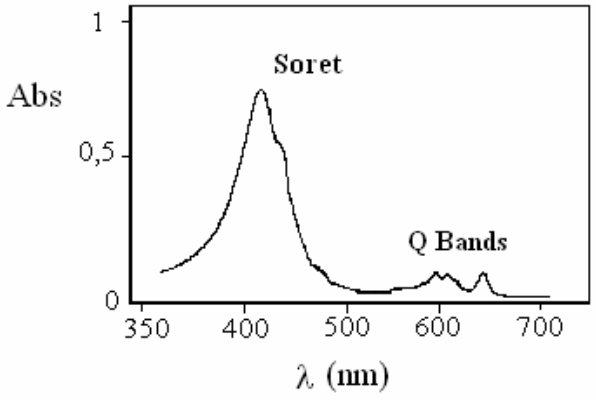

Fig. 3.2 *- UV-visible spectrum of a corrole.*

One of the significant characteristics of corroles is the three protons in the inner core; for this reason the corrole acts as a trianionic ligand different from corrins and porphyrins which are, respectively, monoanionic and dianionic ligands. Corroles are more acidic than porphyrins and the free base derivatives readily form monoanionic species in dilute basic solutions (Fig. 3.3); the monoanionic free base corroles are still aromatic and they retain the Soret band in their electronic absorption spectra. Corroles react with dilute acids to generate monoprotonated derivatives;[1] these monocationic species are aromatic, indicating that the addition of a proton occurs at the inner core nitrogen atom (Fig. 3.3). Stronger acidic conditions cause significant changes in the corrole absorption spectra, with the disappearance of the Soret band. The site of protonation appears to be at the 5 (or 15) position, based on spectroscopic analysis, with resulting interruption of the π conjugated system (Fig. 3.3).

Later studies on the protonation of N-methylcorroles indicated the presence of three protonation steps, but the site of these protonation events is not yet fully known. Furthermore it is not certain that the behavior observed in the case of N-methylcorroles can be generalized, because similar investigations have never been extended to other corroles.

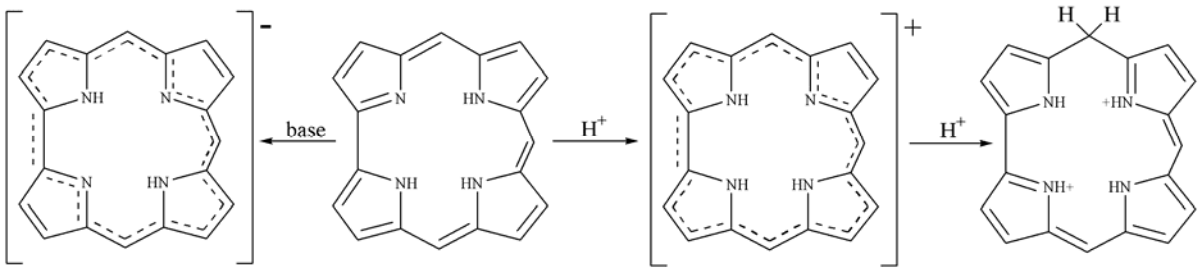

Fig. 3.3 *– Corrole acid-base equilibria.*

It has been demonstrated that octaethylcorrole (OEC) undergoes protonation when oxidized in CH_2Cl_2 solutions to give the corresponding π dication radical[5],

$[(OEC)H_4]^{2+\bullet}$. The identification of such a species was established on the basis of comparison between experimental results obtained by EPR, ENDOR, TRIPLE spectroscopies and molecular orbital calculations (RHF-INDO/SP program); an agreement between measured and calculated spin density distributions was greatly improved by considering $[(OEC)H_4]^{2+\bullet}$ as the oxidation product.[5] This hypothesis was also supported by the fact that the oxidation product of $[(OEC)H4]^{+}$ has spectroscopic properties identical with those of $[(OEC)H_4]^{2+\bullet}$.

3.1.2 Syntheses of Corroles[3,6]

The synthetic chemistry of corroles is far from being as well-developed as that of the porphyrins. Although some of these characteristics of corroles were already known in the past, the chemistry of this macrocycle remained for long time overshadowed among porphyrin analogs. One of the reasons of this lack of interest was probably due to the multi-steps, lengthy and laborious preparation of the macrocycle, which precluded the study of corrole to researchers not familiar with pyrrole chemistry. This scenario changed in 1999, when Gross[7] and our group[8] reported almost contemporaneously the preparation of 5,10,15-triarylcorroles from the reaction of pyrrole and benzaldehydes.

These two seminal reports constituted the starting point for a tumultuous and impressive growth of corrole-devoted papers and the chemistry of this macrocycle has then undergone an unprecedented development. The synthetic approaches to corrole have been further refined and the synthetic chemistry of corrole, yet not developed like that of porphyrins, is nowadays quite versatile.

The main synthetic approaches to corroles can be summarized as follows.

- **Syntheses from pyrroles**

Two different approaches for the synthesis of corroles can be followed starting from monopyrroles. These are the tetramerization of a 2-substituted pyrrole or the condensation of a pyrrole with an aldehyde. Both approaches have been useful and successful routes for the synthesis of porphyrins; in the case of corroles, these routes have not been exploited in part because the competitive formation of the porphyrin has been considered an unavoidable drawback to this approach. However some examples reported in the literature demonstrate the possibility for obtaining corroles starting from monopyrroles.

1. Tetramerization of a 2-substituted pyrrole[9]

The first example for the synthesis of corroles using tetramerization of a 2-substituted pyrrole involved the preparation of octamethyltriphenylcorrole complex, (OMTPC)CoPPh$_3$, from 2-(α-hydroxybenzyl)pyrrole (Scheme 3.1). Pyrrole was first reacted in acidic ethanol after which the reaction mixture was buffered with cobalt(II) acetate in the presence of PPh$_3$ to give the corresponding triphenylphosphine cobalt complex in 25% yield. The presence of cobalt ions was necessary to obtain the corrole ring; in the case of copper, nickel or rhodium salts, for example, the octamethyltetraphenylporphyrin (OMTPP) was always obtained, as expected from a tetramerization of a monopyrrole. The first hypothesis formulated to explain the formation of a corrole was a ring contraction of the intermediate porphyrinogen, catalyzed by the cobalt ion; this reaction is in analogy with what it is proposed to happen in the biochemical synthesis of the corrin nucleus of vitamin B$_{12}$ from uroporphyrinogen III. This hypothesis, however, was later ruled out because the direct reaction of porphyrinogen with cobalt(II) and triphenylphosphine under the same conditions did not afford the corrole complex, but instead gave (OMTPP). A different reaction mechanism has been proposed, involving the formation of dipyrromethene species, which can self-condense in the presence of

cobalt ions to give the ring contracted macrocycle. The formation of this kind of intermediate compound was supported by the presence of an absorption maximum around 515 nm in the reaction mixture[10].

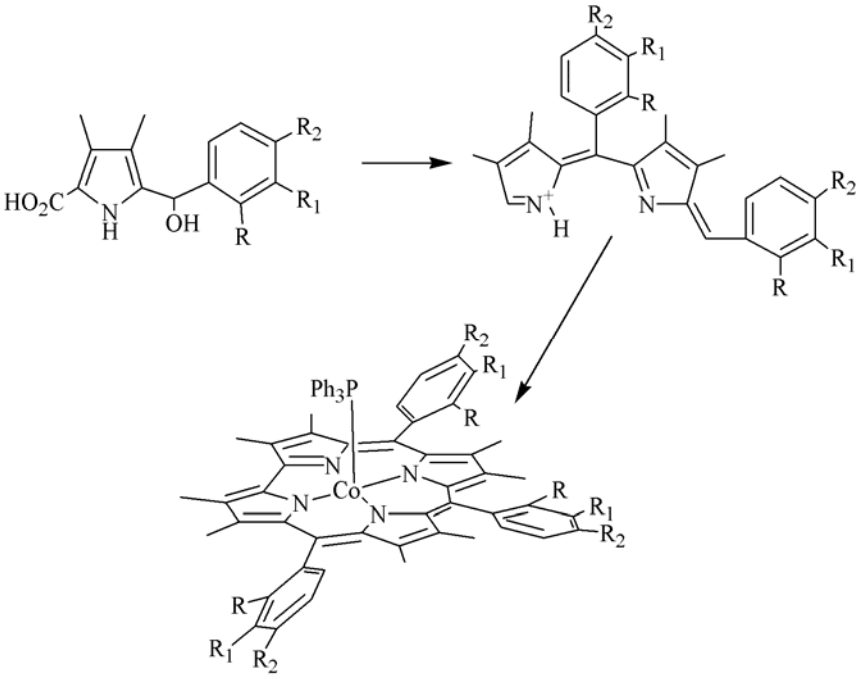

Scheme 3.1 *– Tetramerization of a 2-substituted pyrrole.*

Synthesis of corroles from 2-substituted pyrroles has also been accomplished in the case of 2-formylpyrroles, using the same reaction conditions. In this case cobalt(II) ion is able to drive the reaction to formation of the corrole, whereas nickel(II) and rhodium(III) ions led to porphyrins and iron(III) salts failed to give any macrocyclic products.

2. Condensation of pyrrole and aldehydes

The formation of corrole from the direct reaction of pyrrole and an aromatic aldehyde was reported in 1996, with the formation of *meso*-arylcorrole[11] as by-product of the synthesis of 5,10,15,20-tetrakis-(2,6-dinitrophenyl)porphyrin.

The generality of this approach was however demonstrated in 1999, by Gross group and us and after these papers other examples have been reported in the

literature and it is now possible to choose, among different methods, the best ones for the particular corrole desired.

Reaction of pyrrole and aldehyde in the absence of solvent

The Gross approach consists in the reaction of pyrrole and the aldehyde in the absence of solvent, catalyzed by basic alumina. The yields of the reaction were satisfactory in the presence of pentafluorobenzaldehyde, while in the presence of less reactive aldehydes a significant reduction of yields or the complete failure of the reaction was observed[7].

Following this route, the same group prepared the first *meso*-alkyl substituted corrole while Ghosh[12] and Chang[13] have been able to prepare the *β*-octafluorocorrole and the perfluorocorrole respectively (Fig. 3.4).

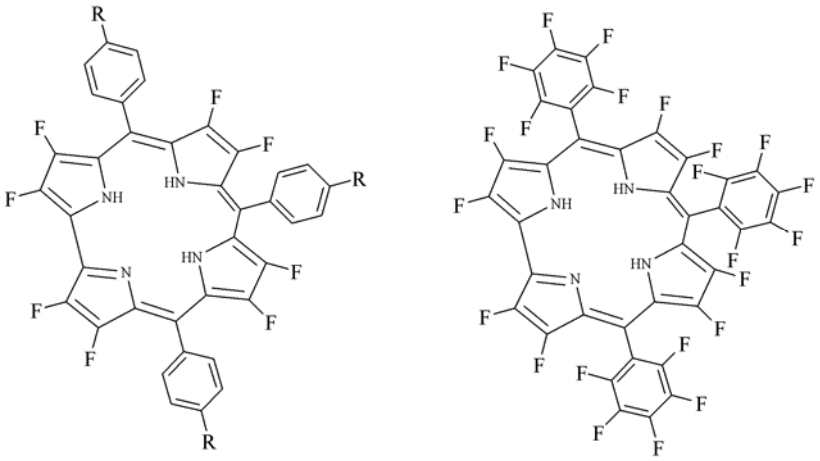

Fig. 3.4 *– β-octafluorocorrole and perfluorocorrole.*

Lee[14] and co-workers, as later reported, demonstrated that the reaction of pyrrole and benzaldehyde catalyzed by trifluoroacetic acid (TFA), following the conditions usually adopted for the formation of *meso*-aryl dipyrromethane, can afford a linear bilane (Fig. 3.5), other than higher linear polypyrroles, by variation of the reagent molar ratio. Subsequent oxidative ring closure, generally carried out with chloranil in open air, gives the corrole ring.

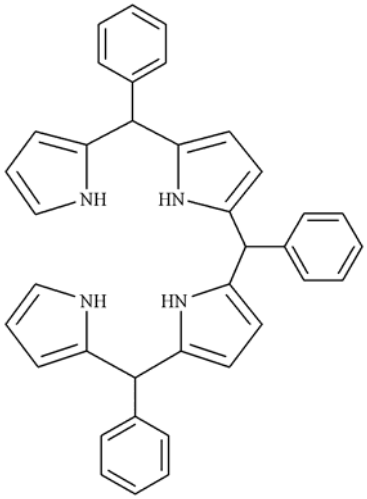

Fig. 3.5 *- Linear bilane structure.*

Following this pathway, Gryko[15] *et al.* proposed a further modification of the reaction protocol between pyrrole and benzaldehydes, carrying out the reaction in two steps: in the first the neat reaction of pyrrole and aldehydes was carried out with the addition of TFA as catalyst and then the reaction was diluted with CH_2Cl_2 and the mixture oxidized with dichlorodicyanobenzoquinone (DDQ).

Gryko and Koszarna optimized the conditions for the formation of corrole from the TFA reaction of pyrrole and benzaldehydes, and they refined three different experimental protocols, depending on the reactivity of the aromatic aldehyde. Highly reactive aldehydes, like pentafluorobenzaldehyde, gave higher yields of corrole in the presence of low amount of the acid catalyst, while less reactive aldehydes needed higher amounts of TFA and an excess of pyrrole. In this way it has been possible to prepare a quite large variety of substituted corroles in the range of 10-20% yields.

Modified Rothemund method[16]

A different approach for the preparation of meso-triarylcorrole has been developed by a simple modification of the experimental conditions of the conventional Rothemund method for the preparation of tetraarylporphyrins, which performs the reaction between pyrrole and aromatic aldehyde in refluxing acetic or propionic acid. To obtain corrole the reaction was carried out in the presence of a

3:1 molar excess of pyrrole. In this way a mixture of corrole and porphyrin is generally obtained, although in some particular cases, such as the reaction with 4-nitrobenzaldehyde, the corrole is the exclusive macrocyclic product of the reaction, in a surprisingly high 22% yield. The scope of the reaction is quite general with mono-substituted benzaldehydes and a wide range of corroles has been prepared following this approach.

In the case of sterically hindered benzaldehydes, such as 2,6-disubstituted derivatives, this approach is not successful and corrole has not been obtained or has been observed in descouraging low yields (0.3 %).

One of the major drawbacks of this approach is however the concomitant formation of the corresponding tetra-arylporphyrin, which makes difficult the chromatographic separation of corrole from the corresponding porphyrin, with the consequent reduction of the total yield of the reaction.

Modified Lindsey method[17]

A third example of preparation of *meso*-substituted corroles involved the reaction of pyrrole and benzaldehydes in acidic CH_2Cl_2, this route can be considered a modification of the Lindsey procedure for the preparation of tetraarylporphyrins. This approach involves a two-step reaction, where pyrrole and benzaldehyde are first reacted in acidic dichloromethane to give the porphyrinogen, which is then oxidized by DDQ to the final porphyrin.

Our group carried out the reaction of benzaldehyde and pyrrole, in 1:10 molar excess, in CH_2Cl_2 with TFA as catalyst Subsequent oxidation with p-chloranil afforded corrole in satisfactory yields, while the corresponding porphyrin was not present or was observed only in traces among reaction products. This approach was also working in the case of 2,6-disubstituted aldehydes, where the modified Rothemund approach failed. Furthermore following this approach it was possible to prepare fully substituted β-octaalkyl, *meso*-triphenylcorroles.

- **Syntheses from dipirromethanes**

A wide range of *meso*-substituted corroles has been obtained using dipyrromethane as starting materials. Two different approaches can be followed (Scheme 3.2).

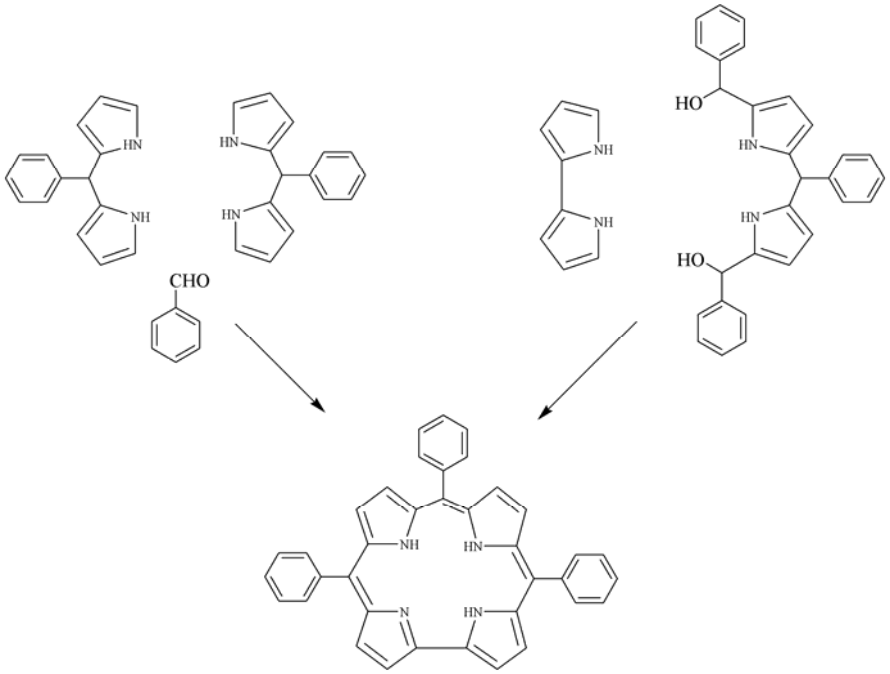

Scheme 3.2 *– Syntheses from dipyrromethanes.*

In the first pathway two *meso*-substituted dipyrromethanes are reacted with an aromatic aldehyde, while the other approach is reminiscent of the McDonalds synthesis of *β*-alkylporphyrins, with the [2+2] acid catalyzed condensation of dipyrromethane and bipyrrin to give the corresponding macrocycle.

The more general pathway, however, is represented by the acid catalyzed reaction of two units of dipyrromethane with a benzaldehyde. Although no evidences have been reported in the literature, it is reasonable that the formation of corrole goes through an intermediate bilane, which is then oxidatively cyclized to give the final corrole ring.

Following this approach, it is also possible to prepare A_2B-substituted corrole, if the final aldehyde is different from that present in the starting dipyrromethane.

The first example of this approach was reported in 2001 by Gryko[18]; the reaction of mesityl dipyrromethane with fluoro substituted benzaldehydes afforded the corresponding A_2B corroles in satisfactory yields. In the preliminary communication the reaction has been reported to be successful only with activated liquid aldehydes and was carried out without the addition of acid as a catalyst. However a detailed study from the same author rationalized this unexpected results, showing that the acid catalysis is necessary for the success of the reaction, and in the first reactions the catalysis was performed by the presence of small amounts of benzoic acids present as contaminants in the liquid aldehydes. Gryko and co-workers pointed out the optimal reaction conditions to increase the corrole yields and to avoid scrambling in the formation of A_2B corroles, using the reaction of mesityldipyrromethane and 2,6-difluorobenzaldehyde as reference reagents. Differently from the protocol used in the porphyrin synthesis, low concentration of acid and high concentrations of substrates favored the formation of corrole ring. TFA and dichloromethane were found to be the best choices for the reaction, while no increase of reaction yields were observed using propionitrile as solvent. The scope of the reaction is quite general and a wide range of different substituted A_2B corroles, including macrocycle bearing pyridine or other nitrogen aromatic bases in the *meso* positions[19] (Scheme 3.3).

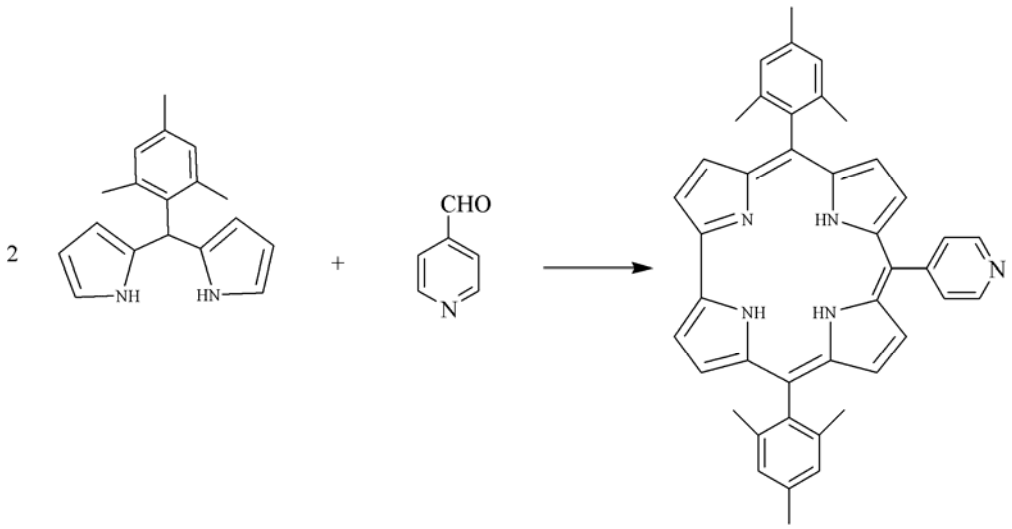

Scheme 3.3 *– A_2B-substituted corrole synthesis.*

- **Syntheses from tetrapyrrolic precursors**

The cyclization of a linear tetrapyrrole has been for long time the unique general route for the preparation of corroles. The oxidative cyclization of the *a,c*-biladiene, has been also the first successful approach for the preparation of this macrocycle.

This linear tetrapyrrolic precursor is generally preparared by the acidic condensation of a dipyrromethane with two equivalents of a 2-formylpyrrole and the obtained *a,c*-biladiene is separated as dihydrobromide salt. For long time basic conditions have been considered as an essential requisite for the formation of corroles, necessary to induce the formation of the dihydrobilatriene, the linear precursor that undergoes the final cyclization step to give corroles. However we recently noted that corroles can also be obtained from *a,c*-biladienes directly in acetic acid or acidic ethanol, demonstrating that the addition of bases is not necessary[20]. More recently we have studied the reaction of *a,c*-biladienes with chloranil in different solvents. Good yields of corrole can be obtained in methanol and the addition of base is not necessary for the cyclization. In $CHCl_3$ the reaction has a completely different pathway, with the formation of the corresponding biliverdin. Addition of small amounts of methanol to the $CHCl_3$ solution, however, induces again the formation of corrole in yields similar to that observed in pure methanol. These results indicated that it is necessary the formation of a fully conjugated species, the dihydrobilatriene cation, to allow the subsequent formation of corrole, (Scheme 3.4).

Methanol or other protic species, induce the formation of this precursor after tautomeric shift of a hydrogen atom, and then the corrole formation. When the formation of this species is prevented, such as in $CHCl_3$, the direct oxidation of the biladiene leads to the biliverdin. When both deprotonation and oxidation are not allowed, as in the case of 10-alkyl substituted *a,c*-biladienes, no reaction is observed and the tetrapyrrole slowly decomposes in solution. The possibility to carry out the

reaction with p-chloranil also in acidic conditions, offers the possibility to point out a two-steps, one-pot synthesis of corroles starting from dipyrromethane and 2-formylpyrroles, avoiding the isolation of the linear precursor.

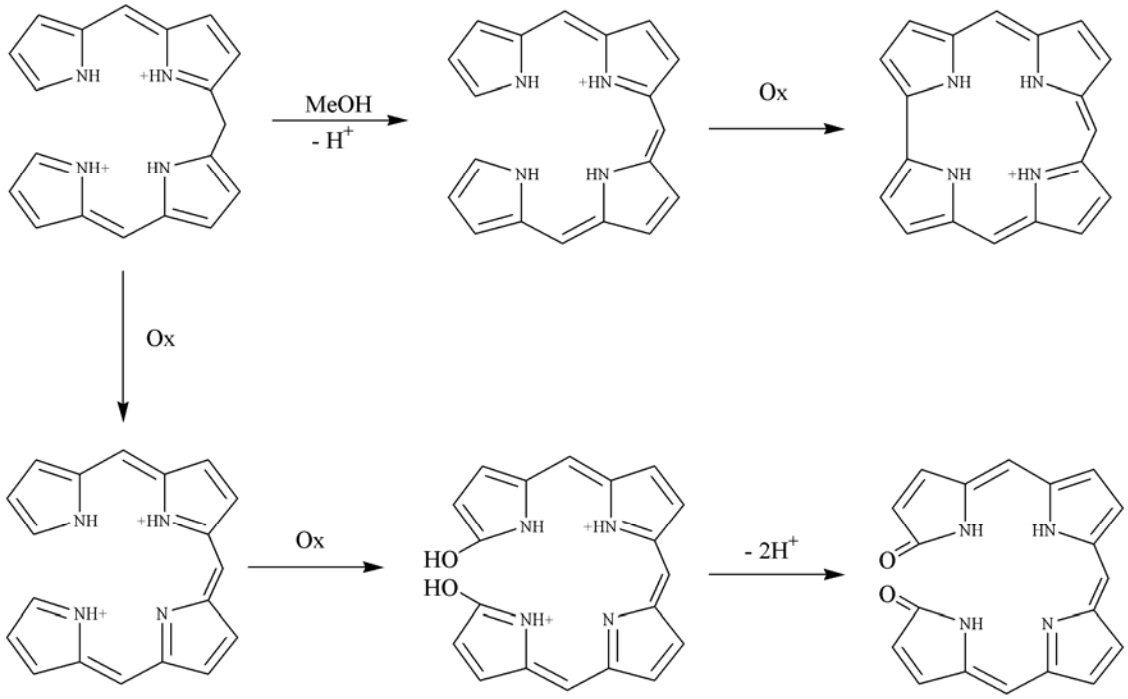

Scheme 3.4 *– Oxidative cyclization of the a,c-biladiene.*

While in the usual preparation of corrole the last synthetic step is the formation of the direct pyrrole-pyrrole link, a different route has been proposed by Bröring and Hell[21], which used as linear precursor a 2,2'-bisdipyrrin, where the pyrrole-pyrrole bond is already present. The cyclization of this precursor was catalyzed by $Mn(OAc)_2$ and the final product is the corresponding Mn(III)Corrole complex. The free base corrole can be obtained in good yields following this route by removal of the Mn(III) ion in HAc/HBr solution. This is also the first example of demetallation of a corrole ring reported in the literature. By using substituted bis-dipyrrins, Bröring and Hell were able to prepare 5,15-diarylcorroles, which could not be prepared by the usual *a,c*-biladiene route.

In the case of 5,10,15-triarylcorroles, the linear precursor is the bilane, formed from the acid catalyzed, neat condensation of pyrrole and benzaldehyde. Highest yields of the bilane were obtained by reduction of the pyrrole: benzaldehyde molar excess to 3:1. The bilane can be purified by chromatography from the other oligo-pyrrolic species formed in this reaction, and subsequently reacted with DDQ, to give the corresponding corroles in good yields. To optimize the experimental protocol the reaction was carried out in different solvents and the influence of the addition of some inorganic salts was also studied. Best results (65 % yield) were obtained by using propionitrile as solvent, where inorganic salts showed no influence. On the other hands, a significant increase of reaction yields by addition of these inorganic salts were observed in acetonitrile or CH_2Cl_2; DDQ was also find to be a better oxidant for the ring closure than p-chloranil.

More recently Guilard and co-workers have reported a different route to the formation of the bilane, by the reaction of a dipyrromethane dicarbinol with pyrrole, which is reminiscent of the *a*,*c*-biladiene pathway (Scheme 3.5).

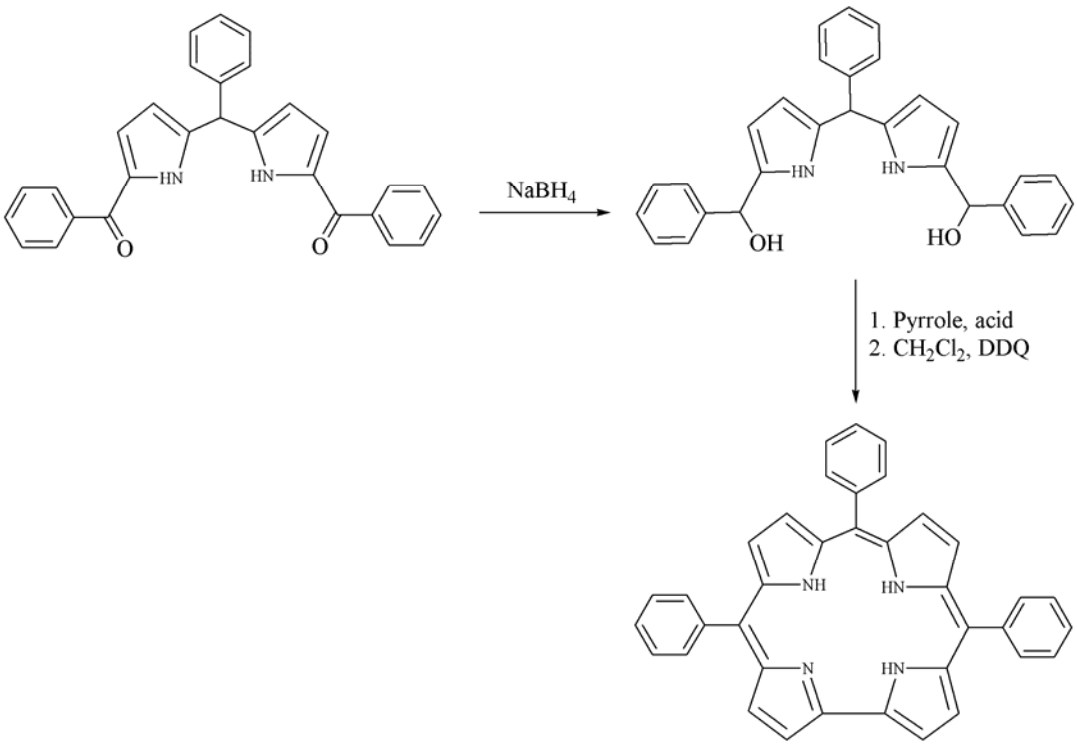

Scheme 3.5 *– Guilard synthetic procedure.*

In this case a diacyl dipyrromethane is reduced by $NaBH_4$ and then condensed in acidic conditions with pyrrole to give the linear species, which is then cyclized with DDQ under the usual conditions to give the corresponding corrole. The bilane can be purified by chromatography and then reacted to give corrole, or the reaction can be carried out one-pot, without the isolation of the linear intermediate. In both cases no porphyrin was observed among reaction products.

Unsymmetrical ABC-corroles can be prepared following this route, starting from unsymmetrical diacyl dipyrromethanes, prepared following the procedure reported by Lindsey and co-workers.

3.2 Metallocorroles

Corroles have been shown to possess excellent chelating properties and at least twenty metal ions have so far been introduced into the macrocycle[22]. Although the coordination chemistry of corroles is far from being as developed as that of porphyrins, it is not unreasonable to believe that the number of metals coordinated to corroles can be greatly expanded in the future. Having three amino and one imino like nitrogen atoms in the inner core, the fully deprotonated form of the corrole acts as a trianionic ligand, different from both corrins and porphyrins, which are, respectively, monoanionic and dianionic ligands. Furthermore, the ability of corroles to stabilize higher oxidation states of the metal as compared to porphyrins, makes its coordination chemistry particularly interesting[23].

For example, iron(IV) porphyrins exist only as unstable inter-mediates while a large number of stable iron(IV) corroles are known[3]. Thus, metallocorroles are of great interest as stable model compounds for the high-valent active intermediates of various heme proteins as well as for general investigations of the electronic structures of high-valent transition metal complexes. In addition, metal complexes

of electron-poor corroles have exhibited promise as catalysts in hydrocarbon oxidations.

3.2.1 The corrolates controversy: "Innocent" or "Noninnocent"[24]

Theoretical calculations have shown that corroles, like porphyrins, obey Gouterman's four-orbital model. Nontransition metal corrole derivatives in C_{2v} have two nearly degenerate HOMOs (a and b) well separated from the rest of the occupied orbitals and two nearly degenerate LUMOs well separated from the other unoccupied orbitals. For example, the two lowest ionization potentials of unsubstituted Ga(III) corrole are extremely close to each other. The two HOMOs of a simple corrole derivative are moderately similar in shape to the a_{1u} and a_{2u} HOMOs of porphyrins. Like the a_{1u} porphyrin HOMO, the a_2 corrole HOMO has zero or relatively small amplitudes at the '*meso*' positions and like the a_{2u} porphyrin HOMO, the b_1 corrole HOMO has large amplitudes at the '*meso*' positions (Fig. 3.6).

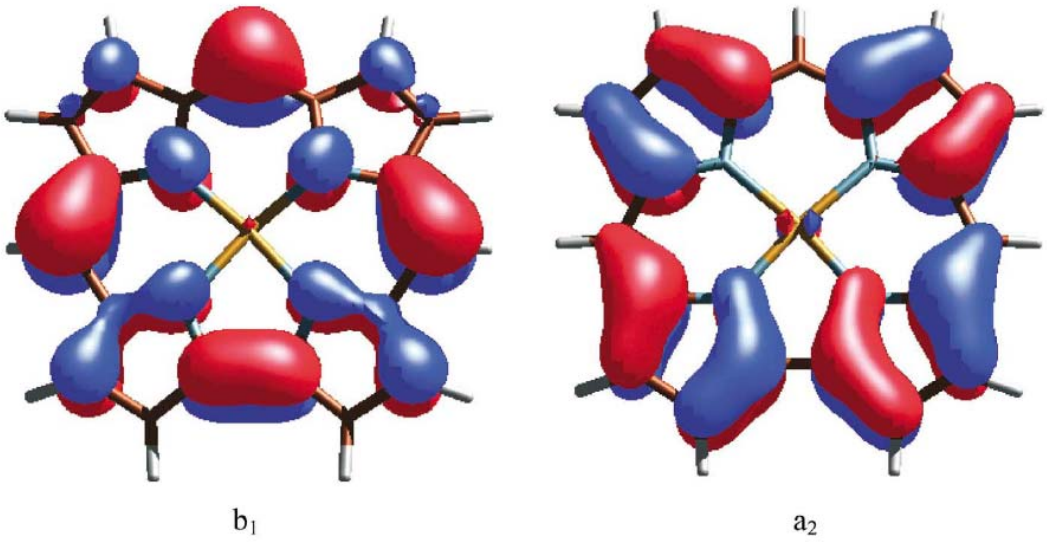

Fig. 3.6 *– The b_1 and a_2 HOMOs of the Ga(III)corrole.*

Corroles are generally more easily oxidized than analogous porphyrin derivatives. For example, the first oxidation potential of Sn(OEC)Cl is 0.67 V compared to 1.36 V (vs. SCE) for Sn(OEP)Cl (OEC=*β*-octaethylcorrole and OEP=*β*-octaethylporphyrin). This poses a paradox: With such low halfwave potentials for oxidation, how do corroles stabilize high oxidation states of transition metal ions? The fact that free-base corroles have three ionizable protons and act as –3 ligands provides a partial explanation for this stabilization. A more intriguing issue and one that has recently provoked controversy involves whether metallocorroles feature 'true' high-valent metal centers or whether the corrole ligand is oxidized (i.e. noninnocent) itself. For this reason, the oxidation states indicated in the various chemical formulae hereafter are meant only as a convenience for the purpose of keeping track of electron counts and do not refer to any actual electronic-structural scenario.

With regard to, the main thesis of a recent Ghosh work is that electrochemical measurements, in addition to magnetic resonance measurements, afford a convenient probe of this question. The picture that emerges from its studies is as follows.

For a relatively electron-rich corrole ligand, the halfwave potentials for oxidation of the Cu(III), Sn(IV)Ph, Fe(IV)Ph, and a Fe(IV)–O–Fe(IV) complexes are significantly lower than those of the Sn(IV)Cl, Fe(IV)Cl, Mn(IV)Cl, and Cr(V)(O) complexes, suggesting that the corrole ligand is relatively electron-rich or 'innocent' in the former group of complexes and that it is relatively electron-deficient or 'noninnocent' in the latter group of complexes. Both the formal charge of the central metal ion and the nature of the axial ligand, if any, appear to be key determinants of the electronic character of the corrole ligand in metallocorrole complexes, a theme that also has interesting resonances with recent findings on high-valent heme protein intermediates. However, for very strongly electron-deficient ligands such as TPFPC and BrTPFPC, the various metal complexes all

exhibit comparable half-wave potentials for oxidation and the ligand may be considered to be relatively innocent.

3.2.2 Syntheses of metallocorroles

Different procedures have been proposed for the preparation of metallocorroles; the cyclization of *a*,*c*-biladiene in the presence of a metal salt is the most direct approach but it cannot be generalized because some metal ions are able to catalyze the cyclization of the open-chain tetrapyrrole without being coordinated and the product of the reaction is then the corresponding corrole free base[25]. In this case it is necessary to react the preformed macrocycle with the appropriate metal carrier (Fig. 3.7); furthermore this method generally affords higher yields of the corresponding metallocorrole.

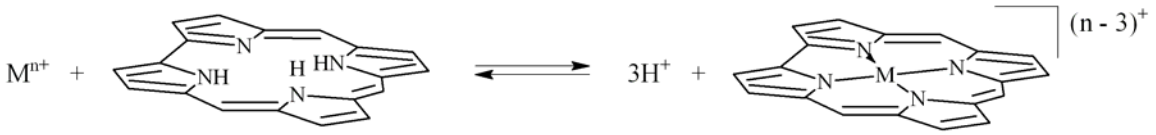

Fig. 3.7 – Metallation reaction scheme.

3.3 Functionalization of Corroles

The modification of the substitution pattern on the corrole ring by the introduction of different groups was a quite unexplored field until the preparation of 5,10,15-triarylcorroles. Indeed these macrocycles constitute a convenient starting platform for the achievement of more elaborated molecular architectures, by analogy with the corresponding 5,10,15,20-tetraphenylporphyrins. Following this

idea, interesting examples of *β*-functionalization of *meso*-triphenylcorroles have been reported in the literature[6], although this field is still in its infancy when compared with that achieved in porphyrin synthetic chemistry. Furthermore, *β*-functionalization of corroles presents higher potential complexity compared with porphyrins, because of the lower symmetry of the corrole system, which can lead to a larger number of possible isomers.

The functionalizations performed on the corrole ring can be divided in two main groups, namely the addition to the inner core nitrogen atoms or substitutions on the peripheral positions. While the alkylation of the corrole inner core has been carried out on both *β*-alkyl and *meso*-triarylcorroles, the functionalization of the peripheral positions has been almost exclusively performed on triarylcorroles, by reaction with electrophilic reagents.

3.3.1 Chlorosulfonation

This reaction was carried out dissolving the tris-(pentafluorophenyl)corrole in cholorosulfonic acid (CSA), which served both as solvent and reagent. Following this approach[26], bis-substituted products were obtained and, among the different regioisomers, only two isomers were isolated (Fig. 3.8), with the 2,17-substituted derivative as the predominant species to respect the 3,17-isomer present in lower amount (94:6 molar ratio).

It is worth mentioning that the reactivity of corrole with CSA is peculiar among tetrapyrrolic macrocycles, in that tetraarylporphyrins have been shown to react preferentially at the *meso*-aryl positions, while phthalocyanines give a complex mixtures of isomers.

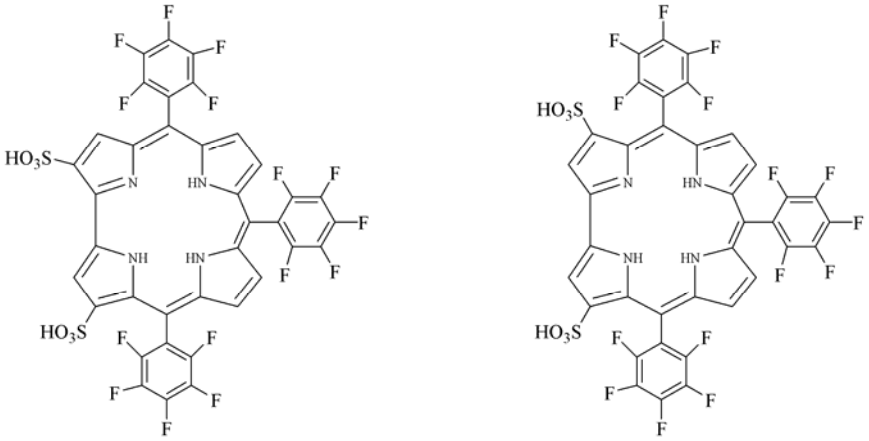

Fig. 3.8 *- Chlorosulfonation reaction prodocts.*

3.3.2 Bromination

The introduction of bromine atoms at the *β*-pyrrolic positions have been carried out on the free-base or on a corrole metal complex. Different from tetraaryl-porphyrins, in both cases the product of the reaction is the *β*-octabromo corrole derivative, where all the *β*-pyrrolic positions are substituted[27].

The reaction on the free base corrole was performed by using N-bromosuccinimmide (NBS) as brominating agent. The yields of this reaction were however quite low, probably due to the decomposition of the corrole in the reaction conditions. When the reaction was carried out using bromine in methanol, the bromination was accompanied by the ring opening of the corrole ring. The *β*-octabromo corrole is quite unstable, probably due to the steric hindrance induced by the peripheral halogen groups, as evident from the UV-vis spectrum, which showed a red-shifted and very broad Soret-like band. Coordination of cobalt ion, using triphenylphosphine as axial ligand, afforded the corresponding penta-coordinated complex in a quantitative yield. X-ray crystallographic characterization of the cobalt

complex of the corrole (Fig. 3.9a), showed only slight deviations from the planarity of the macroring, evidencing the steric relief due to the metal coordination.

When the bromination reaction of corrole was carried out on metal complexes, higher yields were obtained, probably because of the higher stability of the metal complexes of the octabromocorrole. Gross and coworkers prepared the octabromo derivative (Fig. 3.9b), by reaction of the Mn(III)corrole with Br_2 in MeOH, while Ghosh *et al.* obtained the fully brominated product of a series of corroles after the reaction of their copper complexes with Br_2 in $CHCl_3$.

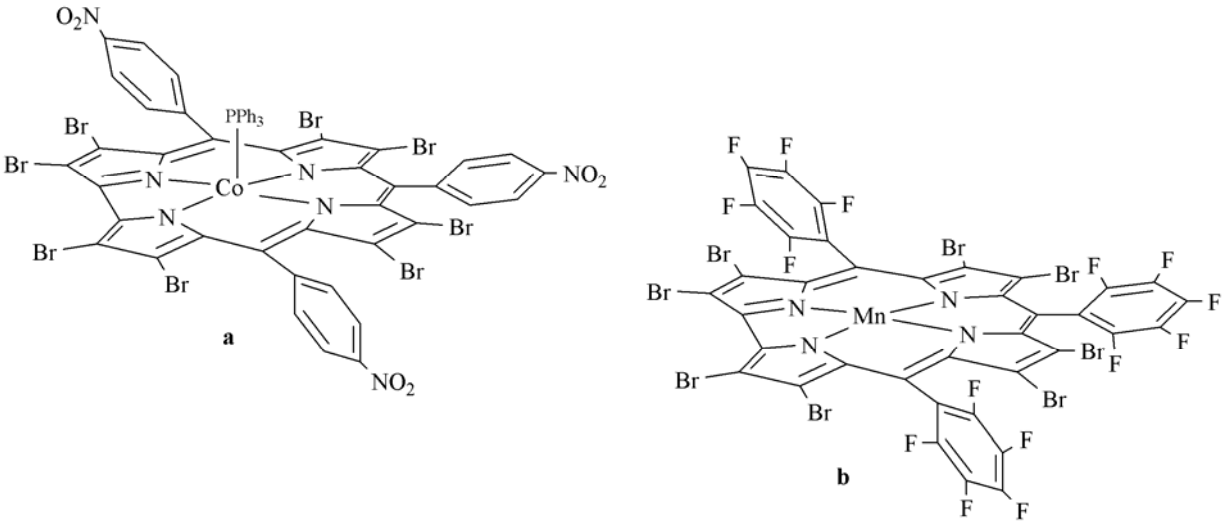

Fig. 3.9 *– Bromination reaction products.*

3.3.3 Formylation

The reagent of choice for this reaction is the Vilsmeier reagent and this system has been used in the case of *β*-alkylcorroles, although in this case a dimethylamino derivative[28], is instead obtained in place of the expected product. The reaction carried out on the Ga complex of tris-(pentafluorophenyl)corrole afforded the 3-formyl corrole or the 2,17-diformyl derivative (Fig. 3.10) depending on the

corrole:Vilsmeier reagent molar ratio. The selectivity was very high and only these regioisomers were obtained.

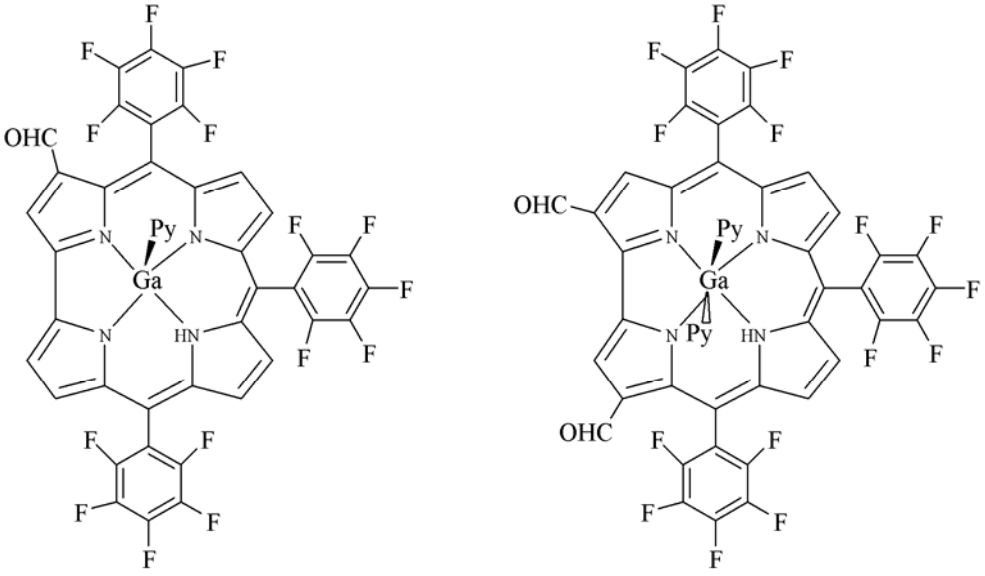

Fig. 3.10 *– Formylation reaction products.*

A peculiar behavior was observed when the reaction was carried out on the free base corrole[30]. The expected 3-formyl derivative was obtained along with a polar compound that became the major product in the presence of an excess of DMF. The X-ray crystallographic characterization of this product allowed us to identify this compound as an inner core ethane bridged derivative (Fig. 3.11). This compound is unprecedented in the case of porphyrins and it is probably obtained from the attack of the Vilsmeier reagent to the inner core nitrogen atoms, followed by a complex series of reactions. Also in this case this peculiar reactivity can be probably inferred to its higher acidity with respect to that of porphyrins, biasing the formation of the corrole anion, which can drive the attack of the Vilsmeier reagent to the macrocyclic core.

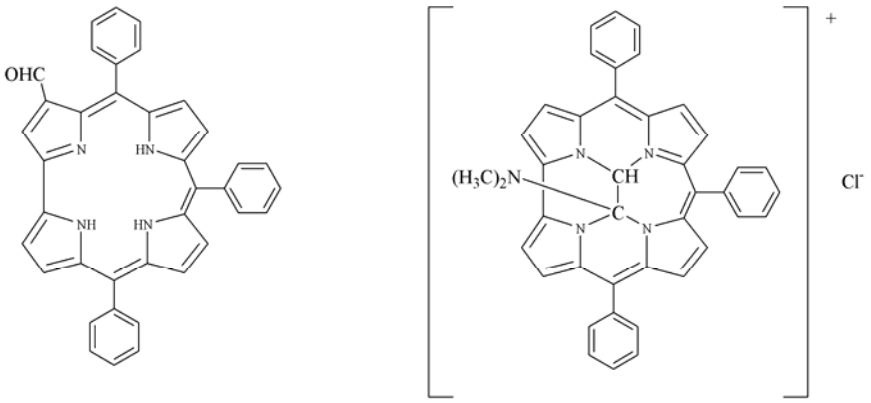

Fig. 3.11 *– Products of the formylation reaction carried out on the free-base corrole.*

3.3.4 Carboxylation

This reaction is similar to the chlorosulfonation and was attempted in order to obtain corroles bearing carboxylic groups at their peripheral positions. The reagent is phosgene and the reaction was firstly attempted on the corrole free base[31]. Also in this case the preferred reaction site was the corrole inner core and the product of the reaction was the bridged carbamide. When the reaction was carried out on the Ga complex, the reaction was successful and the monocarboxylated species was obtained (Fig. 3.12).

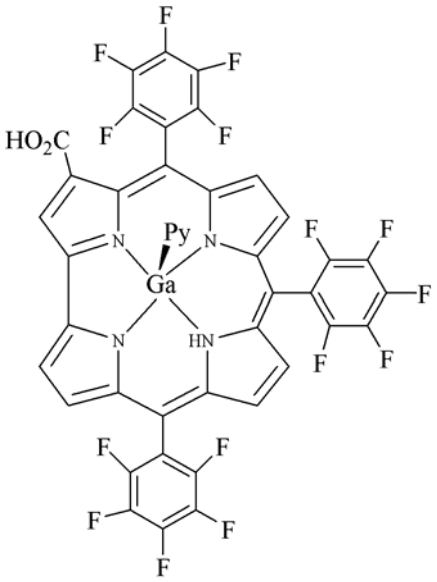

Fig. 3.12 *– Carboxylation reaction products.*

Results and Discussion

3.4 Nitration of Corroles

The β-functionalization of corroles is particularly challenging, because this macrocycle showed in several cases an unpredictable reactivity[27,29,30,33] and furthermore because its lower symmetry than porphyrins leads potentially to the formation of a huge range of regioisomers.

Among the different β-functionalizations, nitration is particularly appealing, because nitro group is a useful starting point for further functionalizations[32]. As an example a β-nitrocorrole is the starting material for the synthesis of a β-fused pyrrole-corrole, a compound particularly intriguing for the construction of more elaborated β-fused architectures, with potential peculiar optical and electronic features.

In literature there is only one example of such reaction, related to the nitration of Ga complex of pentafluorophenyl corrole[29], while this reaction has never been attempted on β-alkylcorroles.

We have been interested in the reaction of corrole free base, because from one side the demetallation of corrole complexes is not so easy and from the other side because free base showed an interesting reactivity.

In the case of bromination we observed a corrole-isocorrole tautomeric equilibrium[27], while hydroformilation afforded an inner core ethane bridged macrocycle in the case of triphenylcorrole and a methyne bridged derivative in the case of β-alkylcorroles[30]. Finally, the reaction with CI_4 gave the corresponding hemiporphycene, by macrocyclic ring expansion [33].

The reaction reported by Gross and co-workers[29] was carried out on the Ga complex of tris-(pentafluorophenyl)corrole firstly with the nitrating systems successfully used in the case of tetraarylporphyrins, such as HNO_3/H_2SO_4, N_2O_4 or $AgNO_2/I_2$. A complex mixture of poly-nitrated derivatives and a significant decomposition of the corrole ring was observed in these conditions, probably due to the strong oxidating character of the reagents.

The successful approach was to use $NaNO_2$ in acetonitrile, with the addition of a small amount of a hexachloroantimonate salt, as one-electron oxidant. In these conditions the reaction was selective and it was possible to obtain the mono-nitro, the 3,17-dinitro and the 2,3,17-trinitro derivative, depending on the amount of the nitrating agent used (Scheme 3.6).

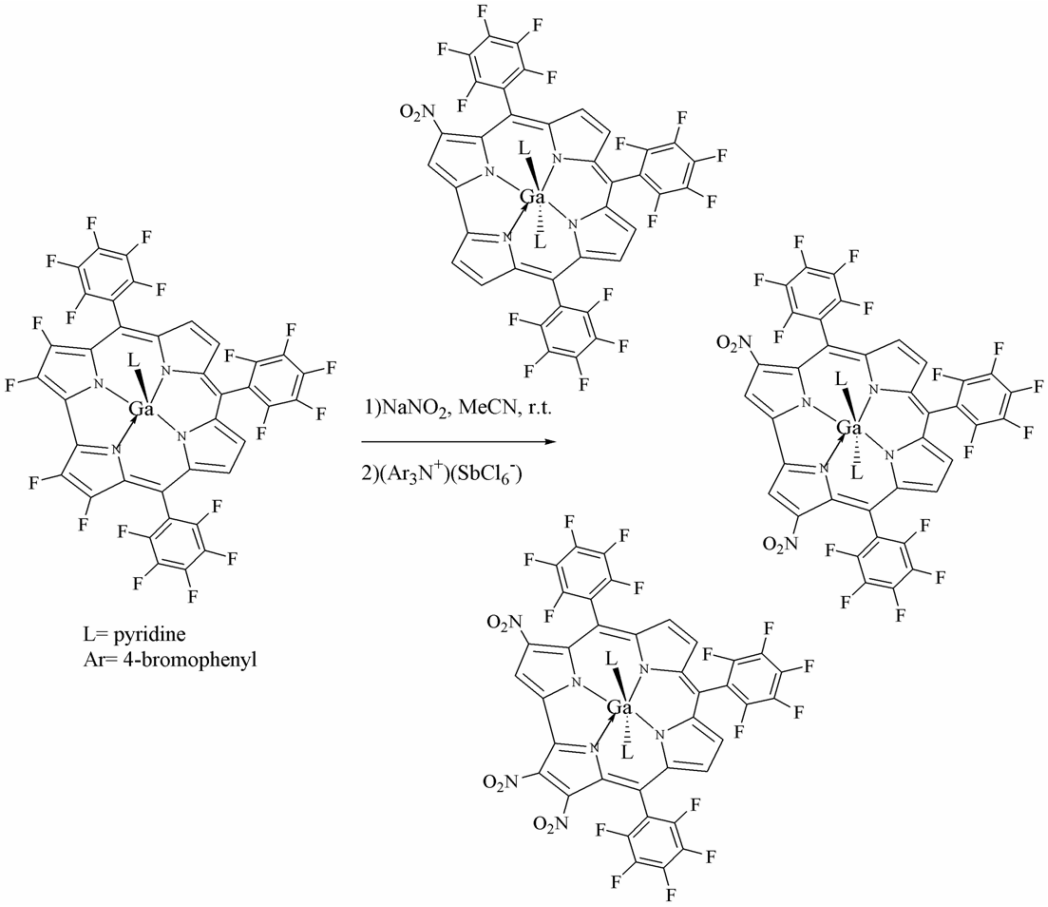

Scheme 3.6 – *Selective nitration of Ga(F_5TPC)(py).*

The mechanism of nitration is not completely elucidated also in the case of porphyrins. More in sight the electronic nature of the nitrating specie (nucleophilic, electrophilic or radicalic) is object of controversies. According to the experimental results Gross indicates a crucial role of the hexachloroantimonate in the oxidation of NO_2^- to NO_2, which is considered the effective nitrating agent.

This hypothesis can be supported by the success of the reaction also with the corresponding tin derivative, which does not form the π-cation radical and by the different regioselectivity observed in this reaction, compared to that commonly featured by other electrophilic substitutions.

3.4.1 Nitration of meso-triarylcorroles

There are a wide range of different nitrating systems that have been successfully used for the preparation of β-nitro derivatives of tetra-arylporphyrins[34].

However in the case of corroles a particular attention should be devoted to the stability of the macrocycle in the reaction conditions. For this reason we did not consider harsh nitrating systems, such as HNO_3/H_2SO_4, considering the sensitivity of corrole ring to oxidation.

Taking in account the good results obtained in the case of porphyrins, we first tried N_2O_4 for the nitration of triphenylcorrole (**TPC**), chosen as reference system. However in this case we did not observe reaction and the starting material remained unchanged at the end of the reaction.

We then exploited $Cu(NO_3)_2$ in acetic anhydride as nitrating system for the reaction on tri-*p*-tolylcorrole (**TTC**). In this case we observed an extensive decomposition of the starting material and a copper corrole complex was obtained in very low yields. The ^1H NMR spectrum (Fig. 3.13) indicated a β-monosubstituted product, but, because of the very low yield of the reaction, we did not attempt to fully characterize this product.

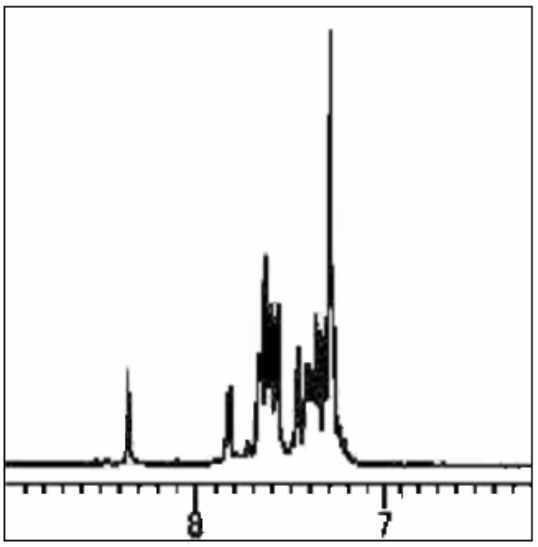

Fig. 3.13 *– ^{1}H NMR spectrum of Cu-(β-NO_2)TTC.*

The formation of this product led us to further consider the reaction of the macrocycle with electrophilic reagent BF_4NO_2, but we obtained the complete decomposition of the starting material.

Our attention turned out to different nitrating system and more satisfying results were obtained when **TPC** was reacted with $AgNO_2/I_2$, commonly used for nitration of tetra-arylporphyrins. Although in this case we still observed some decomposition of corrole, we were able to isolate a product of the reaction in moderate yields.

The complete spectroscopic characterization of this compound revealed the β-nitration of the corrole ring, with also the concomitant coordination of the silver ion to give the corresponding complex.

The reaction seemed to be regioselective, because only one product was formed; our attempts to obtain single crystals of this compound were unsuccessful, so we carried out a ROESY experiment on the product arising from nitration on **TTC**, to characterize the site of substitution.

The spectrum obtained (Fig. 3.14) was consistent with the substitution at position 3, and this result is also in agreement with previous examples reported in

literature, where this position is usually observed as the more reactive in the case of *meso*-triarylcorrole[29].

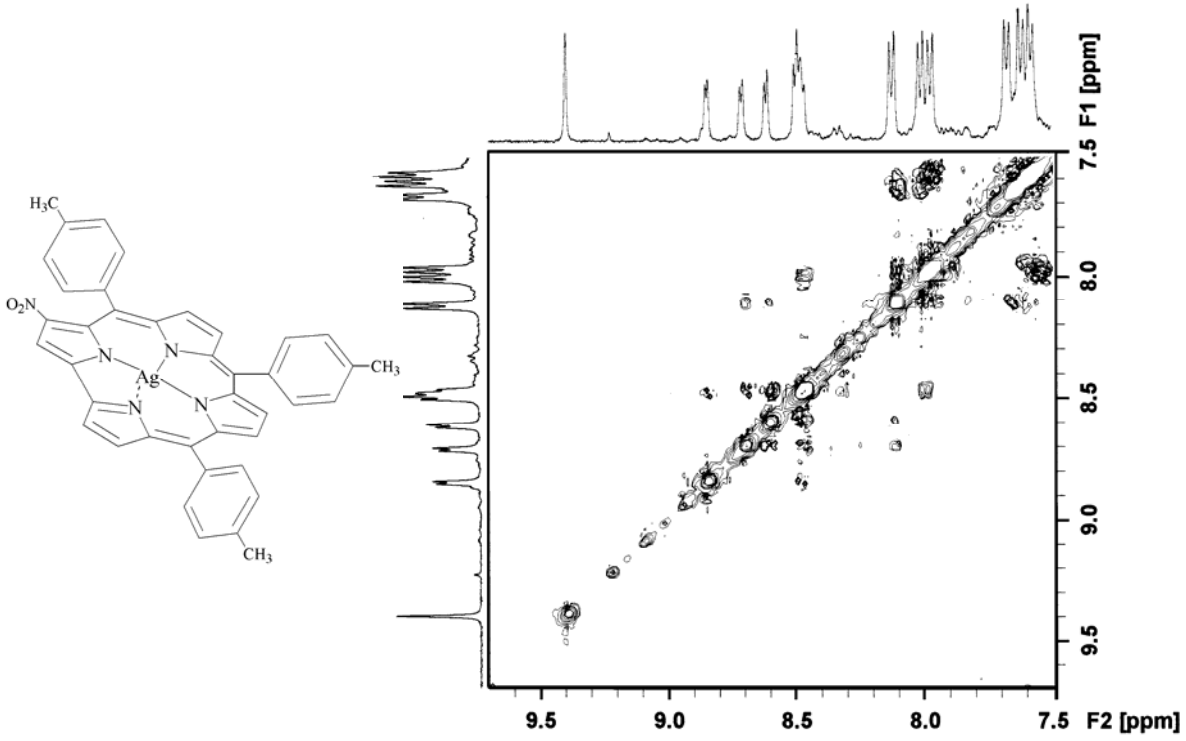

Fig. 3.14 *– ROESY ^{1}H NMR spectrum of Ag-(3-NO_2)TTC.*

Prompted by this promising results, we were interested to check the generality of the reaction, studying firstly the influence of the corrole structure on the reaction. We then performed nitration on different *meso*-substituted triarylcorroles, using $AgNO_2/I_2$ as nitrating system and the results are reported in Table 3.1.

The reaction is clearly favoured by the presence of electron releasing groups on the peripheral phenyl rings. In the case of both ***1c***, ***2c*** and ***3c*** we obtained good yields of the corresponding mono-nitro derivatives, with traces of the non-substituted complexes, while with corroles ***4c*** and ***5c*** we observed mostly decomposition of the corrole ring.

It is worth mentioning that we later noted that I_2 is not necessary for the success of nitration: when the reaction was carried out on ***3c***, we observed that I_2 increased the rate of the reaction, with the reaction complete in about 5 min, but we also observed that without I_2 the reaction gave the same products in 25 minutes (Scheme 3.7). Furthermore in this latter case we obtained better yields of the mononitro derivative, with no significant decomposition of the starting corrole.

Table 3.1. Products of the nitation reaction carried out on different substituted triarylcorroles.

Substrate		Reaction Products
1c	TPC	Ag-TPC + Ag-(3-NO_2)TPC + Open chains
2c	TTC	Ag-TTC + Ag-(3-NO_2)TTC
3c	(4-tBu)TPC	Ag-[(4-tBu)TPC] + Ag-(3-NO_2)[(4-tBu)TPC]
4c	(3,5-F_2)TPC	Monosubstituted product + Open chains
5c	F_5TPC	Open chains

Reaction conditions: $AgNO_2/I_2$ in CH_3CN, at 25°C, under N_2, 5-20min.

This intriguing result led us to further investigate the influence of the reagents in the reaction course.

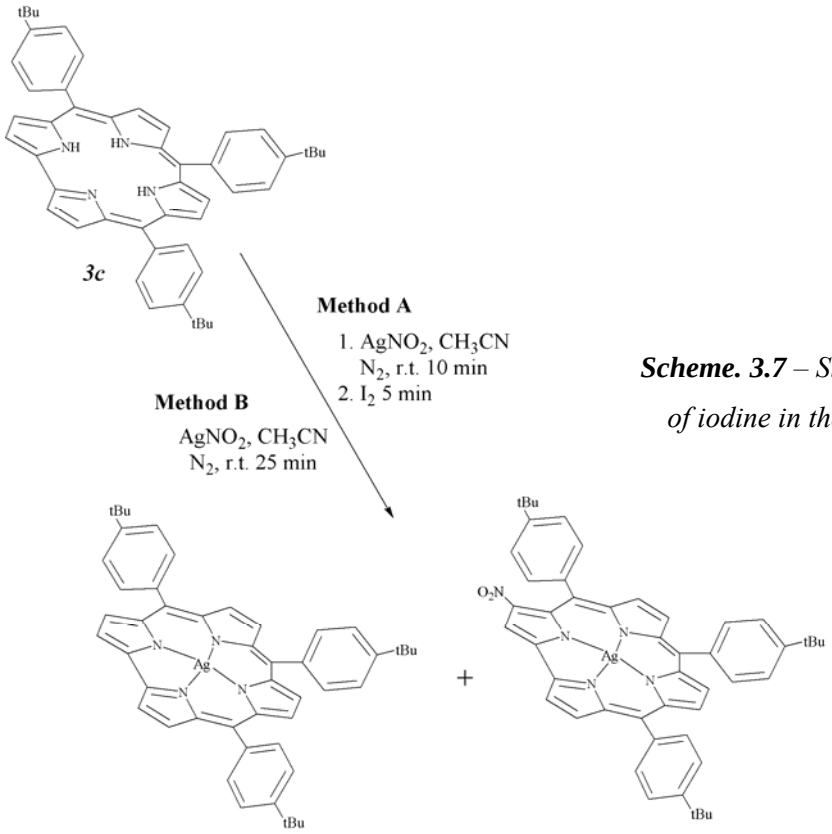

Scheme. 3.7 *– Study of the influence of iodine in the reaction course.*

Firstly we decided to investigate the role of silver ion for the efficiency of the nitration. We decided to react the silver complex **Ag-[(4-tBu)TPC]** ***17c*** with $NaNO_2$ in the same experimental conditions, to check if metal coordination is necessary on the success of the reaction. We observed no reaction in this case, while the product was immediately formed when $AgNO_2$ was added to the reaction mixture (Scheme 3.8).

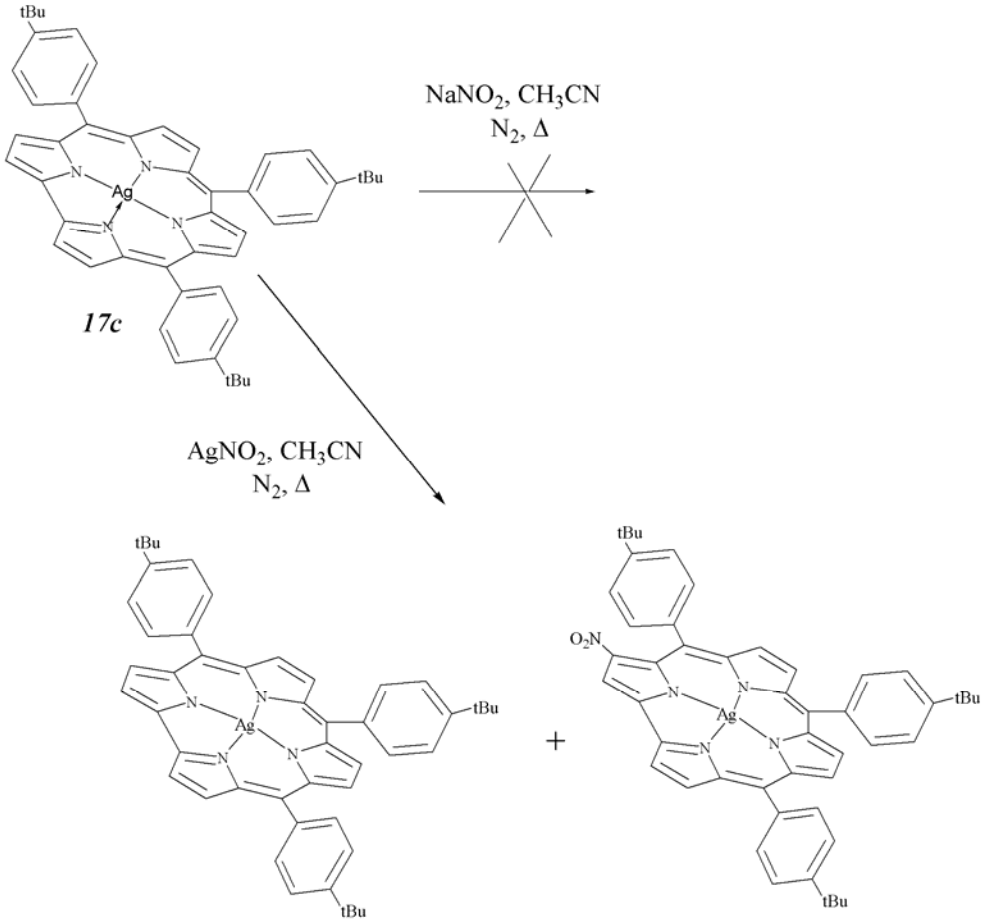

Scheme. 3.8 – *Study of the influence of metal coordination in the reaction course.*

Finally we studied the influence of of the solvent nature on the reaction course. We observed that, using a more polar solvent mixture, like $CHCl_3$/MeOH, in about five minutes the macrocycle was completely decomposed (Scheme 3.9).

All these results led us to propose a plausible mechanism for nitration of triarylcorroles with $AgNO_2$: NO_2^- ion is the nitrating agent, which attacks the π-cation radical of corrole deriving from the oxidation by silver ion.

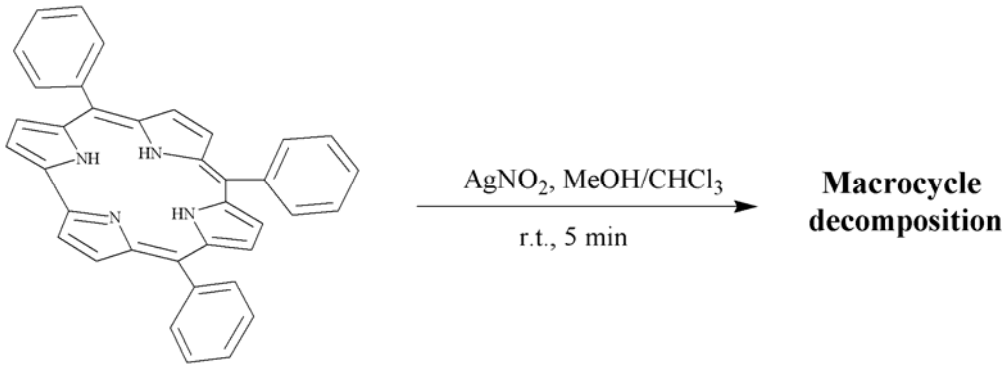

Scheme. 3.9 – *Study of the influence of the solvent nature in the reaction course.*

3.4.2 Nitration on β-alkylcorroles

We also investigated the nitration on *β*-alkylcorroles, in order to verify the generality of the reaction using exclusively $AgNO_2$ as nitrating agent, and evaluate eventually a different reactivity of the *meso* positions compared to the *β* ones.

We firstly reacted corrole ***12c*** with a large excess of $AgNO_2$ in acetonitrile. After 10 min TLC showed the complete disappearance of the starting corrole, and the formation of a single, orange, reaction product (Scheme 3.10).

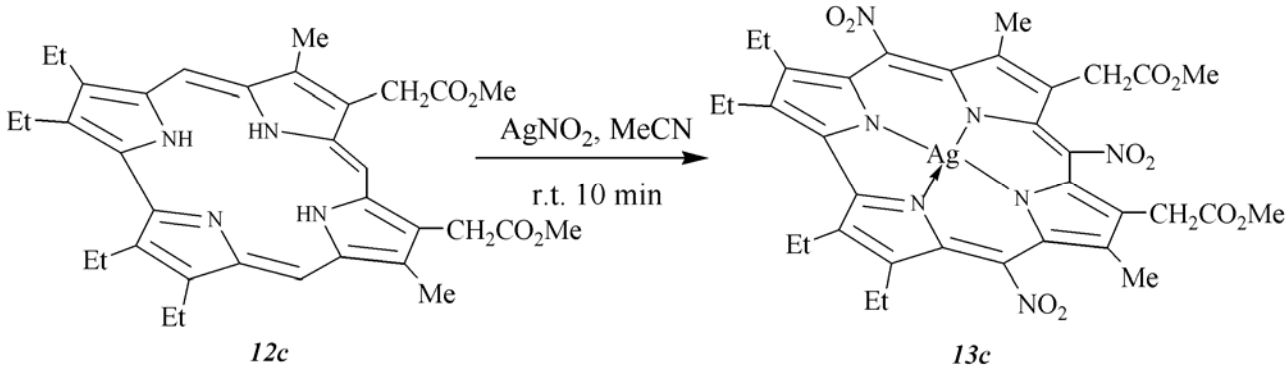

12c ***13c***

Scheme. 3.10 – *Nitration on β- alkylcorrole* ***12c****.*

This product was fully characterized and was identified with the silver corrolate ***13c***, completely substituted on the *meso* positions with nitro groups.

UV-vis spectra of this compound and the starting corrole were completely different; Soret band of the product is red-shifted, as expected in the case of a peripheral functionalization with an electron withdrawing group, such as NO_2.

^{1}H NMR, showed that no signals of the *meso* protons are evident, indicating the complete substitution at these positions.

Finally, X-ray molecular structure confirmed the expected product, evidencing the coordination of the silver ion in the centre of corrole and polynitration.

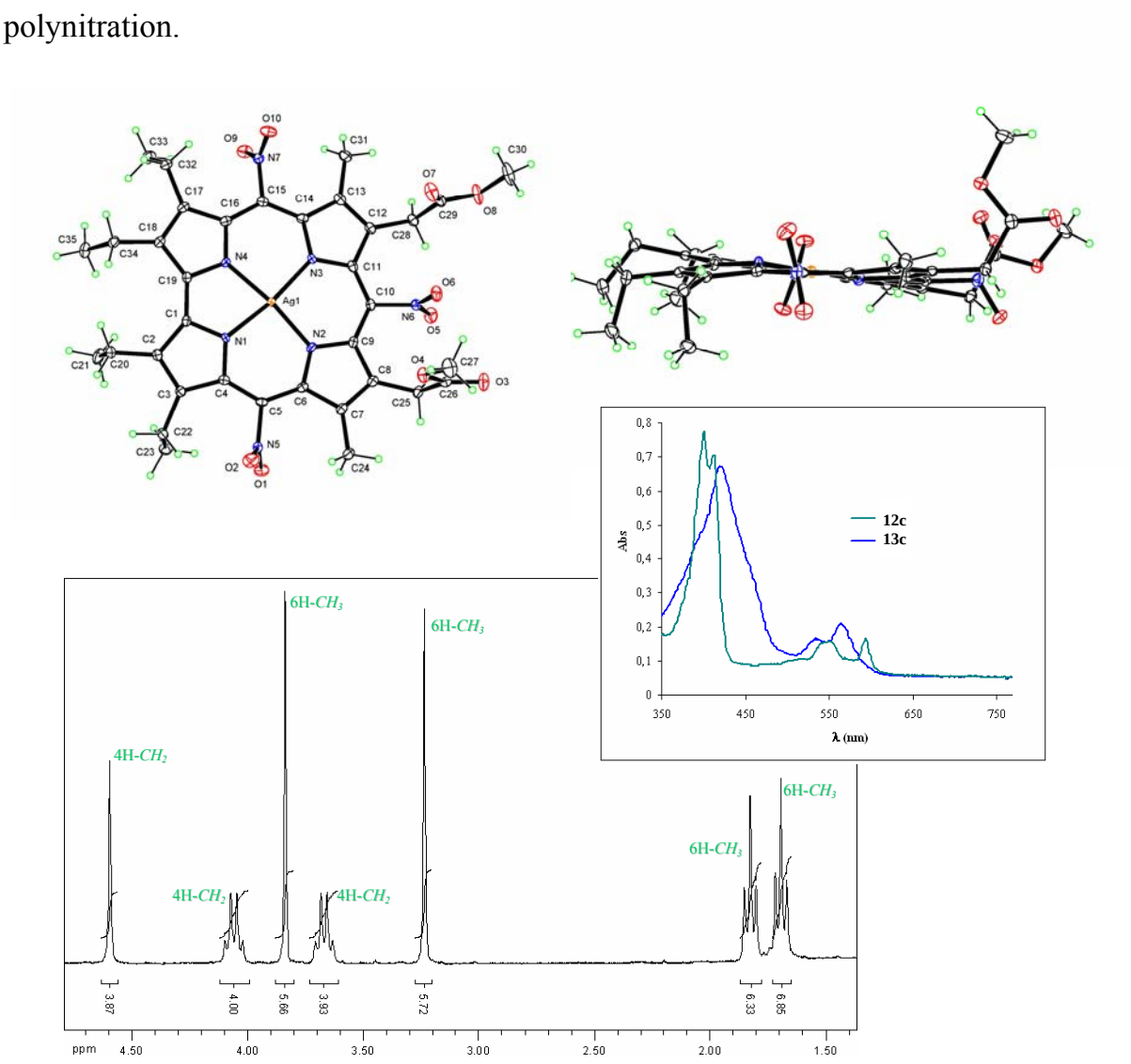

Fig. 3.15 *– Characterization of compound* ***12c****.*

To study the course of the reaction, we reacted corrole ***14c*** in similar conditions, but using DMF instead of acetonitrile as solvent. This choice was due both to the low solubility that this corrole presented in CH_3CN and the need of a polar aprotic medium for the success of the reaction. Moreover the use of DMF allowed us to stop the reaction at different times, by simple addition of brine to the reaction mixture, causing the immediate precipitation of a green powdery solid.

When the reaction was quenched few seconds after the addition of $AgNO_2$, we observed the mono substitution of corrole, but the ^1H NMR spectrum of product ***15c*** showed the presence of two different resonances at ~ 10 ppm (*meso*-protons region) of equal intensity, which indicate the position C5 as the site of substitution.

When the reaction was carried out on longer time, again the fully substituted corrole derivative ***16c*** was obtained, as revealed by ^1H NMR spectrum that showed the disappearance of *meso*-protons.

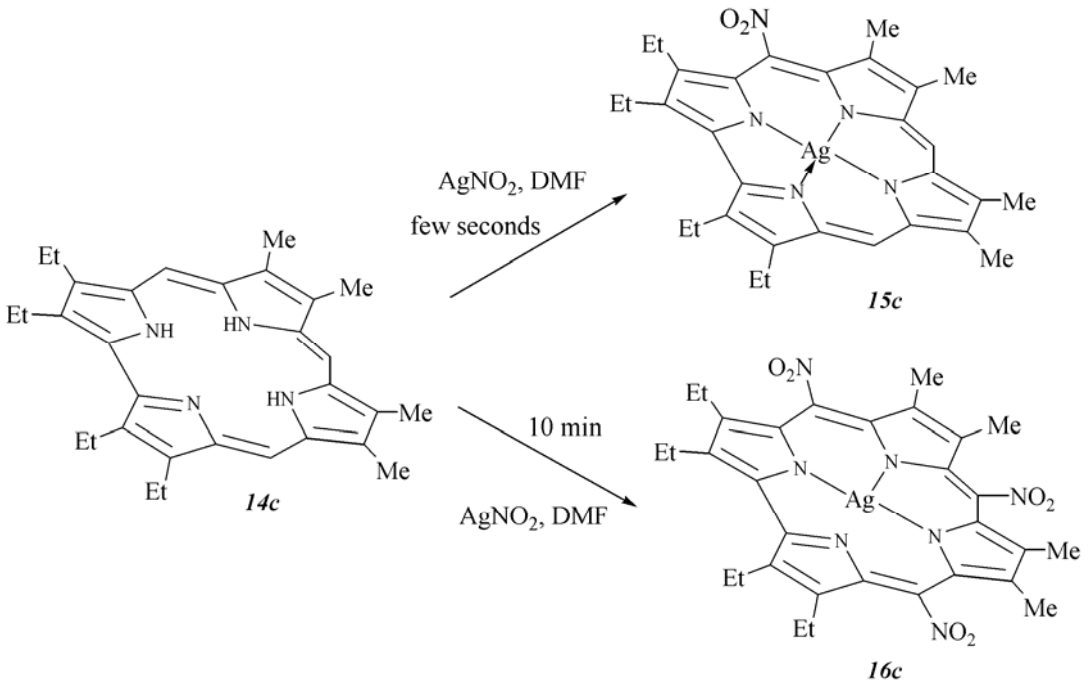

Scheme 3.11 *– Nitration on β- alkylcorrole* ***14c****.*

In Scheme 3.11 the two products obtained at different times by nitration in DMF on corrole **Et_4Me_4Corr *14c*** are reported. Again this feature supports the presence of an intermediate radical species with subsequent attack of nitrite ion, because in the case of reaction with the electrophilic Vilsmeier reagent, for example, we observed that the attack occurred at position 10.

3.5 Nitration on Metallocorroles

In the previous paragraph we described a new synthetic strategy to obtain silver corrolates substituted with nitro groups on the peripheral positions in good yields. Moreover, changing the experimental conditions we were able to propose a plausible pathway for nitration, which seemed to occur by the nucleophilic attack of the NO_2^- ion to the π-cation radical of corrole. The last specie seemed to be formed by means of oxidation occurred in solution.

We have just reported here that a remarkable number of papers has been published about the "innocence" of corrole as a ligand. This feature has been attributed to a one π-electron oxidation process, which leads to the formulation of some metallocorroles as a formally reduced metal ion coordinated to a corrole π-cation radical[35]. Although electrochemical and spectroscopic studies provided crucial informations about these metal complexes in terms of redox potentials, orbital occupation and relative energies, the controversy about the "innocence"of corrole is still in progress and unclosed.

Prompted by the results obtained in the case of nitration on corroles free base, we attempted this reaction on different metallocorroles, previously reported in literature as corrole π-cation radical complexes, both to confirm the proposed reaction mechanism and to provide a new synthetic procedure for the achievement of useful nitroderivatives of these complexes, showing eventually the "non-innocent" character of corrole through an experimental evidence.

3.5.1 Nitration on copper triarylcorrolates

In the last decade a large number of studies were devoted to the exact assignment of the oxidation state of the metal centre in some metallocorroles. In particular, the oxidation state of the central metal in copper *β*-octaalkylcorrolato complexes was shown to be +III[36], and the same assignment was reported by Ghosh and co-workers for the copper complexes of *meso*-triarylcorroles[37].

These complexes display at 25°C in $CDCl_3$ a diamagnetic ^1H NMR spectrum, confirming their diamagnetic character, as expected for a d^8 square planar low-spin Cu(III)complex.

Although the peaks are resolved and found in the general region expected for metallocorroles, the signals assigned to the *β*-protons are shifted and broadened as compared to the *β*-signals in the corresponding diamagnetic Ag(III) or Al(III) complexes. This may be due to a small paramagnetic contribution to the overall spin state of the molecule

Recently, Bruckner and co-workers[38] explained this feature affording some evidences of the equilibrium for [*meso*-triarylcorrolato] copper between two states, the Cu(III) state and the Cu(II)π-cation radical, that is solvent- and temperature-dependent (Fig. 3.16).

In particular, at high temperature the amount of the radical, paramagnetic specie increases.

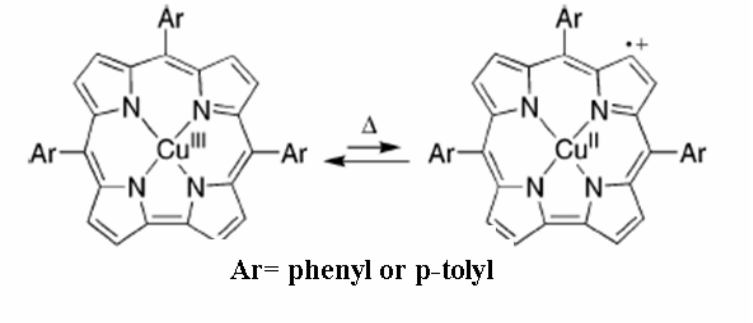

Fig. 3.16 *– Redox equilibrium observed for Cu(III) corrolato complexes*

Then we decided to carry out nitration on two copper triarylcorrolates, whose molecular structures are reported in Fig. 3.17. We surmised that heating the reaction mixture the Cu-complex could be a suitable substrate for the nucleophilic attack of nitro group, affording β-functionalized Cu(III) corrolato complexes.

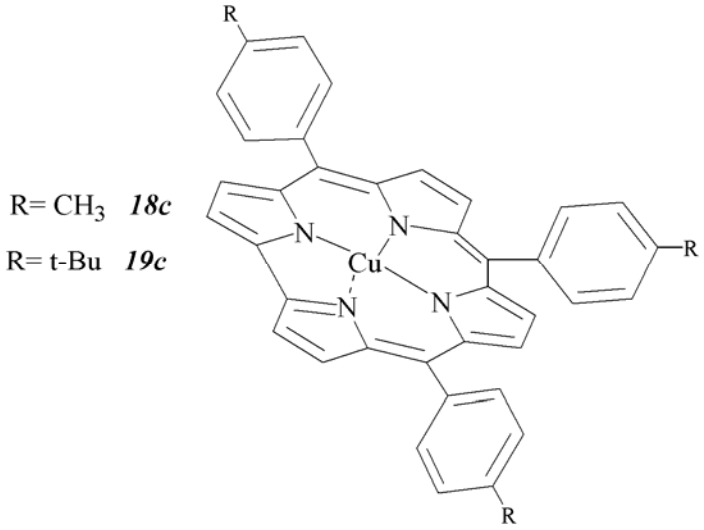

Fig. 3.17 *– Molecular structures of Cu(III) corrolato complexes* ***18c*** *and* ***19c****.*

We reacted corrole complexes ***18c*** and ***19c*** with a large excess of $NaNO_2$ ($[NaNO_2]/[Cu\text{-complex}]=100$) in DMF, heating the mixture to 80°C. The addition of brine to the reaction allowed to stop it at different times, leading to the isolation of different products.

Firstly we quenched the reaction performed on Cu-complex ***18c*** after about 1 hour, obtaining mostly the unreacted complex and another product, which was characterised by ^{1}H NMR spectroscopy. The presence of a single proton resonance at 8.36 ppm together with integrals calculation, led us to identify this compound as the Cu-β(NO_2)TTC.

The reaction was also carried out on Cu-complex ***19c*** in the same conditions, affording the same products. Moreover we observed that heating the reaction for a longer time, about 24 hours, the reaction products were different. In particular the starting material completely disappeared and two main products were formed. ^{1}H NMR spectra of these two compounds allowed to identify them

as the mono- and the di-substituted Cu-[(4-tBu)TPC], showing a single proton resonance at 8.31 and 8.17 ppm respectively.

Finally, we performed nitration on Cu-complex ***18c*** in refluxing DMF (b.p. 153°C). In this case the reaction occurred faster than at 80°C, as witnessed by the quite rapid colour change of reaction mixture from brown to dark green. The reaction afforded mostly a green compound, whose ^{1}H NMR spectrum identified as a polynitrated Cu-complex.

These results clearly supported the presence of the π-cation radical as the reactive specie in nitration. This reasonably corroborates our hypothesis about nitration on triarylcorroles and represents a new synthetic tool to new β-nitroderivatives of Cu(III) corrolato complexes.

Moreover, we observed polynitrated products by increasing temperature: this is particularly intriguing because polyfunctionalization of β positions of corroles is not so trivial. Indeed only tris-nitration on Ga-corrole complexes has been reported in literature by Gross and co-workers[29], while only bis-functionalised derivatives were obtained from other reaction as hydroformylation and chlorosulfonation.

3.5.2 Nitration on chloroiron corrolates

The seminal work in the field of iron corrolates was the report of the Vogel group on iron derivatives of 2,3,7,8,12,13,17,18-octaethylcorroles (OECorr)[39.] In most of these complexes the iron is bound to some anion in addition to the corrole, and thus the formal oxidation state is Fe(IV). This feature is particularly intriguing because Fe(IV) porphyrinates have been proposed as reactive intermediates in some enzymes. It was therefore important to determine if d^4 Fe(IV) was actually stabilized when coordinated to corroles. However, the initial characterization of these iron corrolates did not clearly elucidate their electronic

configurations, because two different structures were thought to be compatible with some of the experimental data: *S*=1 Fe(IV)(Corr)$^{3-}$ or *S*=3/2 Fe(III)(Corr)$^{2-\cdot}$ where the macrocycle is a 1-electron oxidized radical and is antiferromagnetically coupled to the metal unpaired electrons[24,39,40]. In Fig 3.18 are shown the possible electron configurations of the iron corrolates with formal oxidation state Fe(IV). For S = 1 d^4 Fe(IV), the metal electron configuration is expected to be either $(d_{x2-y2})^2$ $(d_{xz})^1$ $(d_{yz})^1$ or $(d_{xz})^2$ $(d_{yz})^1$ $(d_{x2-y2})^1$, while for S = 3/2 d^5 Fe(III), the electron configuration could be either $(d_{x2-y2})^2$ $(d_{xz})^1\times$ $(d_{yz})^1(d_{z2})^1$ or $(d_{xz})^2$ $(d_{yz})^1$ $(d_{x2-y2})^1(d_{z2})^1$.

For the first configuration of each of these oxidation states listed, there is one unpaired electron in each of the π-symmetry orbitals, d_{xz} and d_{yz}, while in the second configuration of each there is only one unpaired electron present, which is shared between the two dπ orbitals.

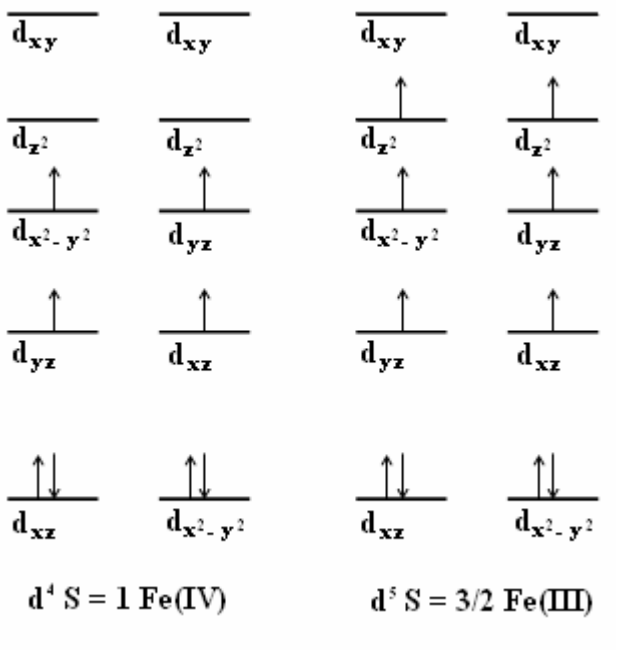

Fig. 3.18 *– Redox equilibrium observed for Cu(III) corrolato complexes*

The other difference in the Fe(IV) and Fe(III) corrolates is the location of the other electrons of the Fe(IV) configuration, or equivalently, from where the fifth

electron of Fe(III) was obtained. These two are interrelated by transfer of one electron of the $(Corr)^{3-}$ macrocycle to the former Fe(IV) to produce a $(Corr)^{2-}$ π-cation radical and Fe(III).

If the Fe(III) has S = 3/2 and there is a way to couple the spins of the metal and corrolate radical, then both S = 1 Fe(IV)$(Corr)^{3-}$ and S = 3/2 Fe(III)$(Corr)^{2-}$ can have S = 1.

The chloride axial ligand appears to play a substantial role in the electron transfer between corrolate macrocycle and iron, both by accumulating positive spin density and also, indirectly, by causing geometrical changes (displacement of the iron out of the corrolate plane), and as a result changes in the interaction of the iron with the corrolate atoms.

Removal of an electron from a corrolate molecular orbital to form a metallocorrolate π-cation radical complex leads to structural changes, or, conversely, structural changes enforce electronic structure changes which may lead to corrolate radical formation.

It should be emphasized that antiferromagnetic coupling of metal spin and corrolate radical spin involves iron (d_{z2})-corrolate (''a_{2u}-like'') overlap, which is facilitated by the out-of-plane displacement of iron. Because of the larger displacement of 0.42Å for the chloroiron corrolates compared to 0.27Å for the phenyliron corrolate, the antiferromagnetically coupled metallocorrolate radical state seems to be more likely for the (OECorr)FeCl and (TPC)FeCl than for the (OECorr)FePh.

All these considerations, together with a large number of experimental and theoretical proofs carried out on these complexes, such as magnetic susceptibility measurements, NMR and Mössbauer spectroscopic investigations, DFT calculations and redox properties evaluations led very recently Walker and co-workers[35b] to definitively describe chloroiron corrolates as S_1= 3/2 Fe(III), S_2= ½ $(Corr)^{2-\cdot}$.

Prompted by these important conclusions, we decided to carry out nitration on different chloroiron corrolates, using only $NaNO_2$ as nitrating agent, being in principle unnecessary in this case the use of an oxidant for the generation of the reactive radical specie.

Moreover our purpose was not only to prepare nitroderivatives of these iron complexes but also to support by experimental evidences the definitive formulations of these complexes as unambiguous chloroiron (III) $(corrolate)^{2-\cdot}$ π-cation radicals.

Furthermore we wanted to verify an eventual substituent effect on the progress of the reaction, by varying the chemical structure of corrole ligand.

Thus, five chloroiron corrolates ***19c***, ***20c***, ***21c***, ***22c*** and ***23c*** have been synthesized and used as substrates for peripheral functionalization with nitro groups. Their structures are reported in Fig. 3.19.

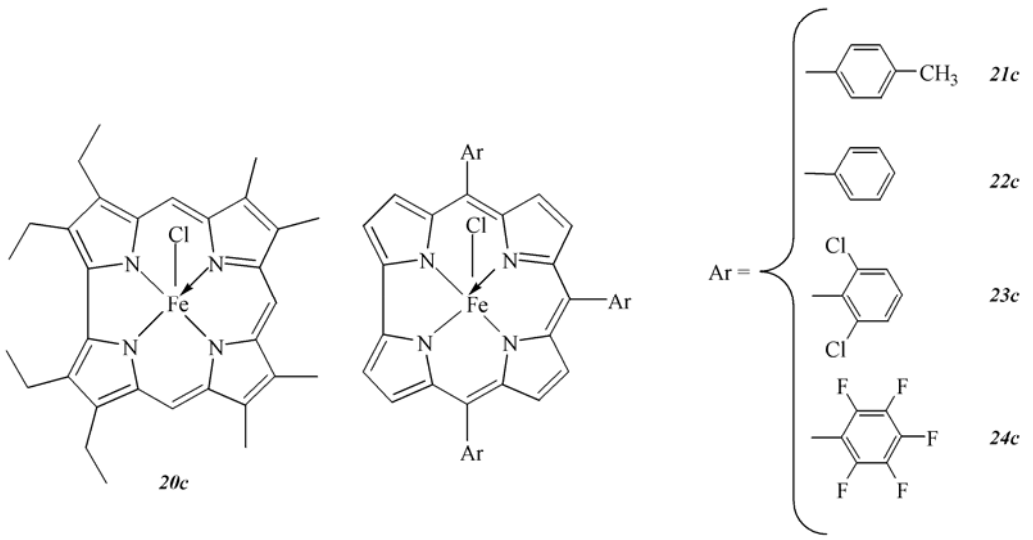

Fig. 3.19 *– Molecular structures of chloroiron corrolates*

The reaction was carried out at room temperature in acetonitrile, using a large excess of $NaNO_2$ ($[NaNO_2]/[Fe\text{-}complex]=100$) and monitoring the reaction course both by UV-vis spectroscopy and TLC. Depending on the substrate we observed different products. In particular nitration on chloroiron corrolate ***20c***

afforded a mixture of products not easy to purify. However, some spectroscopic evidences helped us to understand a plausible identity of the reaction products. More in sight ^{1}H NMR spectrum showed the presence of different *meso*-protons resonances, indicating the functionalization of some *meso* positions with nitro group. Moreover, IR spectroscopy revealed the presence of the stretching band at 1772 cm^{-1} characteristic of a nitrosyl group (Fig. 3.20a) and in accordance with data reported in literature[41]. The reaction products seemed to be a mixture of iron nitrosyl complex and nitrated iron complexes.

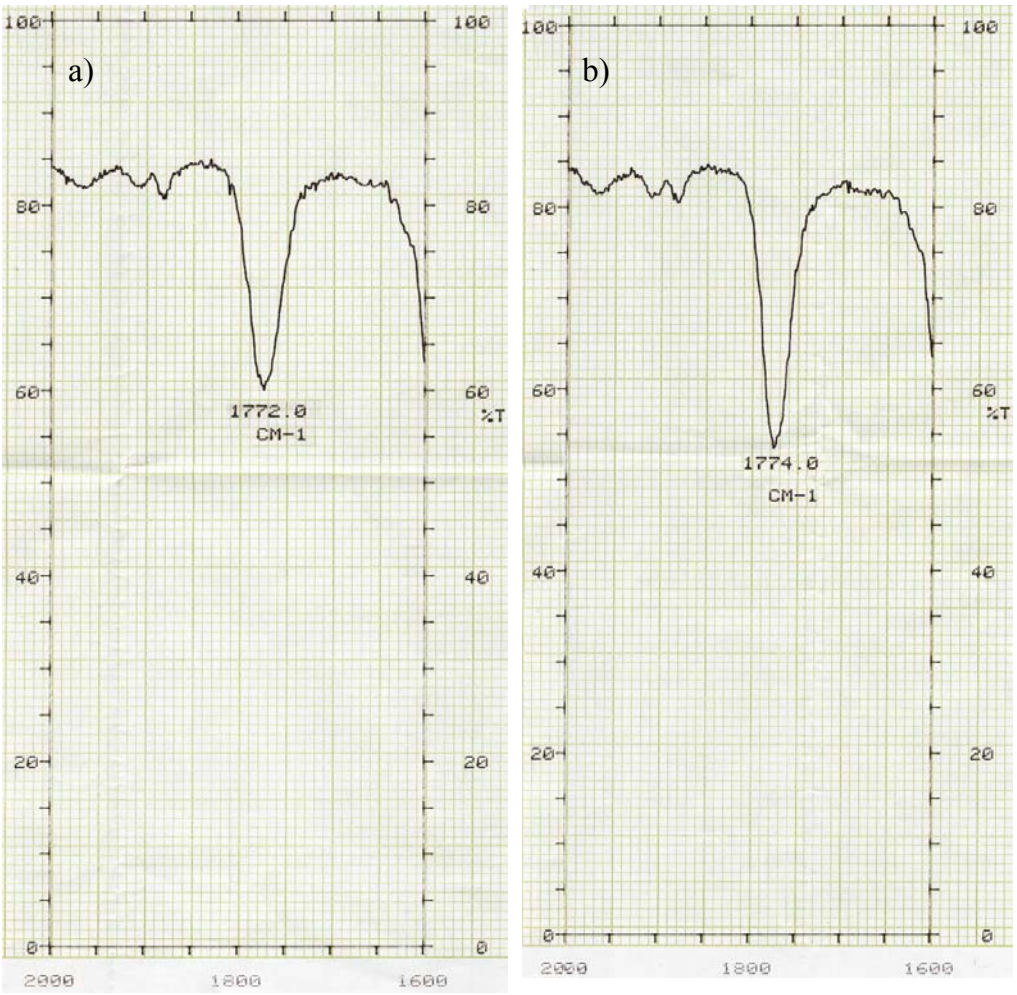

Fig. 3.20 *– IR spectra of nitrosyl complexes of chloroiron corolates* ***20c*** *(a)and* ***21c*** *(b).*

Nitration performed on chloroiron triarylcorrolates afforded some different and more interesting results. A first evaluation was performed on the influence of corrolate structure on the course of the reaction. In the case of compounds ***21c***, ***22c***, and ***23c*** nitration afforded three main products, while in the case of ***24c*** only one product was observed, corresponding to the nitrosyl complex of Fe-(F_5TPC).

The spectroscopic characterization of the products obtained by nitration on complex ***21c*** provided crucial informations to verify the success of the reaction.

The brilliant red crystals of the first band eluting in column was identified by ^{1}H NMR, ESI and IR spectroscopy(see Fig. 3.20b) as the corresponding iron nitrosyl complex, originating by the ligand exchange in the axial position between nitrite ion and chloride anion and its subsequent very fast lack of O atom. Since iron nitrosyl corrolates have been described as a *formally* iron (III) complexes[35b, 41], the generation of this complexes in solution suppressed the π-cation radical character of the starting metallocorrole, leading to an ineffective substrate for nitration as we formulated it. This could be an explanation of the presence of this compound among the reaction products.

The second band afforded by chromatographic column seemed to be a *β*-nitroderivative of the starting iron complex, as witnessed by the presence of a single proton resonance at 8.37 ppm in the pyrrolic region of the ^{1}H NMR spectrum.

The third compound was better characterized and provided intriguing and unexpected results. ^{1}H NMR spectrum is well-defined and resolved compared to the starting iron chloride corrolate, indicating a diamagnetic character of the complex analysed. The presence of a single peak at ~ 8.48 ppm and integrals calculation were consistent with a di-substituted *β*-nitroderivative, and the diamagnetic feature of the sample led us to suppose the presence of NO axially coordinated to the iron ion. As a matter of fact, IR spectrum did not show the

typical stretching signal of this ligand. Fortunately our attempts to obtain single crystals of this compound were successful and we achieved the X-ray molecular structure reported in Fig. 3.21.

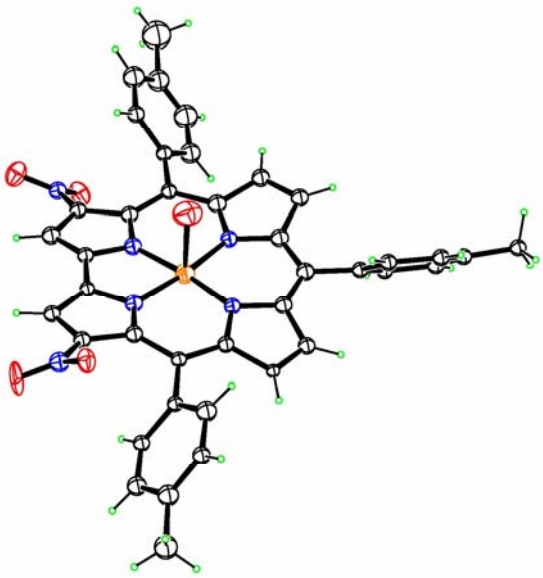

Fig. 3.21 *– X -ray structure of 3,17-$(NO_2)_2$-TTC-Fe(IV)(OH).*

This structure allowed us to mostly identify this compound as a 3,17-$(NO_2)_2$-TTC-Fe(IV)(OH), confirming positions 3 and 17 as the more reactive of the corrole ring. In particular it represents the first experimental evidence of the "non-innocent" character of corrole as a ligand in chloroiron corrolates, and also confirms that nitration on these complexes could be successful, using a very simple nitrating agent, such as $NaNO_2$.

Moreover the X-ray structure revealed other interesting aspects. The axial ligand of the iron corrolate is an OH group, which is a bridge between two macrocycles, leading to a polymeric structure in the solid phase, as illustrated by the X-ray structure reported in Fig. 3.22.

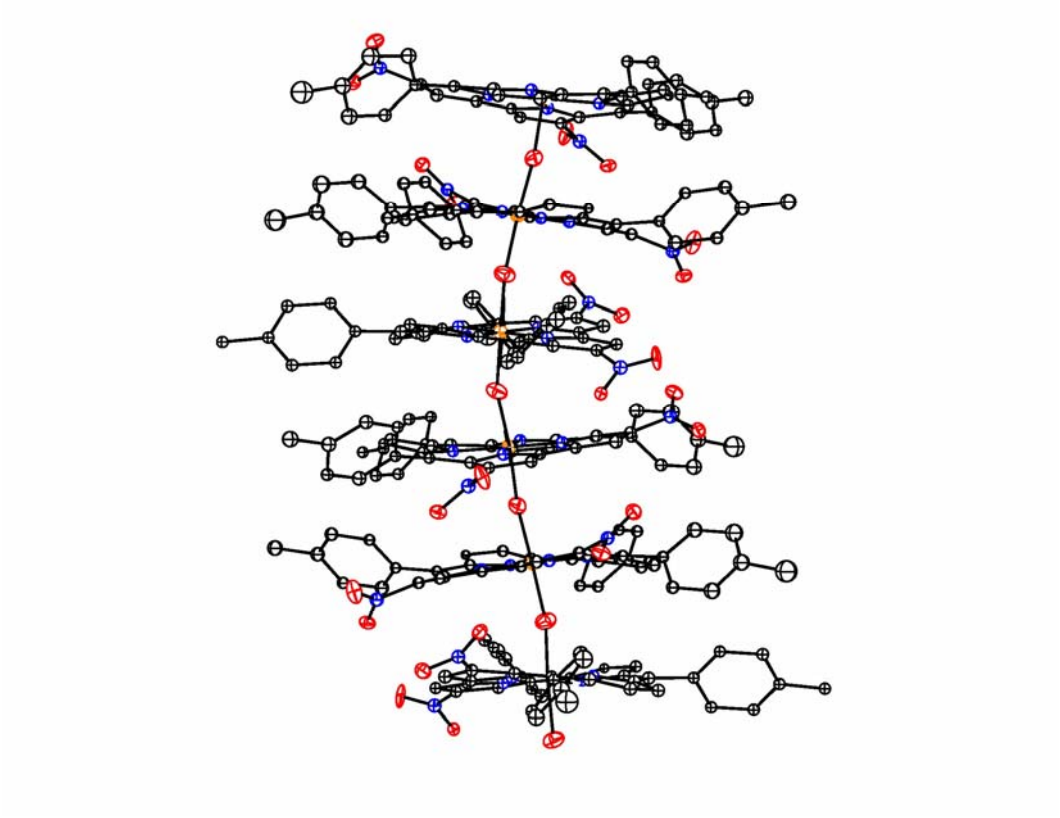

Fig. 3.21 *– X-ray structure of helicoidal arrangement of 3,17-$(NO_2)_2$-TTC-Fe(IV)(OH).*

This helicoidal arrangement is singular and has never been observed in crystallographic packing both of corroles or porphyrins. Nevertheless the information derived from X-ray structure is in conflict with the diamagnetic character of this compound, which is evident from the well-resolved ^{1}H NMR spectrum.

These interesting results clearly need of ulterior studies to determine the definite structures of nitro derivatives of iron corrolates. This topic represents an active field of research in our laboratories.

Experimental Section

➢ *Reagents and materials*

Reagents and solvents (Sigma-Aldrich, Fluka and Carlo Erba Reagenti) were of the highest grade available and were used without further purification.

Silica gel 60 (70 -230 mesh) and neutral alumina (Brockmann Grade III). were used for column chromatography.

Silica gel 60 (Merck) and neutral alumina 60 F_{254}, both on aluminium support, were used for TLC.

➢ *Instruments*

^{1}H NMR spectra were recorded with a Bruker AM400 (400 MHz) or Bruker Advance 300 (300 MHz) spectrometers. Chemical shifts are given in ppm relative to tetramethylsilane (TMS).

Routine UV/Vis spectra were measured on a Varian Cary 50 Spectrophotometer, whereas more precise measurements were performed on a Perkin Elmer λ18 Spectrophotometer equipped with a temperature-controlled cell holder.

IR spectra were recorded with a Perkin-Elmer 983G spectrometer.

Mass spectra (FAB) were recorded on a VG Quattro Spectrometer using m-nitrobenzyl alcohol (NBA, Aldrich) as a matrix in the positive-ion mode.

➢ ***Structures of dipyrromethanes and a,c-biladienes used as precursors of alkylcorroles***

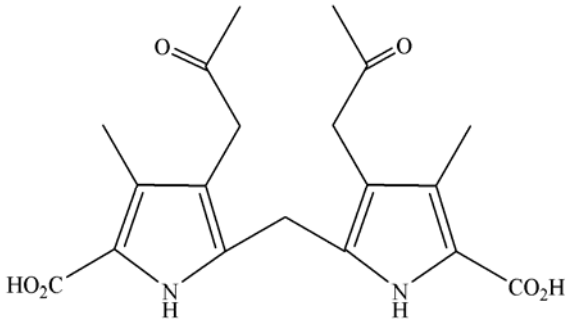

8c

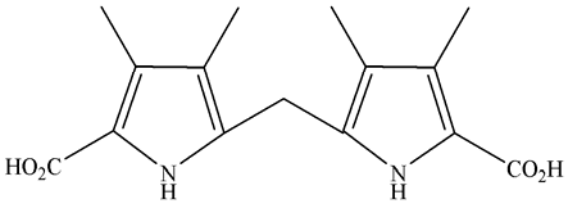

9c

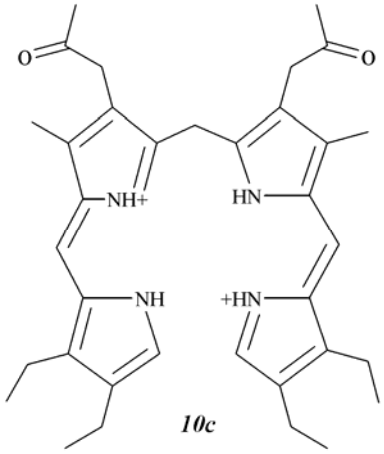

10c

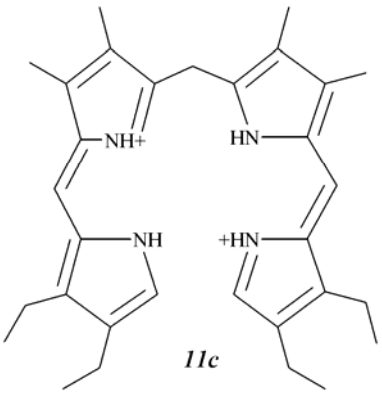

11c

3.6 Syntheses of meso-triarylcorroles

*3.6.1 Syntheses of 5,10,15-triarylcorroles **(1c),(2c),(3c),(4c), (5c),(6c)***

A solution of pyrrole (5.6 mL, 80 mmol) and aldehyde (8.3 mmol) was degassed by bubbling nitrogen for 10 min, before the addition of trifluoroacetic acid (16 μL, 0.2 mmol). The mixture was stirred for 15 min at r.t. and then diluted with CH_2Cl_2 (30 mL). The reaction mixture was left at r.t. for 1 h; chloranil (1.57 g, 6.4 mmol) was then added and the mixture was stirred for a

further 15 min. The solvent and the residual pyrrole were removed under reduced pressure, the crude mixture was dissolved in CH_2Cl_2 and then chromatographed on silica gel (eluant CH_2Cl_2 or CH_2Cl_2/hexane 1:1 in the case of ***5c*** and ***6c***).

Corroles were identified on the basis of comparison of their spectral properties with those in the literature. Yields: 4-15%.

3.7 Syntheses of β-alkylcorroles

*3.7.1 Syntheses of a,c-biladiene dihydrobromide (**10c**) and (**11c**)*

1,6 mmol of the dipyrromethane-1,9-dicarboxylic acid (**8c**), (**9c**), prepared according to literature, was dissolved in trifluoroacetic acid (10 mL) and stirred for 5 min. 2-formyl-3,4-diethylpyrrole (500 mg, 3.3 mmol) in MeOH (90 mL) and 1 ml of HBr/AcOH solution were added and the red solution was stirred at room temperature. Progress of the reaction was monitored spectrophotometrically; when the formation of *a,c*-biladiene was complete, the crude product was precipitated with diethyl ether, then the red-brown crystals were filtered under vacuum.

Yield: 88% (***10c***), 92% (***11c***).

*3.7.2 Syntheses of 2,3,7,8,12,13,17,18-octaalkylcorroles (**12c**) and (**14c**)*

a,c-biladiene dihydrobromide (***10c***) and (***11c***) (0.5g), chloranil (0.5 g) and a spoon of $NaHCO_3$ were dissolved in 100 mL of methanol and stirred at room temperature. Progress of the reaction was monitored spectrophotometrically; when absorbances attributable to the starting material disappeared 1 mL of hydrazine hydrate was added and the crude product was precipitated with water. The resulting solid was redissolved in CH_2Cl_2, then washed with water (3 times)

and dried over anhydrous Na_2SO_4. The solvent was evaporated under vacuum and the crude mixture was chromatographed on silica gel; the column was eluted with CH_2Cl_2 to yield a red-violet fraction which, after evaporation, was crystallized from CH_2Cl_2/hexane. Corroles were identified on the basis of comparison of their spectral properties with those in the literature.

Yields: 51% (***12c***); 58% (***14c***).

3.8 Syntheses of Metallocorroles

3.8.1 Synthesis of the 5,10,15-triarylcorrolato of silver(III) (17c)

meso-triarylcorrole (0.1 mmol) was dissolved in pyridine (10 mL), and silver(I) acetate (0.33 mmol) was added. The deep green corrole solution turns, in due course with the metal insertion, a deep dark red. Quantitative silver insertion takes place upon warming of the solution to ~80 °C (TLC or UV-vis control). Upon completion, the reaction mixture was filtered through a plug of Celite, the solvent was removed on a rotary evaporator, and the residue was chromatographed on silica gel; the column was eluted with CH_2Cl_2 to yield a red-violet fraction. After evaporation, the residue was crystallized from CH_2Cl_2/MeOH, affording 52 mg (65%) of dark red crystals.

3.8.1 Synthesis of the 5,10,15-triarylcorrolato of copper(III) (18c) (19c)

meso-triarylcorrole (***1c***) and (***3c***) (0.1 mmol) was dissolved in $CHCl_3$ (100 mL), and copper(II) acetate (0.33 mmol) dissolved in MeOH was added. The mixture was heated to reflux for about two hours and the progress of the reaction was monitored spectrophotometrically. Upon completion, the solvent was

concentrated and the dark brownn crystals was filtered under vacuum. Yield: 85% (***18c***), 78% (***19c***)

*3.8.3 Syntheses of chloroiron corrolates (**20c**) (**21c**) (**22c**) (**23c**) (**24c**)*

Corrole (0.1 mmol) was dissolved in DMF (10 mL), and iron(II) chloride (0.33 mmol) was added. The mixture was heated to reflux under nitrogen for about three hours and the progress of the reaction was monitored spectrophotometrically. Upon completion, the crude product was precipitated with brine and filtered. The resulting solid was dissolved in CH_2Cl_2, then washed with brine (3 times) and dried over anhydrous Na_2SO_4. The solvent was evaporated under vacuum and the crude mixture was chromatographed on alumina (dis. 5%); the column was eluted with CH_2Cl_2 to yield a brown fraction which, after evaporation, was crystallized from CH_2Cl_2/hexane.

Yields: 65-82%.

3.9 Nitration reaction

*3.9.1 Nitration on 5,10,15-triarylcorroles (**1c**), (**2c**), (**3c**), (**4c**), (**5c**) with $AgNO_2$*

Triarylcorrole (0.1 mmol) was dissolved in CH_3CN (10 mL), and silver (I) nitrite (10 mmol) was added. The mixture was stirred at room temperature and the progress of the reaction was monitored spectrophotometrically. The reaction was complete in about 30 minutes. The reaction mixture was filtered through a plug of Celite, the solvent was removed on a rotary evaporator, and the residue was chromatographed on silica gel; the column was eluted with CH_2Cl_2/hexane (3:1) to afford two main fractions: the first red-violet corresponding to the silver

complex of corrole and the second brilliant green corresponding to the silver complex β-functionalised with NO_2 group. The second fraction, after evaporation, was crystallized from CH_2Cl_2/MeOH.

Yield for Ag-(β-NO_2)Corr 28-32%.

*3.9.2 Nitration on 2,3,7,8,12,13,17,18-octaalkylcorroles (**12c**) and (**14c**) with $AgNO_2$*

Octaalkylcorrole ***12c*** (0.1 mmol) was dissolved in CH_3CN (10 mL), and silver (I) nitrite (10 mmol) was added. The mixture was stirred at room temperature and the progress of the reaction was monitored spectrophotometrically. The reaction was complete in about 10 minutes. The reaction mixture was filtered through a plug of Celite, the solvent was removed on a rotary evaporator, and the residue was chromatographed on alumina dis. 5%, eluting with CH_2Cl_2. The first brilliant orange fraction was collected and crystallized with MeOH, affording compound ***13c***.

Octaalkylcorrole ***14c*** (0.1 mmol) was dissolved in DMF (10 mL), and silver (I) nitrite (10 mmol) was added. The reaction course was stopped in different times.

Quenching of reaction after few minutes with distilled water afforded a main green fraction, which was identified by ^{1}H NMR as compound ***15c***. If the reaction was stopped after 10 minutes, the main compound of reaction was ***16c***.

In both cases, the crude of reaction was chromatographed on silica gel, using CH_2Cl_2 as eluant.

*3.9.3 Nitration on 5,10,15-triarylcorrolato of copper(III) (**18c**) and (**19c**) with $NaNO_2$*

Corrole complex (0.1 mmol) was dissolved in DMF (10 mL), and sodium nitrite (10 mmol) was added. The mixture was heated to 80°C for about one hour, then the solvent was evaporated. The residue was dissolved in CH_2Cl_2, washed three times with distilled H_2O. and dried over anhydrous Na_2SO_4. The solvent was removed on a rotary evaporator, and the residue was chromatographed on silica gel, eluting with CH_2Cl_2.

*3.9.4 Nitration on chloroiron corrolates (**20c**), (**21c**), (**22c**), (**23c**), (**24c**) with $NaNO_2$*

Corrole complex (0.1 mmol) was dissolved in CH_3CN (10 mL), and sodium nitrite (10 mmol) was added. The mixture was stirred at room temperature for about two hours and the progress of the reaction was monitored by TLC (silica gel/CH_2Cl_2). Upon completion, the solvent was evaporated and the residue was dissolved in CH_2Cl_2 and washed three times with distilled H_2O. and dried over anhydrous Na_2SO_4. The solvent was removed on a rotary evaporator, and the residue was chromatographed on silica gel, eluting with CH_2Cl_2.

References

1. Johnson, A.W.; Kay, I.T. *J. Chem. Soc.*, **1965**, 1620.
2. Johnson, A.W. *Chem. Soc. Rev.*, **1980**, *9*, 125.
3. Paolesse, R. In *The Porphyrins Handbook*; Kadish, K.M.; Smith, K.M.; Guilard, R. Eds; Academic Press: New York, **2000**, Vol.II.
4. Ghosh, A.; Jynge, K. *Chem. Eur. J.*, **1997**, *3*, 823.
5. Endeward, B.; Plato, M.; Will, S.; Vogel, E.; Szycewski, A.; Mobius, K. *Appl. Magn. Reson.*, **1998**, *14*, 69.
6. Nardis, S.; Monti, D.; Paolesse. *Mini-Rev. Org. Chem.*, **2005**, *2*, 355.
7. Gross, Z.; Galili, N.; Saltsman, I. *Angew. Chem. In. Ed. Engl.*, **1999**, *38*, 1427.
8. Paolesse, R.; Jaquinod, L.; Nurco, D.J.; Mini, S.; Sagone, F.; Boschi, T.; Smith, K.M. *Chem. Commun.*, **1999**, 1307.
9. Paolesse, R.; Licoccia, S.; Bandoli, G.; Dolmella, A.; Boschi, T. *Inorg. Chem.*, **1994**, *33*, 1171.
10. Licoccia, S.; Tassoni, E.; Paolesse, R.; Boschi, T. *Inorg. Chim. Acta*, **1995**, *235*, 15.
11. Rose, E.; Kossanyi, A.; Quelquejeu, M.; Soleilhavoup, M.; Duwavran, F.; Bernard, N.; Lecas A. *J. Am. Chem. Soc.*, **1996**, *118*, 1567.
12. Wasbotten, I.H.; Wondimagegn, T.; Ghosh, A. *J. Am. Chem. Soc.*, **2002**, *124*, 8104.
13. Liu, H.Y.; Lai, T.S.; Yeung, L.L.; Chang; C.K. *Org. Lett.*, **2003**, *125*, 16300.
14. Littler, B.J.; Miller, M.A.; Hung, C.H.; Wagner, R.W.; O'Shea, D.F.; Boyle, P.D.; Lindsey, J.S. *J. Org. Chem.*, **1999**, *64*, 1391.
15. Gryko, D.T.; Koszarna, B. *Org. Biomol. Chem.*, **2003**, *1*, 350.

16. Lindsey, J.S. In *The Porphyrins Handbook*; Kadish, K.M.; Smith, K.M.; Guilard, R. Eds; Academic Press: New York, **2000**, Vol.I.
17. Paolesse, R.; Marini, A.; Nardis, S.; Froiio, A.; Mandoj, F.; Nurco, D.J.; Prodi, L.; Montalti, M.; Smith, K.M. *J. Porphyrins Phthalocyanines*, **2003**, *7*, 25.
18. Gryko, D.T. *Chem. Commun.*, **2000**, 2243.
19. Gryko, D.T.; Piechota, K.E. *J. Porphyrins Phthalocyanines*, **2002**, *6*, 81.
20. Licoccia, S.; Di Vona, M.L.; Paolesse, R. *J. Org. Chem.*, **1998**, *63*, 3190.
21. Bröring, M.; Hell, C. *Chem. Commun.*, **2001**, 2336.
22. Licoccia, S.; Paolesse, R. In *Metal Complexes with Tetrapyrrole Ligands III*; Buchler, J.W. Ed,; Sprinter-Verlag: Berlin and Heidelberg, Germany, **1995**, *84*, 71-134.
23. Johnson, A.W., In *Porphyrins and Metalloporphyrins*; Smith, K.M., Ed.; Elsevier: Amsterdam, **1975**, 729.
24. Ghosh A.; Steene E. *J. Inorg. Biochem.*, **2002**, *91*, 423.
25. Buchler J.W., In *The Porphyrins*; Dolphin, D., Ed.; Academy Press: New York, **1975**, Vol.I.
26. Mahammed, A.; Goldberg, I.; Gross, Z. *Org. Lett.*, **2001**, *3*, 3443.
27. Paolesse, R.; Nardis S.; Sagone F.; Khoury, R.G. *J. Org. Chem.*, **2001**, *66*, 550.
28. Paolesse, R.; Jaquinod, L.; Senge, M.O.; Smith, K.M. *J. Org. Chem.*, **1997**, *62*, 6193.
29. Saltsman, I.; Mahammed, A.; Goldberg, I.; Tkachenko, E.; Botoshansky, M.; Gross, Z. *J. Am. Chem. Soc.*, **2002**, *124*, 7411.
30. Paolesse, R.; Nardis, S.; Venanzi, M.; Mastroianni, M.; Fronczek, F.R.; Vicente, M.G.H.*Chem. Eur. J.*, **2003**, *9*, 1192.
31. Saltsman, I.; Goldberg, I.; Gross, Z. *Tetrahedron Lett.*, **2003**, *44*, 5669.

32. Paolesse, R.; Jaquinod, L.; Della Sala, F.; Nurco, D.J.; Prodi, L.; Montalti, M.; Di Natale, C.; D'Amico, A.; Di Carlo, A.; Lugli, P.; Smith, K.M. *J. Am. Chem. Soc.*, **2000**, *122*, 11295.
33. Paolesse, R.; Nardis, S.; Stefanelli, M.; Fronczek, F.R.; Vicente, M.G.H. *Angew. Chem. In. Ed. Engl.*, **2005**, *44*, 2.
34. Jaquinod, L. In *The Porphyrins Handbook*; Kadish, K.M.; Smith, K.M.; Guilard, R. Eds; Academic Press: New York, **2000**, Vol.I.
35. a) Ghosh, A.; Stesene, E. *J. Biol. Inorg. Chem.*, **2001**, 739. b) Walker, F.A.; Licoccia, S.; Paolesse, R. *J. Inorg. Biochem.*, **2006**, *100*, 810.
36. Will, S.; Lex, J.; Vogel, E.; Schmickler, H.; Gisselbrecht, J.P.; Haubtmann, C.; Bernard, M.; Gross, M. *Angew. Chem. In. Ed. Engl.*, **1997**, *36*, 357.
37. Wasbotten, I.H.; Wondimagegn, T.; Gosh, A. *J. Am. Chem. Soc.*, **2002**, *124*, 8104.
38. Bruckner, C.; Brinas, R.P.; Krause Bauer, J.A. *Inorg. Chem.*, **2003**, *42*, 4495.
39. Vogel, E.; Will, S.; Schulze Tilling, A.; Neumann, L.; Lex, J.; Bill, E.; Trautwein, A.X.; Wieghardt, K. *Angew. Chem. In. Ed. Engl.*, **1994**, *33*, 731.
40. a) Cai, S.; Walker, F.A.; Licoccia, S. *Inorg. Chem.*, **2000**, *39*, 3466. b) Cai, S.; Walker, F.A.; Licoccia, S. *Inorg. Chem.*, **2001**, *40*, 5795. c) Gross, Z. *Biol. Inorg. Chem.*, **2001**, *6*, 733.
41. Autret, M.; Will, S.; Caemelbecke, E.V.; Gisselbrecht, J.P.; Gross, M.; Vogel, E.; Kadish, K.M. *J. Am. Chem. Soc.*, **1994**, *116*, 9141.

Publications

Publications:

1. Paolesse, R.; Nardis, S.; Stefanelli, M.; Fronczek, F.R.; Vicente, M.G.H. *Angew. Chem. Int. Ed*., **2005**, *44*, 2-4.

Abstracts:

1. Nardis, S.; Stefanelli, M.; Mandoj, F.; Paolesse, R. "Hemporphycene and porphyrin from the expansion of the corrole ring", ICPP-3, New Orleans (Louisiana), July 2004
2. Monti, D.; Paolesse, R.; Stefanelli, M.; Alimelli, A.; Di Natale, C.; Macagnano, A.; D'Amico, A. "Development of chemical sensors based on amphiphilic porphyrin aggregates", Synthetic Receptors 2005, Salisburgo, September 2005
3. Stefanelli, M.; Monti, D.; Ercolani, G.; Venanzi, M.; Paolesse, R. "Chiral supramolecular capsule by self-assembly of resorcinarene-Zn-porphyrin conjugate", VII National Congress on Supramolecular Chemistry, Florence September 2005
4. Stefanelli, M.; Monti, D.; Alimelli, A.; Paolesse, R. "Resorcinarene-Porphyrin coniugate: a new ditopic receptor for chemical sensors", XI Annual Conference AISEM, Lecce February 2006.

5. Stefanelli, M.; Monti, D.; Venanzi, M.; Paolesse, R. “Supramolecular chiral aggregates by self-assembling of functionalized porphyrinoids”, ICPP-4, Rome, July 2006
6. Stefanelli, M.; Mastroianni, M.; Nardis, S.; Paolesse, R. “Novel evidences of the noninnocent character of corrole ligand”, ICPP-4, Rome, July 2006
7. Stefanelli, M.; Monti, D.; Ercolani, G.; Venanzi, M.; Paolesse, R. “Facile generation of supramolecular capsule by self-assembling of Resorcinarene-Znporphyrin conjugate”, ICPP-4, Rome, July 2006
8. Lvova, L.; Verrelli, G.; Stefanelli, M.; Nardis, S.; Paolesse, R.; Di Natale, C.; D’Amico, A.; Makarychev-Mikhailov, S. “Pt(II)- and Pt(IV)-porphyrins as ionophores for solvent polymeric membrane electrodes”, ICPP-4, Rome, July 2006.
9. Nardis, S.; Mandoj, F.; Stefanelli, M.; Paolesse, R. “New developments in corrole chemistry”, ICPP-4, Rome, July 2006.
10. Forleo, A.; Epifani, M.; Francioso, L.; Taurino, A.M.; Siciliano, P.; Nardis, S.; Mandoj, F.; Monti, D.; Stefanelli, M.; Paolesse, R. “Characterization and preparation of metalloporphyrin-tin oxide chemical sensors”, ICPP-4, Rome, July 2006.
11. Stefanelli, M.; Monti, D.; Alimelli, A.; Pomarico, G.; D’Amico, A.; Di Natale, C.; Paolesse, R. “Development and testing of a new sensitive material based on metalloporphyrin-resorcinarene conjugate”, IMCS-11, Brescia, July 2006.

Oral communications:

1. Stefanelli, M.; Monti, D.; Ercolani, G.; Venanzi, M.; Paolesse, R. “Chiral supramolecular capsule by self-assembly of resorcinarene-Zn-porphyrin conjugate”, VII National Congress on Supramolecular Chemistry, Florence September 2005.